

The Synthesis of Highly Selective Immobilised Ligands for Extraction of Toxic Metal Ions from Wastewater

Report to the
WATER RESEARCH COMMISSION

by

**B Barnard, CA Bode-Aluko, O Pereao, OO Fatoba, R Luckay and
LF Petrik**

*Environmental and Nanoscience Research Group
Department of Chemistry
University of the Western Cape*

**WRC Report No. 2391/1/18
ISBN 978-1-4312-0009-5**

August 2018



Obtainable from

Water Research Commission
Private Bag X03
GEZINA, 0031

orders@wrc.org.za or download from www.wrc.org.za

DISCLAIMER

This report has been reviewed by the Water Research Commission (WRC) and approved for publication. Approval does not signify that the contents necessarily reflect the views and policies of the WRC nor does mention of trade names or commercial products constitute endorsement or recommendation for use.

Printed in the Republic of South Africa

© Water Research Commission

EXECUTIVE SUMMARY

BACKGROUND

Toxic metals are classified as inorganic pollutants. They are known to be recalcitrant pollutants in our natural environment. Toxic metal effluents are directly or indirectly discharged into the environment from industries such as metal plating facilities, mining operations, fertiliser plants, paper and other industries, tanneries, batteries, etc., especially in developing countries. South Africa has a rich diversity of mineral deposits and many of these minerals are either toxic themselves or associated with toxic elements. A large percentage of the available water in South Africa is used in mining and heavy industries for cooling, creating slurries, separation processes, etc. Mine dumps contain radioactive elements such as U-235 which are by-products in Au mining. These toxic metal ions dissolve easily and get washed into rivers and streams. Some industries even dump the untreated water directly into rivers and streams. The toxic metal ions of concern in this study are: Cr(VI) (carcinogenic), As(V)(lethal ground water contamination), Sr(II)(radioactive by-product in nuclear power plants), Cd(II)(6th most poisonous substance both for humans and animals), Hg(II)(most Hg compounds are extremely toxic and can result in a perpetual destructive cycle), U(VI)(radioactive and extremely toxic).

The aims of the project were:

- To characterise mine waters for a better understanding of their chemical composition.
- To quantify and identify the toxic elements and radionuclides and the form (isotopes) in which they exist for instance by using neutron activation analysis.
- To synthesise novel ligands for the selective extraction of radionuclides and toxic elements from mine water containing other metals ions.
- To design an ion exchange system that selectively removes radionuclides and toxic elements from mine water.

The purpose of this project was to develop a heterogeneous method that will look into the removal of toxic metals from mine water using ligands supported on suitable substrates. Initially the cost might be perceived as expensive, but the re-use of the ligands and the recovery of the metal ions may in the long term level the financial playing field.

Thus the overall aim of this research was to immobilise selective ligands on inorganic and organic supports, namely a variety of high surface area silicas or polymer nanofibres respectively, for toxic element removal from water through the adsorption process.

SUMMARY OF RESEARCH

The project has focused on three aspects, namely: the synthesis of selective ligands, the immobilisation of the ligands on silica/polymer supports and the applicability of the immobilised ligands for extraction of toxic metals.

The first section of the research focussed on inorganic silica supports for hosting selected ligands. Characterisation of the silica substrates was done using BET, low angle X-ray diffraction and FTIR. Of the chosen silica based supports, MCM-41 had the highest surface area, followed by SBA-15, Si gel (60 Å) and HMS. Although MCM-41 had the largest surface area, it was not the best support to use. HMS and Si gel (60 Å) had almost identical but small surface areas. Yet, Si gel (60 Å) was a better support to use than HMS, and also better than MCM-41. The least useful supports were SBA-15 and HMS. Extraction experiments with just the supports were conducted. The amount of metal ions extracted was below 2.5% and extraction can be considered to be zero. Hence, the silica supports by themselves offered no advantageous adsorption of metals.

Thereafter, two free parent ligands, 1,4,7-tris-[(S)-2-hydroxypropyl]-1,4,7-tri-azacyclodecane (THTD) and 1,4,8-tris-[(S)-2-hydroxypropyl]-1,4,8-tri-azacycloundecane (THTUD), were synthesised. These two ligands are less symmetric due to the carbon bridges between the nitrogen atoms, which differ in length. This gives the ligands the special feature that they can form five- and six membered rings during complexation with the metal ions. The ligands were fully characterised by NMR, mass spectrometry and elemental analysis. A spacer, 3-Glycidyoxypropyl-trimethoxysilane (glymo), was introduced to immobilise the ligands to the silica supports. Solid state NMR and FTIR analysis confirmed that the spacer could indeed be successfully immobilised on the various silica supports. The immobilised ligands were fully characterised with the use of solid state NMR and FTIR. The thermal stability of the immobilised ligands was determined by means of TGA. The immobilised ligands were thermally stable up to 200°C where after they started to disintegrate.

According to literature, 15-crown-5 and 18-crown-6 are suitable ligands for the extraction of Sr^{2+} and UO_2^{2+} . Since these ligands were to be immobilised, both (2-aminomethyl)-15-crown-5 and (2-aminomethyl)-18-crown-6 were used because of the amino group that can be used as an anchor

for immobilisation. The combinations of silica supported ligands explored were: 18-c-6 directly immobilised on the different silica supports, 18-c-6 immobilised with a glymo spacer on different silica supports, 15-c-5 directly immobilised on different silica supports, 15-c-5 immobilised with a glymo spacer on different silica supports, THTD, immobilised with a glymo spacer on different silica supports, THTUD, immobilised with a glymo spacer on different silica supports. To immobilise these ligands onto the activated silica substrates, two methods were used: 1) direct immobilisation onto the substrate by using the amino groups at the end of the carbon arm, and 2) by means of the glymo spacer which connects the (2-aminomethyl)-15-crown-5 and (2-aminomethyl)-18-crown-6 to the silica substrates. The immobilisation was confirmed and the ligand-substrate moiety fully characterised by solid state NMR and FTIR. The thermal stability of the immobilised crown ethers was determined by means of TGA as stable up to 200°C where after they disintegrated.

Metals that were extracted using these materials included As^{5+} , Cd^{2+} , $\text{H}_x\text{Cr}_y\text{O}_z^{-n}$, Sr^{2+} , Hg^{2+} and UO_2^{2+} . Extraction experiments were conducted at 25°C and atmospheric pressure. The extractions were done at pH values of 4.5 and 5.9. The extraction capacity of the immobilised ligands was determined by ICP analysis. As expected, the extraction done at pH 5.9 was significantly better than at pH 4.5.

Arsenic is present in aqueous solutions as two species: as HAsO_4^{2-} or H_2AsO_4^- . The average extraction of H_nAsO^x at a pH of 4.5 with the various ligands immobilised on any of the four supports were less than 2.5% and was therefore considered to be zero. Even with the pH raised to 5.9, the average arsenic extraction with the ligands immobilised on the various supports remained less than 2.5%.

The average extraction of Cd^{2+} at a pH of 4.5 with the various ligands immobilised on Si gel (60 Å), was less than 2.5%. Although THTD showed some extraction with Cd^{2+} , it was still less than 2.5% and is therefore considered to have zero extraction with Cd^{2+} . The other ligands did not extract any Cd^{2+} at all. With the pH raised to 5.9, the average extraction using the immobilised ligands on Si gel (60 Å) increased to 15.2% (ligands are 45% effective). With the exception of 18-c-6 and 15-c-5 with glymo, the other ligands could all be used in the extraction. The only support that failed to extract any of the Cd^{2+} was HMS. The ligands on this support showed no extraction at all. At the higher pH of 5.9, the average extraction of Cd^{2+} increased significantly for the various supports with the exception of HMS. It appears that extraction with THTD, although slightly lower than the crown ether, is more selective towards Cd^{2+} at both pH values since it showed

extraction with all the supports except with HMS, while the crown ethers only extracted Cd^{2+} when supported on Si gel (60 Å) and SBA-15.

Chromium is normally found as one of the following species: $\text{Cr}_2\text{O}_7^{2-}$, CrO_4^{2-} or HCrO_4^- . It appears that the ligands have the right configuration to accommodate the metal ions. The extraction was carried out in an acidic medium, which means that the ligands were partially protonated. The ligands could be positively charged and thus coordinate the negatively charged chromium species. With the solution buffered at 4.5, the average extraction of chromium for the different ligands, immobilised on Si gel (60 Å) were 11.7% (ligands are 34% effective), of which THTD (21.4-64% effective) and THTUD (23.9-90% effective) were the best performing ligands. With the pH raised to 5.9, the average extraction increased dramatically, as expected, to 25.8%. The THTD (33.8-90%) and THTUD (33.7-95%) were again the most effective ligands to use. With the pH at 4.5, MCM-41 was the least effective support to use. SBA-15 and HMS were almost the same with an average extraction of $\pm 10\%$ (ligands are 40% effective). THTD was the best ligand to use. With the pH at 5.9, even the other supports showed a dramatic increase in the extraction capabilities with the various ligands. THTD again proved the most selective ligand of the “six” to use when extracting $\text{H}_x\text{Cr}_y\text{O}_z^{-n}$. With the Si gel (60 Å), it is interesting to note that the extraction increased as the length of the spacer increased. With the MCM-41 and SBA-15, the extraction stayed almost constant, but there was a slight decline when HMS was used as a support. 15-c-5 was the least effective ligand with an average extraction of 18.7% (52% effective). THTD performed the best on all supports and it had an average extraction capability of 33.1% (90% effective). 18-c-6 immobilised with glymo and THTUD were very similar to each other with an average extraction of $\pm 25\%$. $\text{H}_x\text{Cr}_y\text{O}_z^{-n}$ is known as a hard acid, and the ligands that were used contain hard oxygen and borderline/hard nitrogen donors. Therefore it is quite a reasonable assumption that the hard donors and the hard acid will complex very well in the case of $\text{H}_x\text{Cr}_y\text{O}_z^{-n}$. It does not look like the different surface areas of the silica supports had any influence on the working of the ligands because with the higher pH, the extraction was also high in the case of $\text{H}_x\text{Cr}_y\text{O}_z^{-n}$. The only factor that had a profound influence on the degree of extraction was the difference in the pH.

In the case of Sr^{2+} , with the pH at 4.5, it was found that no Sr^{2+} was extracted with any of the ligands immobilised on any of the supports. There was an improvement in the extraction when the pH was increased to 5.9. The average extraction of Sr^{2+} with all the ligands immobilised on Si gel (60 Å) was 10.0% (ligands are 30% effective) and with MCM-41 as a support the average extraction was 9.0% (ligands are 27% effective). The extraction of Sr^{2+} with SBA-15 as support

was less than 1%. The best extraction was obtained using the crown ethers. The 15-c-5 immobilised with the glymo spacer on Si gel (60 Å) gave an extraction of 25.4% (ligand is 75% effective) while 18-c-6 immobilised with the glymo spacer on MCM-41 yielded 24.5%. With the exception of 18-c-6 immobilised directly on HMS (30.2%), it is clear that the better extraction of Sr²⁺ was obtained as the spacer was introduced. THTD and THTUD did not perform as well with the extraction of the Sr²⁺, as was expected. There is an unusual occurrence with the THTD and THTUD immobilised on MCM-41. The nitrogen donating ligands performed better than the crown ethers with the exception of 18-c-6 immobilised with the glymo to the support. It was found that the best average extraction was obtained by using the 18-c-6 ligand (11.0%) and the best support is the Si gel (60 Å). The 15-c-5 and 18-c-6 ligands that were immobilised with the glymo spacer yielded an average extraction of 9.3% and 9.3% respectively.

No extraction of Hg²⁺ occurred at a pH of 5.9 when using any of the ligands in any combination with the supports. Since no extraction was possible at the higher pH, it was decided not to do the extraction at pH 4.5.

The average extraction of U(VI) for the different ligands on the various supports ranged between 13% and 16.5%. HMS was the best support (16.5%) and MCM-41 was the worst (13%). All the ligands showed extraction with the uranyl. The best ligand for the extraction was 15-c-5 (17.5% - ligand is 50% effective) which was directly immobilised on the supports. The second best was the 18-c-6 (15.0%), also directly immobilised on the supports. When the spacer was introduced, the extraction of the uranyl decreased. This trend was observed for the crown ethers on all the supports. The chelator orientation about the uranyl strongly depends on the length of the spacer and it was found that ligands that were immobilised with short flexible spacers coordinated better to the uranyl than the same ligand with a longer spacer. The best extraction was achieved with 15-c-5 (25.7% - ligand is 70% effective), immobilised directly on HMS.

For the silica supported ligands, it is evident that a better extraction was achieved at a higher pH. In this particular study, a pH-value of 5.9 was obtained as optimum. The reason may well be because the ligands are less protonated at the higher pH. This leaves the cavity, as well as the donating atoms exposed and complexation can take place.

MCM-41 had the highest surface area (1020.0 m²/g), followed by SBA-15 (758.0 m²/g), Si-gel 60 Å (469.0 m²/g) and HMS (466.1 m²/g). When comparing the capacities of the ligands supported on different silica supports, it was found that Si gel (60 Å) was the most effective support to use. It did not always have the highest yields, but in all the extraction experiments, some

extraction was obtained when Si gel (60 Å) was used as the support. A reason for this result may be because of the more favourable BET results concerning the surface area of Si gel (60 Å). It would appear that the surface area, pore volume and pore diameters distribute the immobilised ligands more evenly. The area of the Si gel (60 Å) was thus more accessible and can be modified more easily. MCM-41 is also a suitable support to use, but it is very expensive, even more than Si gel (60 Å) and the pore openings are very small which might prevent the ligands and metal ions entering. This could lead to crowding of the ligands on the surface of MCM-41 which in turn leads to less contact area for the metal ions. SBA-15 and HMS showed the least effective results as supports with all of the ligands. Their BET results showed that the usable surface areas were much smaller than that of Si gel (60 Å) or that of MCM-41. The two Si supports that yielded the best results with the immobilised ligands in the competitive extraction with four metal ions were Si gel (60 Å) and HMS. The slight decline in the extraction capacities can be attributed to the amount of metal ions that were introduced to the solution. In this instance, it could be a matter of “first come first served”. Once a metal ion is complexed to the ligand, there is little chance that another metal will replace it.

In summary there was no affinity for As^{5+} or Hg^{2+} at either low or high pH levels. There was slight selectivity for Cd^{2+} extraction by 18-c-6, THTD and THTUD. Cr^{6+} was selectively extracted by all the ligands, independent of the support that was used. Sr^{2+} was selectively extracted by 15-c-5 and to a lesser extent by 18-c-6. Uranyl showed the same preferential affinity towards 18-c-6 and 15-c-5. It was shown that the extraction increased for the same ligands as soon as a spacer was introduced except for the extraction of the uranyl. This was because the metal ions could come into better contact with the ligands because the ligands had more flexibility to move about in the solution, and thus there was less impact from low surface area supports.

Better extraction was achieved at a higher pH, in this particular study, a pH-value of 5.9, compared to 4.5. There is competition between the protons and the metal ion for the ligand. Protonation constants were determined for the free ligands, however, when the ligands are attached (via spacers) to the supports, the protonation constants could be different, because electronically, the immobilised ligands are now different from the free ligands. For coordination of the ligand to the metal ion to take place, the ligand and/or the metal ion must be deprotonated. As the solution became more basic, the metal ions could form hydroxide complexes because of the excess OH^- .

It is proposed that there are a number of H-bonds that keep the crown ethers attached to the silica support. It seems like there is hydrogen bond interactions between the protons of the amine group and the oxygen atoms of the silanol groups. There are in all probability also hydrogen bond

interactions between the lone pair of electrons on the nitrogen of the amine group and the protons of the silanol groups of the silica supports.

It should be noted that regeneration was impossible as the Si supports lost their ligands when being regenerated. The regeneration tests of the ligands required HNO_3 of a particular concentration so as to only release metal ions from the ligand and not to hydrolyse the ligand from the substrate. This aspect was not covered in this part of the study because low pH's reprotonated the ligand and at pH 2 hydrolysis of the ligand from the substrate occurred. Therefore, the reusability of these materials was in doubt.

For this reason further investigations were performed on promising polymer based functionalised nanofiber mats.

Polyacrylonitrile (PAN) was electrospun into nanofibres in dimethyl formamide (DMF) via electrospinning process. The average fibre diameters for polyacrylonitrile nanofibres (PAN-nfs) at optimum concentrations of 8 wt% (PAN) as measured from the HRSEM images were 354 ± 40 nm. 2-pyridine amidoxime (PyAMI) was synthesised through the reaction between 2-pyridine carbonitrile and hydroxylamine hydrochloride and characterised using NMR, FTIR and TGA techniques.

Subsequently, PyAMI was immobilised on PAN-nfs surfaces via two reaction pathways; the base-catalysed immobilisation reaction using NaOH and the acid-catalysed immobilisation reaction using $\text{AlCl}_3 \cdot 6\text{H}_2\text{O}$. A preliminary characterisation of the products from the two reaction pathways using HRSEM showed that the PAN polymer nanofibres surfaces were smooth in the acid-catalysed pathway but disintegrated in the base-catalysed reaction pathway. Therefore the base-catalysed immobilisation reaction pathway was discontinued. The acid-catalysed immobilisation reaction pathway was used to fabricate PAN-PyAMI (PyAMI immobilised on PAN-nfs). The synthesised ligand, PyAMI was characterised using the NMR technique and the resultant PAN-PyAMI was characterised using HRSEM after the immobilisation reaction. The resultant PAN-PyAMI was further characterised using ATR-FTIR and TGA analysis. The ATR-FTIR spectrum of PAN-PyAMI showed that PyAMI was immobilised on PAN-nfs at an optimum reaction time of 60 minutes at 60°C with the presence of peaks such as 1654 cm^{-1} (C=N), 1605 cm^{-1} (N-H bending vibration) and 968 cm^{-1} (N-O) which are attributed to the peaks of PyAMI. The peak in the range of $3181\text{-}3030\text{ cm}^{-1}$ was also assigned to CH stretching of the pyridine ring. A peak at 1145 cm^{-1} (C-O) was also assigned to the new bond formed. The TGA results showed that PAN-PyAMI started losing volatiles at a temperature of around 240°C (instead of 270°C for pristine

PAN-nfs) due to the loss of organic ligands on the nanofibres. The acid stability of PAN-PyAMI was tested in different pH solutions and it was found according to ATR-FTIR spectra that the ligand was stable on the PAN support at pH higher than 4.5 and less stable at pH lower than 4.5. Moreover, 0.1 M HNO₃ and 0.1 M EDTA were used to test for the stability of the ligand-PyAMI upon PAN. The ATR-FTIR results after the stability tests showed that PAN-PyAMI could be regenerated using 0.1 M EDTA, as all the peaks attributed to PyAMI was retained but disappeared with 0.1 HNO₃.

Thereafter, the functionalised PAN-PyAMI mats were used to remove Pb²⁺ or Sr²⁺ from simulated water. PAN-PyAMI and the pristine PAN-nfs were used for adsorption of Pb²⁺ in batch experiment by investigating the effect of initial pH, initial concentration, and the contact time. The effect of initial pH played the most important role in adsorption of Pb²⁺ as the removal was greatly increased as pH increased. The results showed that PAN-PyAMI could adsorb Pb²⁺ far better than the PAN-nfs at the same conditions (0.1 g weight of adsorbent, pH 4.9, concentration 200 mg/L and contact time 60 minutes, at 25°C). The maximum adsorption capacity of PAN-PyAMI for Pb²⁺ was 4.70 mg/g (or 22.5%), while PAN-nfs gave 1.37 mg/g (or 8%). Meanwhile, the adsorption capacity of PAN-PyAMI decreased as the pH increased further from 4.9 to 6.1. This was due to the formation of hydrated lead (II) ions at a pH above 4.9 resulting in the decreased binding capability of Pb²⁺. At a Pb²⁺ concentration of 150 mg/L, the equilibrium capacity of PAN-PyAMI of 3.17 mg/g (21%) was achieved. The experimental data were fitted with the Langmuir isotherm, indicating that the monolayer adsorption of Pb²⁺ occurred on the homogenous surface of PAN-PyAMI. The rate of adsorption of Pb²⁺ on PAN-PyAMI increased steadily from 10 to 60 minutes and the kinetic rate was best described as pseudo second-order. The adsorption capacity of Pb²⁺ at equilibrium time (80 minutes) was calculated to be 3.29 mg/g, (34%). PAN-PyAMI was then used to selectively remove Pb²⁺ from a simulated solution containing both Pb²⁺ and Sr²⁺. The selectivity of PAN-PyAMI was conducted as batch adsorption experiments at the optimum conditions of Pb²⁺ adsorption. At the optimum conditions, PAN-PyAMI was selective for Pb²⁺ as it could remove significantly more Pb²⁺ than Sr²⁺ from separate aqueous test solutions and PAN-PyAMI was fairly selective for Pb²⁺ in the presence of Sr²⁺ in the same aqueous solution. To check for the factor responsible for the disparity in the adsorption capacities of PAN-PyAMI for Pb²⁺ and Sr²⁺, the effect of solution pH was performed on the adsorption of Sr²⁺ using PAN-PyAMI. The maximum adsorption capacity of PAN-PyAMI for Sr²⁺ was 2.28 mg/g at pH 6.1, whereas, for Pb²⁺, it was 4.70 mg/g at pH 4.9. This implies that at the optimum pH for adsorption of Pb²⁺, PAN-PyAMI will perform poorly for the adsorption of Sr²⁺, which allows selective extraction via process conditions.

After use, PAN-PyAMI was regenerated using EDTA but could not be regenerated using HNO_3 . 1 M EDTA gave the highest Pb^{2+} desorption of 95% (4.92 mg/g) out of 5.16 mg/g previously adsorbed. 0.1 M EDTA desorbed 89% (4.85 mg/g) out of 5.44 mg/g while 0.01 M EDTA gave the lowest result, desorbing 25% (1.31 mg/g) out of 5.10 mg/g previously adsorbed on PAN-PyAMI. However, after Pb^{2+} desorption using 1 M EDTA, PAN-PyAMI became brittle and could no longer be re-used. Therefore PAN-PyAMI was regenerated using 0.1 M EDTA after each adsorption experiment and was subsequently reused for 4 times. For the first cycle, out of 5.65 mg/g previously adsorbed by PAN-PyAMI, 4.54 mg/g, (80%) was desorbed. Thereafter, for the Pb^{2+} adsorption cycles with PAN-PyAMI, 85%, 84% and 59% desorption was achieved for second, third and fourth desorption cycles respectively. SEM-EDS and SEM-EDS mapping were used to check the availability of Pb^{2+} on PAN-PyAMI after the 1st and the 4th adsorption cycles and it was lower, thus Pb^{2+} was not irreversibly adsorbed. Therefore reduction in adsorption capacity could be attributed to the reduction in active adsorption sites as a result of loss of ligands on PAN-PyAMI. The ATR-FTIR after every regeneration showed that the ligand peaks on PAN-PyAMI were gradually eroding and that only 4 regeneration cycles could be done on PAN-PyAMI.

RECOMMENDATIONS

This study has opened another avenue for removal and separation of toxic metals; therefore, further research should be carried on the immobilisation of ligands on silica and nanofibres for selective adsorption and metal separation purposes.

In the case of the inorganic supports, two novel ligands were synthesised and separately two crown ether derivatives were all immobilised onto four different silica supports. These immobilised ligand systems were used to extract six different toxic metal and metalloid ions in water. The extraction capacities of the different immobilised ligands were compared so as to determine whether the substrates had any influence on the extraction capabilities of these ligands and it was shown that both the support and the type of ligand impacted upon the selectivity and removal capacity. These fundamental findings could be used for the further development of stable and selective adsorbents. The recovery of metals from the immobilised ligands was attempted by re-protonating the ligands so as to displace the metal ions, but the ligand-support bond was not stable thus would need further consideration.

This research is also reporting for the first time the fabrication of a combination of nanofibres prepared via electrospinning process followed by the immobilisation of a selective ligand on the

nanofibers, namely 2-pyridine amidoxime (PyAMI) which was synthesised through the reaction between 2-pyridine carbonitrile and hydroxylamine hydrochloride. Electrospun PAN-nfs was used as support for PyAMI ligands to produce new adsorptive, PAN-PyAMI in non-woven mat format. The nanofibres have shown potential in adsorption of specific toxic metal contaminants from water and the nanofiber mats could be regenerated. However, the stability of the ligand bond to the polymer should be looked into in order to overcome the instability in acids, which limits the cycles of reuse. This research has been able to contribute new knowledge to the use of nanofibres as supports. The immobilisation of 2-pyridine amidoxime on nanofibres has not been previously studied.

OUTPUTS

Four articles and two PhD theses have been published from this project and are listed below:

Articles/thesis from the report:

1. Bode-Aluko, C.A., Perea, O., Ndayambaje, G. and Petrik, L. (2017). Adsorption of toxic metals on modified polyacrylonitrile nanofibres: A Review, *Water, Air, & Soil Pollution*, 228: 35, DOI: 10.1007/s11270-016-3222-3.
2. Bode-Aluko, C.A., Perea, O., Fatoba, O. and Petrik, L. (2017). Surface-modified polyacrylonitrile nanofibres as supports, *Polymer Bulletin*, Vol. 74, pp. 2431-2442, DOI: 10.1007/s00289-016-1830-0.
3. Perea, O. K., Bode-Aluko, C., Ndayambaje, G., Fatoba O. and Petrik, L.F. (2017). Electrospinning: Polymer nanofibres adsorbent applications for metal ion removal, *Journal of Polymers and the Environment*, DOI: 10.1007/s10924-016-0896-y.
4. Bernardus Francis Barnard. 2014. The Synthesis of Selective Immobilized Ligands for the Extraction of Toxic Metal Ions from Water Doped with these Contaminants. Unpublished PhD thesis, University of Stellenbosch
5. Chris Ademola Bode-Aluko. 2017. Functionalisation of Polymer Nanofibres and Track-Etched Membrane for Removal of Organic and Inorganic Pollutants from Water. Unpublished PhD thesis, University of the Western Cape

Article related to the report:

6. Ndayambaje, G., Laatikainen, K., Laatikainen, M., Beukes, E., Fatoba, O., Van der Walt, N., Petrik, L. and Sainio, T. (2016). Adsorption of nickel(II) on polyacrylonitrile nanofiber modified with 2-(20-pyridyl)imidazole, *Chemical Engineering Journal*, Vol. 284, pp. 1106-1116.

ACKNOWLEDGEMENTS

The project team wishes to thank the following people for their contributions to the project.

Reference Group	Affiliation
Dr Jo Burgess	Water Research Commission (Chairperson)
Dr R Luckay	Stellenbosch University
Mr Terry Harck	Solution H Plus
Prof. B Pletschke	Rhodes University
Dr E Beukes	University of the Western Cape

TABLE OF CONTENTS

EXECUTIVE SUMMARY	iii
Background	iii
Summary of Research.....	iv
Recommendations	xi
Outputs	xii
ACKNOWLEDGEMENTS	xiv
1 INTRODUCTION.....	1
2 LITERATURE REVIEW	3
2.1 Water pollution.....	3
2.2 Potential water pollutants from industrial wastewaters	4
2.2.1 Chromium.....	4
2.2.2 Arsenic.....	4
2.2.3 Strontium.....	5
2.2.4 Cadmium.....	5
2.2.5 Mercury	5
2.2.6 Uranium.....	6
2.3 Water treatment technologies.....	6
2.4 Immobilised ligands	8
2.5 Polymer as an Immobilisation Substrate	16
2.6 Silica as an Immobilisation Substrate	17
3 Synthesis and Immobilisation of Ligand on Silica support	19
3.1 Experimental procedure of the preparation of THTD and THTUD.....	19
3.1.1 Protection of the amines by means of tosylation.....	19
3.1.2 Protection of the diol by means of tosylation	20
3.1.3 Preparation of the tosylated triamine disodiumsalt (diethylenetriamine and the bis-(3-aminopropyl)-amine)	20
3.1.4 Synthesis of the macrocycles	20
3.1.5 The addition of the pendant arms.....	21
3.2 Characterization of THTH and THTUD.....	21
3.2.1 NMR spectra of THTD	21
3.2.2 NMR spectra of THTUD	23
3.3 Immobilisation of THTD and THTUD Ligands on Silica substrate.....	25
3.3.1 Silica gel (60 Å) (Si gel).....	25

3.3.2	Mobil composition of matter (MCM-41)	25
3.3.3	Santa Barbara armophous (SBA-15)	25
3.3.4	Hexagonal mesoporous silica (HMS).....	25
3.4	Results and Discussion for Immobilisation experiment	26
3.4.1	Fourier transform infra red (FTIR) spectra.....	26
3.4.2	NMR.....	28
3.4.3	Brunauer-Emmett-Teller (BET) results.....	32
3.5	Extraction of Toxic Elements using Silica supported ligands	34
3.5.1	Results and Discussion.....	35
3.6	Conclusions.....	58
4	Synthesis of ligand and immobilisation on polymer nanofibers	59
4.1	Electrospinning process	59
4.1.1	Electrospinning of PAN solution	59
4.2	Synthesis of 2-pyridine amidoxime (PyAMI).....	60
4.3	Immobilisation of 2-pyridine amidoxime on PAN-nfs (PAN-PyAMI).....	60
4.3.1	Acid-catalysed immobilisation of PyAMI on PAN-nfs	62
4.3.2	Stability of PAN-PyAMI in EDTA & HNO ₃ solutions.....	63
4.4	Results and discussion	63
4.4.1	Polyacrylonitrile nanofibres (PAN-nfs)	63
4.4.2	(High resonance scanning electron microscope (HRSEM) of PAN-nfs	63
4.4.3	Attenuated total reflectance-FTIR of PAN-nfs	68
4.4.4	TGA profile of PAN-nfs	69
4.4.5	Characterisation of PyAMI and PAN-PyAMI	69
4.4.6	Preparation of PAN-PyAMI.....	72
4.5	Extraction of metals using polymer supported ligand.....	75
4.5.1	Adsorption experiments.....	75
4.5.2	Effect of solution pH.....	76
4.5.3	The effect of initial concentration.....	78
4.5.4	The effect of contact time.....	80
4.5.5	Desorption and reusability experiments	81
4.5.6	Competitive adsorption.....	86
5	Conclusions.....	89
6	References	91

LIST OF FIGURES

Figure 2.1: The chemical structure of TPEN.	10
Figure 2.2: Examples of natural biological macrocycles: a) the porphyrin ring of the haem-protein, b) the chlorin ring of chlorophyll and c) the corrin ring of vitamin B12 (Constable, 1999).	12
Figure 2.3: Examples of synthetic macrocycles: phthalocyanine (a) which can be used as semi-conductors, catalysts or colouring agents and natural antibiotics such as nonactin (b) and valinomycin (c) (Constable, 1999)	13
Figure 2.4: Reaction of nitrile and hydroxylamine to produce amidoxime group.....	15
Figure 2.5: Amidoxime and imidazole groups for extraction of UO_2^{2+}	15
Figure 2.6: A chelating molecule that is directly immobilised on the silica surface will produce steric hindrances at the silanol site	18
Figure 3.1: The FTIR spectrum of the direct immobilisation of 18-c-6 on silica gel. This spectrum is representative of 15-c-5 and 18-c-6 on all four supports.	26
Figure 3.2: The FTIR spectrum of 15-c-5 on silica gel 60 Å by means of the glymo spacer. This spectrum is representative of 15-c-5 and 18-c-6 on all four supports.	27
Figure 3.3: The FTIR spectrum of THPTD immobilised by the glymo spacer on silica gel (60 Å).....	28
Figure 3.4: The solid state ^{13}C NMR spectrum of 18-c-6 directly immobilised on a silica support. This spectrum is also representative of 15-c-5 immobilised directly onto the silica support.....	29
Figure 3.5: The solid state NMR spectrum shows the direct immobilisation of the crown ethers on the silica supports. This spectrum is representative of both crown ethers immobilised on all four supports.....	29
Figure 3.6: The spectrum is a representation of the immobilised glymo spacer on the silica.	30
Figure 3.7: The solid state spectrum ^{13}C -NMR is representative of the immobilisation of the crown ethers onto the silica supports by means of the glymo spacer.	31
Figure 3.8: The solid state ^{13}C NMR spectrum is representative of the immobilisation via the glymo spacer, of the aza-crown ethers onto the silica supports.....	31
Figure 3.9: The extraction of As(V) with various ligands immobilised on four different silica supports	36
Figure 3.10: The extraction of Cd(II) with various ligands immobilised on four different Si supports.....	39

Figure 3.11: The extraction of Cr(VI) with various ligands immobilised on four different Si supports.....	41
Figure 3.12: The extraction of Sr(II) with various ligands immobilised on four different Si supports.....	43
Figure 3.13: The extraction of UO_2^{2+} with various ligands immobilised on four different Si supports.....	45
Figure 3.14: The extraction of 2 metal ions with various ligands immobilised on four different Si supports	47
Figure 3.15: The extraction of metal ions with various ligands immobilised on four different Si supports.	49
Figure 3.16: The extraction of various metal ions with 15-c-5, directly immobilised on different silica supports.	50
Figure 3.17: The extraction of various metal ions with 18-c-6, directly immobilized on different silica supports.	51
Figure 3.18: The extraction of various metal ions with 15-c-5, immobilised with a glymo spacer on different silica supports.	52
Figure 3.19: The extraction of various metal ions with 18-c-6, immobilised with a glymo spacer on different supports.....	53
Figure 3.20: The extraction of various metal ions with THTD, immobilised with a glymo spacer on different silica supports.	54
Figure 3.21: The extraction of various metal ions with THTUD, immobilised with a glymo spacer on different silica supports.	55
Figure 3.22: Structures of the neutral, free ligands, THTD and THTUD.	57
Figure 4.1: Electrospinning set-up.	59
Figure 4.2: Brønsted acidity of $AlCl_3 \cdot 6H_2O$	61
Figure 4.3: Formation of carbocation on PAN-nfs in acidic medium.	61
Figure 4.4: Reaction of PyAMI using nitrogen with PAN-nfs from Figure 3.3.	61
Figure 4.5: Reaction of PyAMI using oxygen with PAN-nfs from Figure 3.3.	62
Figure 4.6: De-protonation of PyAMI on the hydroxide.	62
Figure 4.7: Reaction of PyAMI from Figure 3.6 with PAN-nfs.	62
Figure 4.8: HRSEM images of PAN-nfs at different concentrations in dimethyl formamide.	65
Figure 4.9: HRSEM images of PAN-nfs at (a) 10 wt% and (b) 12 wt% concentrations in dimethyl formamide.....	65

Figure 4.10: The relationship between the average fibre diameters of PAN-nfs and the polymer concentration.	66
Figure 4.11: Fibre diameter distributions of PAN-nfs at different concentrations in dimethyl formamide.	67
Figure 4.12: ATR-FITIR of 8 wt% PAN-nfs and PAN powder.	68
Figure 4.13: TGA profile of 8 wt% PAN-nfs under nitrogen.	69
Figure 4.14: ATR-FITIR spectrum of synthesised PyAMI.	71
Figure 4.15: TGA profile of PyAMI under nitrogen.	71
Figure 4.16: ATR-FITIR spectra of acid-catalysed immobilisation of PyAMI on PAN-nfs as function of reaction time.	72
Figure 4.17: HRSEM images of (a) pristine PAN-nfs (b) PAN-PyAMI 20 mins (c) PAN-PyAMI 40 mins and (d) PAN-PyAMI 60 mins.	73
Figure 4.18: Thermal profile of pristine PAN-nfs and PAN-PyAMI under nitrogen.	74
Figure 4.19: ATR-FITIR spectra of PAN-PyAMI showing regeneration studies in EDTA or HNO ₃	75
Figure 4.20: Effect of initial pH on quantity adsorbed of Pb ²⁺ (initial concentration; 200 mg/L, weight of adsorbent; 0.1 g, contact time; 1 hour).	76
Figure 4.21: Effect of initial pH on the percentage adsorption of Pb ²⁺ by PAN-PyAMI and PAN-nfs (initial concentration; 200 mg/L, weight of adsorbent; 0.1 g, contact time; 1 hour).	77
Figure 4.22: Effect of initial concentration on quantity adsorbed of Pb ²⁺ on PAN-PyAMI at pH; 4.9, weight of adsorbent; 0.1 g, contact time; 1 hour.	79
Figure 4.23: Effect of initial concentration on percentage adsorption of Pb ²⁺ on PAN-PyAMI at pH; 4.9, weight of adsorbent; 0.1 g, contact time; 1 hour.	79
Figure 4.24: Effect of contact time on quantity of Pb ²⁺ adsorbed using PAN-PyAMI (initial concentration; 200 mg/L, weight of adsorbent; 0.1 g, initial pH; 4.9).....	80
Figure 4.25: Effect of contact time on percentage adsorption of Pb ²⁺ using PAN-PyAMI (initial concentration; 200 mg/L, weight of adsorbent; 0.1 g, initial pH; 4.9).....	81
Figure 4.26: Regeneration of 0.1 g PAN-PyAMI loaded with Pb ²⁺ using different concentrations of EDTA.	82
Figure 4.27: Desorption and reusability test of PAN-PyAMI on Pb ²⁺ (initial concentration 200 mg/L, weight of adsorbent; 0.1 g, initial pH; 4.9, contact time; 1 hour, 0.1 M EDTA)...	83

Figure 4.28: Percentage desorption of Pb^{2+} adsorbed onto PAN-PyAMI with respect to number of cycles using 0.1 M EDTA (initial concentration 200 mg/L, weight of adsorbent; 0.1 g, contact time; 1 hour).	83
Figure 4.29: SEM-EDS {(a) PAN-PyAMI after 1st adsorption cycle of Pb^{2+} and (b) PAN-PyAMI after 4th adsorption cycle of Pb^{2+} } and (c) SEM-EDS mapping of PAN-PyAMI after 1st adsorption cycle of Pb^{2+}	84
Figure 4.30: ATR-FTIR spectra of regenerated PAN-PyAMI using 0.1 M EDTA.	85
Figure 4.31: Selectivity test of PAN-PyAMI for separating Pb^{2+} and Sr^{2+} in solution (Weight of adsorbent; 0.1 g, pH; 4.9, contact time 1 hour,).....	87
Figure 4.32: Percentage Pb^{2+}/Sr^{2+} adsorbed onto PAN-PyAMI (Weight of adsorbent; 0.1 g , pH; 4.9, contact time; 1 hour).	87
Figure 4.33: Effect of initial pH on the adsorption of Pb^{2+} and Sr^{2+} on PAN-PyAMI (Initial concentration; 200 mg/L, weight of adsorbent; 0.1 g, contact time; 1 hour).....	88

LIST OF TABLES

Table 3.1: ^1H and ^{13}C NMR of the 1,4,7-tris[2(S)-hydroxypropyl]-1,4,7-triazacyclodecane.....	22
Table 3.2: ^{13}C NMR data of the 1,4,8-tris[2-(S)-hydroxypropyl]-1,4,8-triazacycloundecane.	24
Table 3.3: The surface areas of Si-gel 60 Å and MCM-41	32
Table 3.4: The surface areas of SBA-15 and HMS	32
Table 3.5: The average size of the pore diameters and average pore volumes for MCM- 41 and Si-gel (60 Å) are shown in the table below.	33
Table 3.6: The average size of the pore diameters and average pore volumes for HMS and SBA-15 are shown in the table below.	33
Table 3.7: The average pore diameter for Si-gel 60 Å and MCM-41 was determined by BET and is shown in the table below.	33
Table 3.8: The average pore diameter for HMS and SBA-15 was determined by BET and is shown in the table below.	33
Table 3.9: The metal salts that were used for the preparation of the different solutions.	34
Table 3.10: The comparison between the stability constants ($\log K$) of THPTD, THPTUD, [10]-ane-N ₃ , THETAC and TETA are shown (Barnard, 2008)	37
Table 3.11: The pK _a values of the two free azamacrocyclic ligands are shown (Barnard, 2008) .	37
Table 3.12: The $\log(K)$ values of ligands with similar structures to THPTD and THPTUD.	57
Table 4.1: Assignment of NMR spectra of PyAMI.	70

This page was deliberately left blank

1 INTRODUCTION

Contamination of water by toxic metals has steadily increased over the last decades as a result of over population and expansion of industrial activities (Barakat, 2011). Toxic metals could also originate from natural sources (contaminations from the bedrock) or from anthropogenic sources. The anthropogenic source of toxic metals in the soil and water can be as a result of mining activities, smelting and aerosol deposition (Fu and Wang, 2011). The source can also be an outcome of working on the soil such as the application of fertiliser (agriculturally induced), which can in turn pollute the soil and water bodies close by (Topolska et al., 2004). Mining is arguably the largest anthropogenic source of toxic metal contamination into the environment (Tutu et al., 2008). Geochemical processes acting upon mining wastes initiate the process of transporting toxic metals from contaminated areas and redistributing them to the surrounding soils, streams and groundwater (Yin, 2010). Toxic metals in their aqueous solutions behave the same way in the natural aquatic environment (Akçay et al., 2003). They can be transported via sorption, dissolution and precipitation and can even form complexes with organic molecules present in the water. Toxic metals also respond to changes in physicochemical variables such as pH, redox conditions or ionic strength and hydrodynamic effects (which are responsible for sediment transportations) (Akçay et al., 2003). Because of their high solubility in the aquatic environments, toxic metals can be absorbed by living organisms either by direct intake or through the food chain (Islam et al., 2015). Once they find their way into the food chain, these toxic metals may accumulate in certain organs of the human body and if the metals are ingested beyond the permitted concentration, they can cause serious health problems such as poisoning and cancer (Islam et al., 2015; Meena et al., 2008). Therefore, it is necessary to treat metal contaminated wastewater prior to its discharge to the environment; at least this will substantially reduce the discharge from human activities to the environment.

As mentioned, several techniques have been used to remove toxic metals from contaminated water. These techniques include; ion-exchange, chemical precipitation, coagulation-flocculation, flotation, membrane filtration, electrochemical treatment, reverse osmosis and adsorption (Fu and Wang, 2011; Kurniawan et al., 2006). Among these techniques, adsorption is arguably the simplest and most effective technique and its efficacy largely depends on the fabrication of high capacity adsorbents (Fu and Wang, 2011). Adsorption has been used to remove toxic metal ions from various aqueous solutions even at low concentrations (Bode-Aluko et al., 2017a; 2017b; Perea et al., 2016). The performance of these adsorbents largely depends on their physical and chemical properties. It is noteworthy that adsorption is a surface phenomenon and therefore the efficiency

of adsorbents largely depends on their ability to adsorb metal ions from solution onto their surfaces in order to remove the metal ions from the solution. However, the purpose of adsorption is not to permanently keep the metal ions (chemisorption) on the adsorbents, since adsorbents should be able to release the metals afterwards (physisorption). This is important for the purpose of recovery of metals and regeneration of adsorbents (Eldridge et al., 2015; Hong et al., 2015; Kampalanonwat and Supaphol, 2014).

In recent years, the use of chelating agents for the selective extraction and concentration of toxic metal ions has been on the rise especially from dilute industrial wastewaters (Ndayambaje et al., 2016; Nilchi et al., 2008a; Bilba et al., 1998). The selectivity of an adsorbent could be used to separate different metals in the same solution (Nilchi et al., 2008b; Bilba et al., 1998). This has led researchers to grafting chelating ligands on hydrophilic supports for extraction of metal ions in a solid-liquid system (Ndayambaje et al., 2016; Nilchi et al., 2008a; Jal et al., 2004). The supports can be organic (polymer, resins, fibres) or inorganic materials (silica gel) (Ndayambaje et al., 2016; Jal et al., 2004; Bilba et al., 1998). The surface of adsorbents can either be chemically activated through direct reactions or can serve as a support for the chelating ligands (Ndayambaje et al., 2016; Horzum et al., 2012). The performance of these chelating adsorbents therefore depends on the chelating group they are carrying which would bring about the selective metal-ligand complexes (Eldridge et al., 2015).

Metal ions adsorbed on solid materials such as silica and the polymer matrix are usually removed using acidic or basic solutions (Kwon and Jeon, 2012; Pakade et al., 2011; Saeed et al., 2008). The desorbing agents can be EDTA, NaOH, NaCl, HCl, H₂SO₄ and H₃PO₄. In the desorption of Pb²⁺ Qing-Zhu et al. (2009) found that HCl was the ideal solution for desorbing the lead ion since it yielded a high percentage recovery. Kwon and Jeon (2012) reported a high percentage (79%) recovery efficiency of indium using ethylenediamine-tetraacetic acid (EDTA) and nitrilotriacetic acid whereas HCl resulted in 74

% recovery. Saeed et al. (2008) has reported 90% recovery of the adsorbed Cu²⁺ and Pb²⁺ on PAN nanofibres using a solution of HNO₃. The stability of the attached ligand on the adsorbent materials can be determined during the material regeneration. The adsorbing solution should not degrade the chemically attached ligand in order to keep the adsorbent's capability for reuse.

2 LITERATURE REVIEW

2.1 Water pollution

Water is a unique natural resource essential for maintaining life. However, the world human population increases by about 85 million per year, and anthropogenic, industrial and domestic activities are increasing pollution of ground and surface water and decreasing the availability of fresh water resources per person (Hanjra & Qureshi, 2010; Stikker, 1998). Highly industrialised and fast developing countries rely substantially on large-scale industries to boost their global economic competitiveness. Economic growth, which is spurred by robust manufacturing industries, has also generated significant quantities of organic, inorganic and metal contamination of the earth's surface environment, particularly the surface water environment over the past century (Yin, 2010).

Mining in South Africa (SA) has been taking place for over 100 years because SA has huge mineral resources and the wealth created from mining has contributed to the development of the country. However, the quality of water has also been affected by this activity. In the gold mining industry, uranium is one of the by-products that are produced. It is known that uranium in any of its forms is radio-active. Radionuclides are atoms with an unstable nucleus characterized by excess energy. Some of these radionuclides such as uranium-238 and thorium-232 occur in nature while radionuclides such as the strontium ion are a by-product of certain nuclear reactions.

In South Africa, the presence of these radionuclides in rivers is inevitable because of gold mining. It has been reported that gold mining areas in the Witwatersrand basin produce radionuclides, consisting mainly of uranium isotopes and their radioactive daughter products (Winde and Sandham, 2004; Winde, 2006). It was reported by Madzivire et al. (2012) that the concentration of radionuclides in Rand Uranium mine water was above the target water quality range (TWQR) for potable water set by the Department of Water Affairs (DWA) (now Department of Water and Sanitation (DWS)) and World Health Organization (WHO, 2011). The gross alpha radioactivity was 6.01 Bq/L and gross beta radioactivity was 6.05 Bq/L in Rand Uranium mine water. This was 12 and 6 times more than the required limit for potable water respectively. Radioisotopes analysis of Rand Uranium mine water showed that U-235 was 4.71 Bq/L which was above the TWQR for potable water of 0-1 Bq/L. Generally, a discharge of toxic and radioactive elements such as uranium, thorium and strontium to surface and ground water comes from active and abandoned mines.

2.2 Potential water pollutants from industrial wastewaters

Metal contamination and pollution of our aquatic environment is receiving global attention due to the environmental abundance, toxicity and persistence in water over decades. These metals may enter the human food chain and result in health problems from contaminated residues which accumulate in micro-organisms, fauna and aquatic flora. Uncontrolled discharge of untreated industrial waste into water bodies has led to the release of hazardous metals into rivers. These toxic metal ions have been associated with water quality problems that can be linked with health issues to humans, and adverse impacts upon the environment (Armitage et al., 2007).

The behaviour of metals in the aquatic environment is a function of their transport due to dissolution, sorption, precipitation and complexation phenomena. The chemical processes in polluted water are complicated because the processes respond to changes in physicochemical variables such as pH, ionic strength or redox conditions; hydrodynamic processes that affect sediment transport; formation of authigenic particles, with pollutant sorption on particles and particle solutions (Akçay et al., 2003; Dassenakis et al., 1998). The toxic metal ions of concern in this study will include: Cr(VI), As(V), Sr(II), Cd(II), Hg(II), and U(VI).

2.2.1 Chromium

Cr⁶⁺ is very hazardous in cases of skin contact (it is easily absorbed through the skin), eye contact, inhalation or ingestion. Cr⁶⁺ is a confirmed carcinogen (tumorigenic) as well as a mutagen (genetic material). This metal ion causes damage to the kidneys, liver, gastrointestinal tract, the upper respiratory tract, skin and eyes (Khezami and Capart, 2005). Other health risks include fetotoxicity or post-implantation mortality and birth defects. It dissolves easily in water and since it is used by motor manufacturers, it tends to find its way into streams and rivers (MSDS).

2.2.2 Arsenic

Arsenic causes many problems in many third world countries where groundwater is contaminated with arsenic derivatives. Arsenic can enter the body on dermal contact, eye contact, inhalation or ingestion. It is a confirmed carcinogen which increases the risk of cancer, especially of the bladder. It causes damage to the blood, kidneys, lungs and liver (Jaishankar et al., 2014). Arsenic is extremely poisonous and potentially lethal. It is thus of the utmost importance to clean up mining water, since this seeps into groundwater that is used by a large portion of the human population (MSDS).

2.2.3 Strontium

Strontium (Sr) with atomic number 38 is an alkaline earth metal that is highly reactive chemically. It occurs naturally as celestine, putnisite and strontianite. Natural strontium is stable but upon contact with water reacts to form strontium hydroxide and hydrogen gas. The human body absorbs strontium as if it were calcium. The removal and recovery of $^{90}\text{Sr}^{2+}$ from nuclear waste has received a lot of attention since the 1940s. Since the end of the 60s and mid-70s, two kinds of extractants, crown ether derivatives and cobalt bis (dicarbollide) derivatives (Grüner et al., 2002), received quite a lot of attention because these derivatives showed some very promising results in the separation and recovery of $^{90}\text{Sr}^{2+}$ and $^{137}\text{Cs}^+$ from high level radioactive liquid waste (HLRLW). HLRLW has been generated from the reprocessing of spent nuclear fuel. The main hazard of HLRLW consists of unrecovered U and Pu as well as some minor actinides. There are also some radioactive fission products such as $^{90}\text{Sr}^{2+}$ (Tian et al., 2005).

2.2.4 Cadmium

Cadmium (Cd) with atomic number 48 is similar to zinc and mercury with a low melting point. It is commonly found in the +2 oxidation state and is mainly obtained in the metallurgical processing as a by-product of extracting metals such as copper, lead and zinc (Gupta et al., 2001). Although cadmium is an extremely toxic metal, it is still used extensively as pigments, in electroplating, in metallurgical products and various other industries (Rodríguez et al., 2005). Even at low concentration, cadmium is considered to be one of the most toxic metals. Human exposure can occur through fossil fuel combustion, cement production, municipal waste incineration etc. The entry of cadmium into the body can occur through eye contact, inhalation or via ingestion. Cadmium can cause lung, blood and kidney diseases. It is also a suspected carcinogen and it is very harmful to the environment since Cd^{2+} is highly soluble in water.

2.2.5 Mercury

Mercury (Hg) with atomic number 80 is the only metal liquid at standard conditions for temperature and pressure. It occurs naturally as cinnabar. Hg and most of its compounds are toxic. It is released during coal combustion and gold production as well as from non-ferrous metal production and smelters as well as cement production. The route of entry into the body is the same as for all the other metal ions discussed. Mercury can also be transferred to the offspring of mammals, because it is secreted in the maternal milk (Kumari, 2011). It is toxic to the kidneys, lungs, nervous system and mucous membranes. Tremors, impaired cognitive skills and sleep disturbances occur when exposed to mercury vapours, even at very low levels. Mercury has a tendency to accumulate in fish and shellfish (Sharma et al., 2014). Since fish is a substantial source

of food in South Africa, it is important to rid streams of mercury to prevent contamination of fresh water fish, but also to prevent the mercury from reaching the ocean.

2.2.6 Uranium

Uranium (U) with atomic number 92 is weakly radioactive because all its isotopes are unstable. The concentration of uranium in seawater is approximately 3.3 µg/L. In fresh water the uranium concentration is lower than in seawater (Madrakian et al., 2007). The real problem arises in industry where uranium is a by-product in gold mining, and ends up on mine dumps. Rain water then washes the uranium into the environmental water. South Africa used to be the largest supplier of gold (Au) in the world. Uranium, often found in association with Au, is a fairly mobile element in surface or near-surface environments. Not only is uranium extremely toxic and radioactive (Lewis, 1996; Domingo and Corn, 1993), It is also very precious as a fuel for nuclear power stations or nuclear power plants. Uranyl (UO_2^{2+}) is nephrotoxic. It is also chemically toxic and carcinogenic in bone (Gorden et al., 2003). It may cause mutagenic or teratogenic effects. There is also the danger of cumulative effects.

2.3 Water treatment technologies

Due to the shortage of fresh water supplies and the growing concern over the role of toxic metals in the environment, several water reclamation technologies have been studied and/or implemented to various degrees (Kurniawan et al., 2006; Crini, 2005; Wang et al., 2003). Some of the treatment technologies are discussed here below.

Chemical precipitation has the advantages of being simple, non-selective and cheap. The main disadvantages are; production of large sludge volumes containing metals; this results in high sludge disposal cost and high maintenance. Ion exchange is very selective such that relatively pure metals can be recovered and resins can be regenerated and reused. The disadvantages include that the technology works over a small pH range and it is costly to implement as well as to maintain. Coagulation- flocculation is capable of bacterial inactivation and the sludge has good settling rates and dewaterers quickly. Its main set back is the high chemical consumption and the high volume of sludge generated during the treatment of water using coagulation and flocculation. Flotation is a process that can handle high concentrations of metals in the wastewater, has low retention time and is capable of removing very small particles from wastewater. The main disadvantages of this technology include high initial capital costs, high maintenance and operation costs. Membrane filtration technology, when used for the treatment of wastewater, results in some solid waste

generation, but low chemical consumption. The plant requires little space and has the possibility to be selective to a particular metal. The disadvantages of this technology are: high initial capital cost, high maintenance and operational costs; membrane fouling is very likely and membranes have a limited flow-rate and lifetime. Electrochemical treatment requires no chemicals, can be engineered to tolerate suspended solids and can be moderately metal selective to treat effluent. The main set back of this technology is its high initial capital cost. Adsorption deals with a wide variety of target pollutants, and has high capacity and fast kinetics and there is possibility of selectivity depending on the adsorbent. The performance depends on the type of adsorbent and chemical derivatisation to improve its sorption capacity. Regeneration remains an issue.

Currently water treatment processes at power stations include water recovery through desalination, ion exchange regeneration for water softening to produce boiler feed water and cooling systems which produce blow down. While in mines, desalination, particularly reverse osmosis, treats rising underground water to potable quality. However, desalination technologies have problems associated with managing the concentrated inorganic waste products (sludge and brines) that are being produced. It is necessary to develop cost effective ways and a holistic integrative solution to manage wastes for long term sustainability as it relates to pre-treatment, beneficiation, disposal and concentration of the wastes. The selection of a wastewater treatment method is based on the concentration of waste and the cost of treatment. Adsorption by ion exchange resins is one of the popular methods for the removal of major, minor and toxic metals from wastewater and aqueous media (Yavuz et al., 2003).

Ion exchange resins have been developed as a major option for treating wastewaters over the past few decades (Anjum et al., 2017). Non-specific sorbents, such as activated carbon, metal oxides, silica and ion-exchange resins have also been used (Kantipuly et al., 1990). Specific sorbents consisting of a ligand i.e. ion-exchange material or chelating agents, that interacts with the metal ions specifically and a carrier matrix that may be an inorganic material (i.e. aluminium oxide, silica or glass) or polymer microspheres (i.e. polystyrene, cellulose, polyhydroxyethyl methacrylate) have been considered for more specific removal (Igwe and Abia, 2006; Denizili et al., 1998). Selectivity is achieved by new types of ion exchangers with specific affinity to definite metal ions or groups of metals. Chelating ion-exchange resins which are also known as complexing or specific ion resins are designed to have high specificity for an ion or groups of ions. These types of ion-exchange resins adsorb metal ions through a combination of ionic and coordinating interactions instead of the simple electrostatic interactions in conventional cation or anion ion exchange. As a consequence, chelating resins offer greater selectivity than conventional resins.

2.4 Immobilised ligands

In water treatment, the widespread use of metal chelating resins and immobilised (adsorbed or chemically bonded) chelates is applied for concentration and/or separation of trace metals from a variety of matrices.

The donor atoms involved in forming chelates usually include oxygen, nitrogen, phosphorous and sulfur atoms present in phenol, carbonyl, carboxylic, hydroxyl, ether, phosphoryl, amine, nitro, nitroso, azo, diazo, nitrile, amide, thiol, thioether, thiocarbamate, bisulphite, etc. However, the selectivity of the surface with the immobilised functional groups towards metal ion(s) depends on factors like size of the modifier, activity of the loaded group and the characteristics of hard-soft acid-base. The insertion of suitable specific functional groups into the polymeric matrix makes them capable of reacting with metal species under certain favourable conditions to form metal complexes (Mahmoud and Soliman, 1997; Pearson, 1963).

The organic chelates (ligands), which have a tendency to form metal complexes with various metal ions in solution, play a very important role in pre-concentration as well as separation of analytes when sorbed on a suitable support material (Seeber et al., 1999). For instance, 8-hydroquinoline (8HQ), a versatile ligand, reacts with over 60 metal ions in homogenous solution to form complexes of varying stability. Poly(L-cysteine) (PLC), a larger, flexible chelating molecule, is a poly (amino acid) consisting of linear chains of cysteine. It has the possibility for intra-chain complexation involving the SH groups, much like a polydentate ligand, even if the individual poly(amino acid) chains are widely dispersed on the surface (Jurbergs and Holcombe, 1999).

Marshall and Mottola in 1983 characterised an azo-immobilised 8HQ with respect to Cu^{2+} capacity and acid-base properties of its nitrogen and phenol binding groups (Marshall and Mottola, 1983). A study of the potential of immobilised Poly(L-cysteine) (PLC) as a pre-concentration reagent as well as an investigation of the metal-binding properties of a poly(amino acid) showed that PLC has high selectivity for Cd solutions at pH 5 and above, with an increasing strong-site capacity as the pH is increased. Poly(L-cysteine) should find application for concentration or isolation of soft acid metals such as Cd, Pb, Cu and Hg in matrices where there is significant competition from harder acid transition metals as well as Group I and II metals (Jurbergs and Holcombe, 1997).

The use of chelating agents, especially macrocyclic ligands, has increased dramatically recently. Toxic metals are fairly easily absorbed in the intestinal tract to form complexes with proteins and enzymes, for example As^{3+} , Cd^{2+} and Hg^{2+} which have a high affinity for soft donors. Therefore, the removal of toxic metal ions from water is essential and is based primarily on the concepts of

soft-hard acid-base (SHAB) and the principles of coordination chemistry. The use of ligands containing N, S and/or other soft donors is very useful (Martell and Hancock, 1996). Nowadays, there is a growing interest in synthetic macrocycles and their metal complexes. This interest depends on the fact, firstly, that these compounds may mimic naturally occurring macrocycles in their structural and functional features and secondly, on their rich chemical behaviour. For instance, 12- to 16-membered cyclic tetra-amine ligands have a strong tendency to coordinate in a co-planar fashion with 3d transition metal ions to form strong complexes. These in-plane metal-nitrogen interactions are modulated according to the size of the ligand cavity (Sabatini and Fabbrizzi, 1979). Typically, macrocycles contain a central hydrophilic cavity, ringed with either electropositive or electronegative binding atoms. The exterior framework is flexible and exhibits hydrophobic behaviour. The hydrophobic exterior allows the macrocycle to be soluble in ionic substances and in non-aqueous solvents, making it useful in a variety of media (Christen et al., 1974).

Because of the great number of selective ligands available nowadays, solvent extraction became a very useful method for the selective separation and concentration of metal ions from complex aqueous solutions. Separation by solvent extraction is generally considered to be economical for concentrations from 0.01 to 1.0 mol.dm⁻³ (Akita & Takeuchi, 1990; Deorkar & Tavlarides, 1997).

Although alkali and alkali earth metal ions are “less” toxic, there is also an interest in the extraction thereof from aqueous solutions. This can be done by means of macrocycles. Another method is to make use of calixarenes, which are also a type of macrocycle. Calixarenes are bucket-shaped macrocycles containing phenol groups that form the “bottom of the bucket”. For Sr²⁺, the best extractant up to now was shown to be calix[8]arene actamide (Casnati et al., 2001). It is also shown that Sr²⁺ is extracted by dicyclohexano-18-crown-6 (DCH18C6) into ionic liquids (Stepinski et al., 2005).

In recent years, new areas of interest opened up for the use of macrocycles (Huskens, & Sherry, 1996; Beer et al., 1999). One such area is the selective extraction of precious metals in hydrometallurgy. Previously, it was reported that extraction was done from solutions containing Cu²⁺, Ni²⁺, Co²⁺, Zn²⁺, Mn²⁺, Fe²⁺ and U³⁺ at levels between 0.2 and 0.8 g.L⁻¹ in a sulphate medium at a pH of 2 (Green & Hancock, 1982). Various macrocyclic and spherical ligands, as well as their open-chain counterparts are nowadays used in analytical detection, material preparation, catalytic function, medical use and nanoscopic devices (Gloe et al., 2001). The liquid-liquid extraction of UO₂²⁺ with organic solutions of crown ethers for example, was studied intensively by S.K. Mundra and co-workers (Mundra et al., 1987), N.V. Deorkar and S.M. Kopkar (Deorkar & Khopkar, 1989)

and M. Shamsipur and co-workers (Shamsipur et al., 1999). It was found by Shamsipur and co-workers that the extraction properties of the ligands depended on the number of ester oxygen atoms and on the nature of the substituents present in the macrocyclic molecule. They also found that most elements were likely to be extracted when in their highest oxidation state. The best result for the extraction of UO_2^{2+} was obtained when complexed to DCH18C6.

Studies carried out by Gupta and co-workers (Gupta et al., 2001) in the extraction of Cd^{2+} , along with other elements, from a hydrochloric acid medium using Cyanex 923 showed that extraction capacity of 91-92% was obtained. A recovery of 98-99% was achieved with Cyanex 923 and the Cyanex 923 could be used for up to 15 cycles for the extraction and stripping of Cd^{2+} . Rodríguez et al. (2005) also investigated the liquid-liquid extraction of Cd^{2+} by Cyanex 923 in a solid-supported liquid membrane system, but the process was not as successful as was hoped for. As the temperature was increased, the extraction decreased because the extraction process is exothermic. It was also found that the extraction is dependent on the extractant concentration, but not upon the initial metal ion concentration.

Takeshita and co-workers (Takeshita et al., 2003) synthesised a hexa-nitrogen ligand, *N,N,N',N'*-tetrakis(2-pyridylmethyl)ethylenediamine (TPEN), that can coordinate and enclose metal ions (Figure 2.1). They found that Cd^{2+} was selectively extracted by the semi-cyclic structure containing nitrogen donors in the BTP gel (2,6-di(5,6-dipropyl-1,2,4-triazin-3-yl)pyridine).

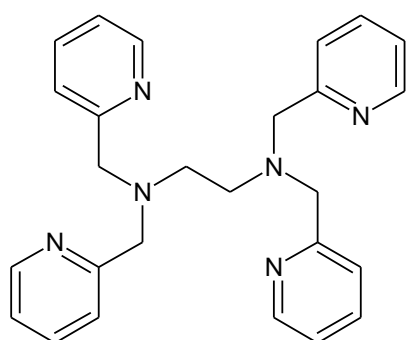


Figure 2.1: The chemical structure of TPEN.

A study was done by B. Wassink, D. Dreisinger and J. Howard, (Wassink et al., 2000) to separate Zn^{2+} and Cd^{2+} , from Co^{2+} and Ni^{2+} . A 30% Aliquat 336, a strong base anion exchanger, in either a chloride (R_4NCl) or thiocyanate (R_4NCSN) form was used for the separation and there appeared to be a slight advantage of Cd^{2+} over the extraction of Zn^{2+} . Fenton and co-workers

(Fenton et al., 2002) studied complexes with mixed donor atoms in the macrocyclic ring with a variety of metal ions. The transition metal ions show complexes that are six coordinate, but Cd^{2+} is an exception, being eight coordinate, so this must be kept in mind. Hydrogels were used by Essawy and Ibrahim (Essawy and Ibrahim, 2004) for the extraction of Cu^{2+} , Ni^{2+} and Cd^{2+} . It was found that Cd^{2+} was the least extractable with these specific hydrogels.

One of the methods for the extraction of U^{6+} is known as a cloud point extraction. This process uses a mixture of the ionic surfactant, cetyl trimethylammonium bromide (CTAB) and a non-ionic surfactant, TritonX-114, for the extraction of U^{6+} from an aqueous solution. This method has a detection limit of 0.06 ng/mL and is used for the determination of U^{6+} in tap water, wastewater and well samples. It has been reported that amongst other methods and materials, activated Si gel is used for the enrichment of U^{6+} from dilute solutions. In 2009, Sadeghi and Sheikhzadeh used Murexide that was chemically bonded to silica gel immobilised by 3-aminopropyl trimethoxysilane (APMS) for the extraction of UO_2^{2+} . A maximum sorption of 1.13 mmol g^{-1} was obtained (Sadeghi and Sheikhzadeh, 2009). This happened prior to its determination with the use of various analytical techniques (Domingo and Corn, 1993).

Poly-dentate oxygen-donating ligands are known to form high-affinity complexes with hard Lewis acids from the f-block (Gorden et al., 2003). The uranyl (UO_2^{2+}) ion is known to be a hard Lewis acid and therefore will have an affinity for hard donor groups. It is thus clear that UO_2^{2+} will be oxophilic and this is one reason why crown ethers are considered as ligands for the extraction of U^{6+} (Kaltsoyannis & Scott, 1999). Because of the size of UO_2^{2+} , the ligand does not accept the uranyl into the cavity, but it would stay on the outside of the crown ether (Hassaballa et al., 1998). Sakama and co-workers used diamyl amyolphosphonate $(\text{C}_5\text{H}_{11}\text{O})_2\text{C}_5\text{H}_{11}\text{PO}$ for the extraction of hexavalent UO_2^{2+} from 2 mol. dm^{-3} HNO_3 (Sakama et al., 2007).

Uranium adopts a hexavalent oxidation state that is usually linear. This linearity will be maintained as far as possible. This means that coordination can only take place in the equatorial plane that is perpendicular to the $\text{O}=\text{U}=\text{O}$ vector. The apical moieties are almost non-reactive, except with the appropriate macrocyclic ligands. The orientation of the chelator around the UO_2^{2+} depends very strongly on the length of the spacer that connects the ligand to the substrate. Short, flexible linkers were found to work best, and $\text{N}_{\text{amide}}-\text{H}\cdots\text{O}_{\text{phenolate}}$ hydrogen-bonding stabilised the deprotonated metal chelated ligands (Sadeghi & Sheikhzadeh, 2009; Arnold et al., 2006). It was found that ethylsulfanyl groups disrupt the planar conjugated ligand arrangement with UO_2^{2+}

introduced to the thiophene linker. The new arrangement forms a dimeric structure in which each ligand spans two uranyl centres $(\text{UO}_2)_2\text{L}_2$.

A macrocyclic ligand is by definition a cyclic molecule with at least three potential donor atoms in a ring which contains a minimum of nine atoms (Constable, 1999). This means no macrocyclic ligand can be classified as normal or small.

Macrocyclic ligand transition metal complexes are involved in a number of biological systems, for instance the porphyrin ring of the haem-protein (Fe containing ring – Figure 2.2a), the chlorin ring of chlorophyll (Mg containing ring – Figure 2.2b) and the corrin ring of vitamin B₁₂ (Co containing ring – Figure 2.2c).

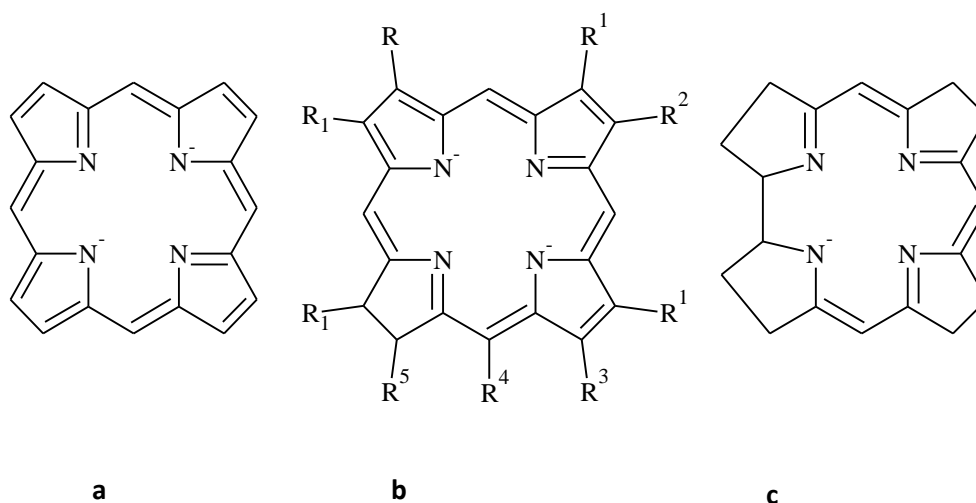


Figure 2.2: Examples of natural biological macrocycles: a) the porphyrin ring of the haem-protein, b) the chlorin ring of chlorophyll and c) the corrin ring of vitamin B₁₂ (Constable, 1999).

It was in the '60s that strong complexes were observed involving Na^+ , K^+ and other related cations, but these were limited to biological materials only. Macrocyclic Polyethers (crown ligands) have an almost unique property in their tendency to form complexes with alkali salts and other salts with similar cations. These complexes are held together by electrostatic interactions between the cation and the negative end of the C-O dipoles. Some of the cations that are of interest in this study that were observed to form stable complexes with crown ligands, are Sr^{2+} , Cd^{2+} and Hg^{2+} (Greene, 1972; Pioda et al., 1967)

Currently a large number of synthetic macrocyclic ligands have been prepared and investigated, for example phthalocyanine (Figure 2.3a), which can be used as semi-conductors, catalysts or

colouring agents. Crown ethers react in a manner similar to that of naturally occurring antibiotics such as nonactin (Figure 2.3b) and valinomycin (Figure 2.3c) (Greene, 1972).

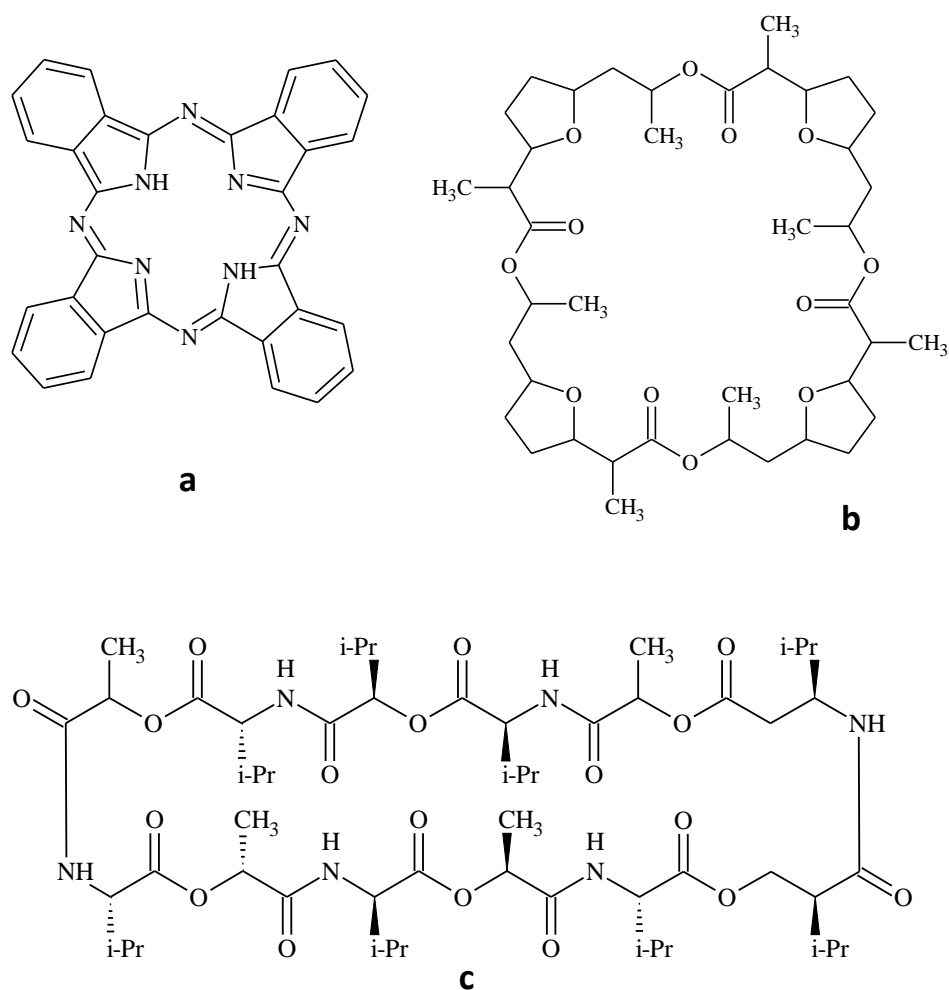


Figure 2.3: Examples of synthetic macrocycles: phthalocyanine (a) which can be used as semi-conductors, catalysts or colouring agents and natural antibiotics such as nonactin (b) and valinomycin (c) (Constable, 1999)

Macrocycles are also used extensively in the medical field. β -thalassemia, commonly known as Cooley's anaemia, is treated with desferral, a macrocyclic ligand which contains hard oxygen donors to get rid of the iron overload (Martell and Hancock, 1996).

Macrocyclic ligands are widely used in solvent extraction of metal salts, and more importantly, in the recovery of precious metals and the removal of toxic elements from wastewater of industrial plants. Macrocyclic ligands form very stable complexes with various metal ions, but they are very selective towards certain metal ions. This attribute now opens up the possibility to selectively

isolate specific metal ions from a mixture of ions by using tailor made macrocyclic ligands (Tasker et al., 2004; Gloe, 2005).

Methods have been widely studied and tested in sea water for adsorption of the uranyl ions through binding to organic ligands (Horzum et al., 2012). This gives a solid background for the selective extraction of uranyl ion in industrial effluents as well. The uranyl ion, due to its unique linear shape, allows for the use of specific ligands tailored towards these properties. Meanwhile, the precipitation and adsorption behaviour of the uranyl ion is governed by the complexes it forms in solution.

For the specific purpose of uranyl ion extraction, several promising ligand groups have been identified and prepared for uranyl sorption and some are in current use. For example, organic phosphorous oxides mostly bounded to a solid matrix are in use in a commercial uranyl extraction system (Kim et al., 2003; Borkowsky and Cahill, 2003; Chen et al., 2003). Modern adsorbents include hydrous titanium hydroxide, amidoxime capped polymers, and synthetic organic ligands that can be attached to a solid supports (Carboni et al., 2013; Abney et al., 2013). Organic ligands on solid supports, especially nanofibers, make good adsorbents due to their affinity, high surface area, selectivity, also their stability and ability to function in various conditions, and ultimately their reusability. However, research to achieve better ligands on solid supports continue. It is worthy to note that these adsorbents must come in contact with a large amount of contaminated water, slowly accumulating for capturing the uranyl ion. After a lengthy accumulation time, the uranium can then be extracted (Carboni et al., 2013).

To improve the sorption capacity of adsorbents, many attempts have been made to chemically modify their surfaces by grafting ligands of functional groups such as amidoxime (Pekel and Guven, 2003; Saeed et al., 2008), imidazole (Pekel et al., 2000), metal oxides (Sadeghi et al., 2012; Comarmond et al., 2011; Zou et al., 2009), and carboxyl or phosphoryl derivatives (Yakshin et al., 2010). Phosphoryl functional groups are good candidates for uranium sorption under acidic conditions, and present promising alternatives to organic polymer sorbents in uranium extraction from nuclear waste. As commonly used sorbents are in powder form, their utilisation as a filter material is not convenient due to the difficulty in the isolation of the solid from the solution medium following the sorption stage. Therefore, additional treatments might be needed, such as the anchoring of these sorbents onto a supporting surface, to efficiently use them for uranium removal and regeneration as well. Attention has recently been paid to the amidoxime chelating adsorbent in removing toxic heavy metals and/or selective recovering of precious metals

(Takeda et al., 1991). Pekel and Guven (2003) studied uranyl ion uptake by amidoximated poly(acrylonitrile/N-vinylimidazole) complexing adsorbents (Figure 2.4).

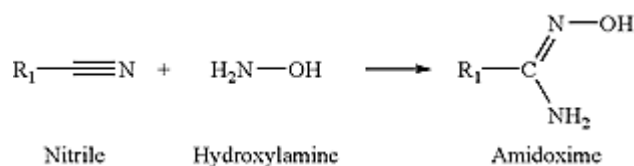


Figure 2.4: Reaction of nitrile and hydroxylamine to produce amidoxime group

It was reported that uranyl adsorption was achieved via the complexation abilities of the vinylimidazole and amidoxime groups. A series of uranyl-amidoxime derivatives were investigated to examine the role of electron donation on uranyl bond strength in the study above. The distance from uranium to the oxime function decreased as electron donation increased, as did the O=U=O bond angle and U=O bond index. Electron donation was further increased by attaching the oxime function to an imidazole or imidazolidin rings (Figure 2.5), giving the most thermodynamically favoured uranyl complexes investigated in the study.

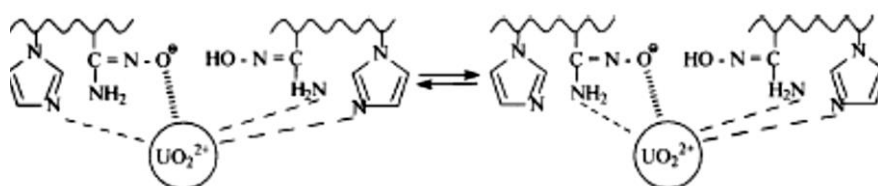


Figure 2.5: Amidoxime and imidazole groups for extraction of UO_2^{2+}

Solvent extraction of uranyl in HNO_3 medium with different extractants has been studied using several organic solvents such as xylene, n-hexane, cyclohexane, benzene, chloroform, toluene etc. as diluents (Kumar et al., 2011). The choice of the diluent depends on the functional group of the extractant. The class of ligands that have been extensively used for removing radionuclides in solvent-solvent extraction are the crown ethers. Examples are dicyclohexano-18-crown-6, benzo-18-crown-6, dibenzo-18-crown-6, benzo-15-crown-5 and calixarenes (Choppin et al., 2006). Studies of crown ethers with actinide ions indicated that they can form either inclusion or secondary sphere coordination compounds. This depends on the solvent and anions present. In the absence of protic solvents like water and ammonia and the presence of non-coordinating anions such as $\text{BF}_4^-/\text{ClO}_4^-/\text{CF}_3\text{SO}_3^-$, they form inclusion compounds. However in the presence of protic solvents and coordinating anions, they form secondary sphere coordination compounds

(Draye et al., 2008; Kannan et al., 2001; Karkhaneei et al., 2001). Yaskshin, et al. (2010) used dicyclohexano 18-crown-6 in 1, 2 dichloroethane to extract uranyl ion from aqueous hydrochloric acid. The distribution ratio D of UO_2^{2+} in the system depended on the HCl concentration; however D was maximum in 6-8 M HCl. The ability of di-tert-butyl-dicyclohexano 18-Crown-6 (DtBuCH18C6) to selectively remove Sr^{2+} has been studied extensively (Wu et al., 2012; Zhang et al., 2010; Zhang et al., 2008; Rawat et al., 2006). DtBuCH18C6 was immobilised by impregnation into the macropores of SiO_2 -polymer with molecular modifiers such as tri-*n*-butyl, 1-dodecanol and, 1-octanol. The modified macroporous silica based polymeric DtBuCH18C6 composite was used to remove Sr^{2+} in 2M HNO_3 (Zhang et al., 2004). The distribution ratio D , of Sr^{2+} increased considerably when the contact time with the resin DtBuCh186 was increased. In an attempt to immobilise dicyclohexano 18-Crown-6 (DCH18C6) on silica, Ye et al. (2012) and Bai et al. (2013) followed a post modification approach by preparing the DCH18C6 moieties with amino groups and attaching them to a polymerised silica matrix. The resultant immobilised ligand had a good thermal stability and was acid resistance. It removed Sr^{2+} effectively from the high acidic medium.

2.5 Polymer as an Immobilisation Substrate

The development of organic polymer based sorbents address the two limitations of silica based sorbents as they are stable over a wide pH range and they do not possess any free silanol groups. Modern porous polymer sorbents are generally copolymers of styrene and divinylbenzene processed to enhance their properties for Solid Phase Extraction (Poole, 2003). Modifying polymer surfaces provide a possible way of immobilising ligands on the surfaces for the extraction and recovery of metal ions from solutions. This will also provide a way for the recovery and reuse of the ligand. There are quite a number of synthetic routes for the chemical modification of polymer surfaces for instance by modifying the surface of polymers with 3-aminopropyltriethoxysilane (APTES). The reaction proceeds by initial APTES adsorption to the substrate, lateral bonding and then multilayer formation which make this analogous to silane multilayer formation.

There are three principal methods by which crown ethers can be incorporated into polymer matrices. The first mode is direct polymerisation of the crown ether through a step-growth mechanism; the second mode is polymerisation through a chain-growth mechanism; and the third mode is post-functionalisation wherein crown ether is covalently bound to a pre-formed polymer backbone. The last method requires the crown to have a reactive functional group that can bond to the polymer and the choice of polymer can influence the degree of ionic accessibility onto the grafted crown ether (Salamone, 1998; Tunca & Yagci, 1994).

2.6 Silica as an Immobilisation Substrate

Silica has been the support of choice in many of these applications. Silica is a polymer of silicic acid, consisting of inter-linked SiO_4 tetrahedra, which have the stoichiometry SiO_2 . Silica gel is a porous, granular form of silica, synthetically manufactured from sodium silicate or silicon tetrachloride or substituted chlorosilane/orthosilicate solution. Silica exhibits good mechanical strength and swelling stability as required for use in a separation technique. Immobilisation reactions on silica are relatively simple, especially when compared to immobilisations involving organic polymers. Faster metal ion exchange kinetics were observed with silica-based chelating ion exchangers than with many other organic polymer-based chelating ion exchangers (Waddell et al., 1981).

The properties of porous solids are of great scientific and technological significance due to their interactions with atoms, ions and molecules. One of the most exciting discoveries in the field of material synthesis is the formation of mesoporous silicate sieves with liquid crystal templates and since then have attracted much attention because of large surface areas, well-defined pore structures, inert framework and non-toxicity. M41S silica was discovered in 1992. A series of inorganic silica meso-structures such as M41's, HMS and SBA-n have been synthesised by different methods and their applications range from catalytic supports in fine chemistry and pharmaceutical chemistry to the production of special polymer products. The immobilisation of extractive ligands on silica supports has advantages over immobilisation on organic polymer supports. Some of the advantages are: short time for equilibration, excellent swelling resistance in different solvents and easy modification of the surfaces (González et al., 2009; Lasseter et al., 2004; Mayani et al., 2006; Zaporozhets et al., 1999).

There is an increasing utilisation of mechanically stable synthetic matrices as solid supports. Solvent impregnated resins and chelating polymeric resins were used for the extractive concentration of metal ions from aqueous solutions and wastewater. Silica gels in particular lend themselves to be modified as such supports. The surfaces are modified either by impregnation of organic ligands directly onto the surface, or by covalent grafting through spacer units for metal ion extraction purposes. Inorganic supports have also been used successfully as stationary phases for extraction chromatographic separation (Braun and Ghersini, 1975). Since the mid 70s, major efforts have been made to immobilise different chelating agents on silica gels by covalent bonding (Marshall and Mottola, 1983). Izatt and co-workers were some of the first groups to immobilise macrocyclic ligands onto silica gel in 1988 (Izatt et al., 2000; Izatt et al., 1988). These studies

concentrated mainly on the immobilisation of crown ethers and not so much on aza-macrocycles (Deorkar and Tavlarides, 1997).

The preparation of modified silicas with an adsorbed reagent was found to be rather easy, and their chemical-analytical properties are not affected by the sorbent with covalent grafted reagents. These types of solid-phase reagents have huge possibilities for analytical work in varied applications (Zaporozhets et al., 1999). The active hydrogen atom of the silanol groups on the silica substrates has the ability to react with organosilyl groups to give some organic nature to the precursor inorganic carrier. These are covalent bonds and these bonds are resistant to removal from the surface by organic solvents or water. The immobilisation of the desired reactive groups causes the silica gels to have a wide variety of uses. They can be used as an ion exchanger, stationary phases in chromatography, enzyme catalysts, and metal ion extractors, heterogeneous catalysts or even in the use of biotechnological processes (Santos and Airoidi, 1996). It was considered that the covalent bond attached to the surface will prevent the attached molecule from detaching itself from the support, thus providing a stable matrix (Figure 2.6).

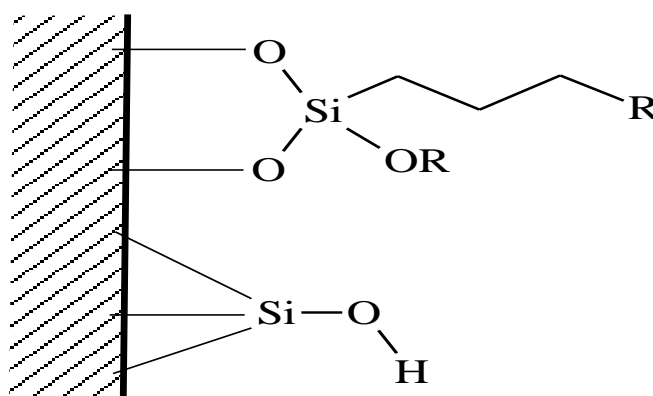


Figure 2.6: A chelating molecule that is directly immobilised on the silica surface will produce steric hindrances at the silanol site

It must be stressed that the chemical and analytical properties of the chelating agent, including the complex forming ability, may differ from the free ligand to that of the same ligand immobilised on a solid support (Myasoedova et al., 1985). Another factor to remember is that, by introducing organic functional groups to the silica surface, the partial conversion of the silanol groups will be changed to a new organo-functional surface that will now possess organophilic properties. This may be the reason why the immobilised ligands and the support surface functions may be totally different from the original molecules (Pyell and Stork, 1992).

3 Synthesis and Immobilisation of Ligand on Silica supports

The method implemented in this study made use of the direct synthesis method, described by Sabatini and Fabbrizzi (1979), Koyama and Yoshino (1972) and Atkins and co-workers (1978). Studies on macrocyclic ligands have shown that when it comes to triazamacrocycles, the bridges between the nitrogen atoms were all equal in length, either being 3 ethylene bridges, [9]-ane-N₃, or 3 propylene bridges, [12]-ane-N₃, including all their derivatives. By synthesising THTD and THTUD, the gap between these ligands, [9]-ane-N₃, and [12]-ane-N₃ is closed and it was hoped that these two more unsymmetrical ligands would produce an interesting selectivity pattern with a number of transition and post-transition metal ions. All reactions are performed under standard atmospheric conditions, unless stated otherwise. The materials used were Toluene-4-sulfonyl chloride, diethyl ether, diethylenetriamine, bis-(3-aminopropyl)-amine, 1,3-propanediol, DMF, ethylene glycol, ethanol, NaOH and all other chemicals were obtained from Sigma-Aldrich and the molecular weights were used as indicated on the containers.

3.1 Experimental procedure of the preparation of THTD and THTUD

3.1.1 Protection of the amines by means of tosylation

3.1.1.1 *Tosylation of diethylenetriamine*

Toluene-4-sulfonyl chloride (114.390 g - 0.600 mol) is dissolved in approximately 700 mL of dry diethyl ether. A solution of NaOH (3.000 mol dm⁻³) was prepared by dissolving NaOH pellets (24.000 g - 0.600 mol) in water (200.0 mL). Diethylenetriamine (20.630 g - 0.200 mol) was then added to the freshly prepared NaOH solution. The solution of toluene-4-sulphonyl chloride was added dropwise over a period of 2 hours to the diethylenetriamine and stirred mechanically for 3 hours. A thick, white precipitate formed. This precipitate was filtered through a no. 4 sintered glass filter and washed, first with water and then with ether to ensure that the product was clean. The tosylated product was dissolved in hot absolute ethanol and left to crystallise at room temperature. The crystals were left in an open atmosphere at room temperature for 3 days to dry completely. The yield mass was 112.950 g.

3.1.1.2 *Tosylation of bis-(3-aminopropyl)-amine*

This reaction is analogous to the tosylation of the diethylenetriamine as is described in section 3.1.1.1, but differs in that we used bis-(3-aminopropyl)-amine (26.244 g - 0.200 mol). The yield mass was 118.760 g.

3.1.2 Protection of the diol by means of tosylation

3.1.2.1 Tosylation of 1,3-propanediol

1,3-propanediol (15.220 g - 0.200 mol) was added to triethylamine (200 mL). Toluene-4-sulphonyl chloride (76.260 g - 0.400 mol) was dissolved in approximately 400 mL of dry diethylether and added dropwise to the 1,3-propanediol solution over a time period of 2 hours. The mixture was then mechanically stirred overnight. A thick, white precipitate was formed. This white precipitate was filtered through a no.4 sintered glass filter and washed first with water, and then with ether. The tosylated product was then crystallised from hot ethanol (99.99%) and the crystals were left for 3 days to dry completely in an open atmosphere at room temperature. The yield mass was 76.894 g.

3.1.2.2 Tosylation of ethylene glycol

The reaction is analogous to the tosylation of the 1,3-propanediol as was described in section 3.1.2.1, but we used ethylene glycol (12,414 g - 0.200 mol). The yield mass was 74.089 g.

3.1.3 Preparation of the tosylated triamine disodiumsalt (diethylenetriamine and the bis-(3-aminopropyl)-amine)

The procedure was carried out under inert conditions (N_2), in a 2 L round bottom flask, fitted with a $CaCl_2$ drying tube. Na (9.196 g - 0.400 mol) was reacted with approximately 1.2 L of ethanol. The tosylated tri-amine (0.200 mol) was then added bit by bit to the Na solution and stirred overnight by means of a mechanical stirrer. A white precipitate formed which is the Na-salt of the tri-amine. This precipitate was filtered through a no. 4 sintered glass filter, and washed with ethanol and diethyl ether. A yield of 90% was obtained (mass = 114.790 g). The synthesis described is analogous for the tosylated diethylenetriamine as well as the tosylated bis-(3-aminopropyl)-amine. A yield of 92% was obtained (mass = 112.180 g).

3.1.4 Synthesis of the macrocycles

3.1.4.1 Synthesis of tosylated 1,4,7-triazacyclodecane

The tosylated diethylenetriamine di-sodium salt was immediately dissolved in approximately 900 mL of DMF and placed in an oil bath at 120°C. The tosylated 1,3-propanediol (15.22 g - 0.200 mol) was then dissolved in 450 mL DMF and added dropwise (over a period of 2 hours) to the freshly prepared solution of tosylated diethylenetriamine di-sodium salt while stirring vigorously

with an overhead stirrer. This solution was then stirred for a further 8 hours. A clear orange solution formed. This clear orange solution was filtered through a no. 4 sintered glass filter and it was then added slowly to approximately 8 L of ice water. A white precipitate formed immediately when added to the water and the solution was left for 24 hours for the maximum amount of product to precipitate. The precipitate was filtered off and recrystallised from ethanol (99.99%).

3.1.4.2 Synthesis of tosylated 1,4,8- triazacycloundecane

The reaction is analogous to section 3.1.4.1, using the tosylated bis-(3-aminopropyl)-amine and the tosylated ethylene glycol.

3.1.5 The addition of the pendant arms

The procedure was analogous for both the macrocycles and the reaction must be carried out under inert (N₂) conditions. Na metal (0.414 g - 0.018 mol) was reacted with approximately 100 mL ethanol (99.99%) to form sodium ethoxide. The macrocyclic-HBr-salt (0.006 mol) was then added to the sodium ethoxide solution and stirred for approximately 2 hours. A white precipitate -NaBr- formed which was filtered off by using normal no. 4 filter paper. (*S*)-(-)-propylene oxide (1.5 mL - 0.018 mol) is added to the solution to attach the arms to the macrocycle. This solution was then stirred at room temperature for 7 days. On completion of the reaction, the volume of the solution was reduced with the use of a rotary evaporator. A white precipitate (NaBr) formed which was removed. Since NaBr and the product are soluble in water, it was decided to add CH₂Cl₂ to the solution because the product is more soluble in the CH₂Cl₂ than is NaBr. The NaBr was removed by filtration through a no. 4 filter paper. This procedure was repeated a few times to ensure that all the NaBr was removed. The product (filtrate) was dried by means of a rotary evaporator and afterwards placed on a vacuum pump to ensure a dry product.

3.2 Characterization of THTH and THTUD

3.2.1 NMR spectra of THTD

Nuclear magnetic resonance (NMR) spectra were recorded in D₂O. The spectra were compared with previously resolved structures that were published (Barnard, 2008).

Table 3.1: ^1H and ^{13}C NMR of the 1,4,7-tris[2(S)-hydroxypropyl]-1,4,7-triazacyclodecane.

Assignment	δ / ppm
^1H	
Pendant arms (without the CH_3 - and the OH- groups)	3.11-4.25
Ring structure	2.30-3.02
OH	1.47
CH_3	0.99-1.22
^{13}C	
$\text{C}^{12, 15, 18}$	76.4
$\text{C}^{11, 14, 17}$	66.8
$\text{C}^{2, 3, 5, 7, 9, 10}$	66.6
C^6	18.8
$\text{C}^{20, 21, 22}$	15.2

3.2.1.1 ^{13}C NMR spectrum of THTD

The chemical shifts for the signals of the ^{13}C NMR spectrum of THTD can be seen in Table 3.1 above. Although the signals are fairly weak, they could be assigned unambiguously. The signal for the CH chiral centre at C^{12} , C^{15} and C^{18} is shifted far downfield due to the OH groups of the pendant arms. This signal can be observed at 76.4 ppm. The resonance at 66.8 ppm is the signal of the CH_2 groups (C^{11} , C^{14} , C^{17}) of the pendant arms, while the signal at 66.6 ppm is ascribed to the protons of the CH_2 groups (C^2 , C^3 , C^5 , C^7 , C^9 , C^{10}) of the carbon bridges. The carbon atom, C^6 , is the lone CH_2 of the propyl bridge at 18.8 ppm and the signal at 15.2 ppm represents the methyl groups (C^{20} , C^{21} , C^{22}) of the pendant arms.

3.2.1.2 ^1H NMR spectrum of THTD

The chemical shifts for the ^1H NMR spectrum of THTD can be seen in Table 3.1 above. The ligand may appear as a symmetrical molecule, but due to overlapping of the signals, the assignment of the peaks proved to be problematic. A comparative study (Barnard, 2008) was made and only

chemical environments could be used to identify the different protons. The integration showed that the protons do match the structure of the ligand.

The signals for the CH₂ and CH₃ -groups of the pendant arms are found in the chemical environment between 3.1 ppm and 4.3 ppm. These are shifted downfield because of the OH groups. The region between 2.3 ppm and 3.1 ppm can be divided into two areas. These areas contain the signals for the protons of the parent ligand, the ring itself. The first part is likely to be the propyl bridge while the latter parts are the ethylene bridges. Between 0.9 ppm and 1.3 ppm is the signal for the methyl groups. From the integration it can be seen that the number of protons were correct as well as the chemical environment where they were situated.

Based on the ¹³C and the ¹H NMR spectra together, it was concluded that the THTD had indeed formed. The proton spectrum on the other hand does not give conclusive evidence. The ligand was thus further characterised by elemental analysis, melting point determination and mass spectrometry to confirm its structure.

3.2.2 NMR spectra of THTUD

The NMR experiments were carried out in D₂O. The spectra were compared with previously resolved structures that were published (Barnard, 2008).

3.2.2.1 ¹³C NMR spectrum of THTUD

Table 3.2 shows the chemical shifts for the signals of the ¹³C NMR spectrum of THTUD. The CH-groups (C¹³, C¹⁶, C¹⁹), attached to the OH groups are furthest downfield and the signal is found at 76.4 ppm. At 66.3 ppm and 67.0 ppm are two resonances that are very similar to each other. These signals are the CH₂-groups (C¹², C¹⁵, C¹⁸) of the pendant arms that are attached to the nitrogen atoms of the ring. The chemical environment is slightly different for these three groups, splitting them into two signals. The prominent signals at 64.1 ppm are the CH₂-groups (C², C³, C⁵, C⁷, C⁹, C¹¹) of the ring, that are attached to the nitrogen atoms. At 18.8 ppm is the resonance for the CH₂-groups of the propyl bridges (C⁶, C¹⁰). The methyl groups (C²¹, C²², C²³) give a signal at 15.2 ppm.

Table 3.2: ^{13}C NMR data of the 1,4,8-tris[2-(S)-hydroxypropyl]-1,4,8-triazacycloundecane.

Assignment	δ / ppm
^1H	
H ^{21,22,23}	1.00-1.16
Ring	1.80-2.10
Pendant arms (CH ₂)	3.05-2.80
Pendant arms (CH)	3.86-4.02
^{13}C	
C ^{13,16,19}	76.4
C ^{12,15,18}	66.3, 67.0
C ^{2,3,5,7,9,11}	64.1
C ^{21,22,23}	18.8
C ^{6,10}	15.2

3.2.2.2 ^1H NMR spectrum of THTUD

Table 3.2 shows the approximate chemical shifts of the signals of the proton. The resonances for the methyl groups (H²¹, H²², H²³) are found between 1.00 ppm and 1.16 ppm. Between 1.88 ppm and 1.56 ppm the resonances for the ethylene bridge (H², H³) of the parent ring can be found. The signals for the protons of the propyl bridges (H⁵, H⁷, H⁹, H¹¹) are observed between 2.00 ppm to 2.74 ppm. This region also includes the OH groups of the pendant arms. The signals of the CH₂-groups (H¹², H¹⁵, H¹⁸) on the pendant arms can be seen between 2.80 ppm and 3.05 ppm. The CH-groups (H¹³, H¹⁶, H¹⁹) of the arms are represented by a broad signal between 3.86 ppm and 4.02 ppm.

Based on the ^{13}C and the ^1H NMR spectra together, it was concluded that the THTUD had indeed formed. The proton spectrum on the other hand did not give conclusive evidence. The ligand was thus further characterised by elemental analysis, melting point determination and mass spectrometry to confirm its structure.

3.3 Immobilisation of THTD and THTUD Ligands on Silica substrate

There are two different ways of immobilisation. The first method is the homogeneous method in which the silylant compound is first bound to the inorganic carrier. The second route is the heterogeneous route and here the molecule is directly immobilised on the support through a silanising agent.

3.3.1 Silica gel (60 Å) (Si gel)

Silica gel (60 Å) was bought from Sigma-Aldrich and had a particle size of 70-230 mesh and a pore diameter of 60 Å. Silica gel is an inorganic, amorphous polymer of which the bulk consists of siloxane groups (Si-O-Si). The outside surface is made up of silanol groups (Si-OH). Commercial silica gel has very little silanol groups available for modification, therefore it is necessary to activate the silica gel prior to modification.

3.3.2 Mobil composition of matter (MCM-41)

MCM-41 is a hexagonally ordered mesoporous molecular sieve, developed by a scientist from the Mobil Corporation in 1992. Depending on the alkyl chain length of the surfactant template and the synthesis conditions, the particle sizes may vary from 2 to 10 nm.

3.3.3 Santa Barbara amorphous (SBA-15)

SBA-15 is a meso-porous molecular sieve with a large surface area and homogeneous pore diameters. It is nowadays commonly used as the basis for catalysts and adsorbants. SBA-15 can be prepared over a wide range of uniform pore sizes and wall thicknesses depending on the temperature at which it is prepared. The pores can be as wide as 30 nm. These properties give SBA-15 higher thermal and chemical stability. SBA-15 is a very attractive carrier because of its large surface area, well ordered meso-porous structure, tuneable pore sizes and volumes and well defined surface properties for modification.

3.3.4 Hexagonal mesoporous silica (HMS)

Of all the silica supports, HMS has the smallest surface area. It also has the smallest pore volume as well as the smallest pore diameters. Although HMS is smaller in all aspects, it can still be modified as a carrier for selective ligands. In certain aspects, it might even be a better support to

use since the pores are very small and therefore will not allow too many molecules, solvent or metal, to enter into the pores, forcing them to complex to the ligands that are immobilised on the surface.

3.4 Results and Discussion for Immobilisation experiment

3.4.1 Fourier transform infra red (FTIR) spectra

3.4.1.1 Spectra of the direct immobilisation of the crown ethers

Figure 3.1 shows the FTIR spectrum of 18-c-6 immobilised on silica gel (60 Å).

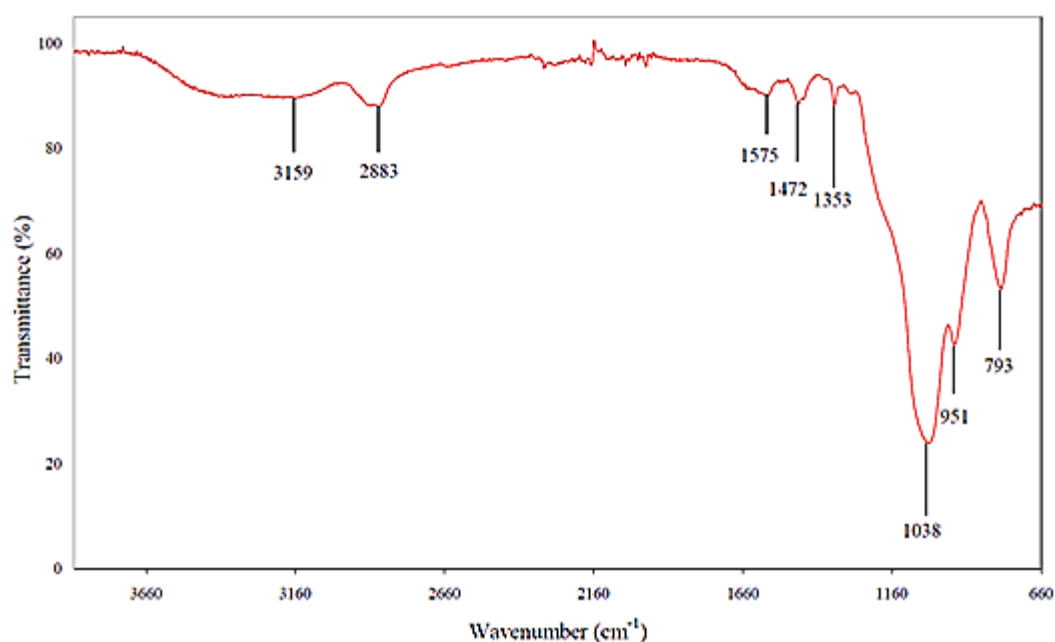


Figure 3.1: The FTIR spectrum of the direct immobilisation of 18-c-6 on silica gel. This spectrum is representative of 15-c-5 and 18-c-6 on all four supports.

According to Deorkar and Tavlarides, FTIR spectral studies show van der Waals type of interactions between the alkyl chain of the extractant and the functional groups bonded to the silica surfaces. It is proposed that there are a number of H-bonds that keep the crown ethers attached to the silica support. It seems like there is hydrogen bond interactions between the protons of the amine group and the oxygen atoms of the silanol groups. There are in all probability also hydrogen bond interactions between the lone pair of electrons on the nitrogen of the amine group and the protons of the silanol groups of the silica supports.

The signals for the CH₂ stretch in the crown ethers can be seen in the 2883 cm⁻¹ region. The bend motion is visible at 1472 cm⁻¹. The NH stretch signal is obscured by the very broad signal at 3159

cm^{-1} , but the bend motion can clearly be seen at 1575 cm^{-1} . The CN single bond signal is observed at 1353 cm^{-1} . The FTIR spectrum of 15-c-5 (on Si gel (60 \AA)) is similar to that of 18-c-6 with the signals in the same regions. The FTIR of SBA-15 was used to verify that the ligands did in fact attach to the substrate and was compared to that in the literature. The interpretation of the signals corresponds to that of the immobilised 18-c-6 on Si 60 \AA .

3.4.1.2 Spectra of the immobilised crown ethers by means of the glymo spacer

The FTIR spectrum of the glymo spacer with the immobilised 15-c-5 (Figure 3.2) is representative of all the crown ethers that were immobilised with the glymo spacer. The CH_2 stretch frequencies can be seen at 2866 cm^{-1} . The bend frequency is clearly visible at 1456 cm^{-1} . The NH stretch signal is obscured by the broad signal at 3373 cm^{-1} . The bend motion for NH is clear at 1586 cm^{-1} . The CN single bond stretch frequency can be seen at 1352 cm^{-1} . The crown ether signal is very clear in the 1033 cm^{-1} region.

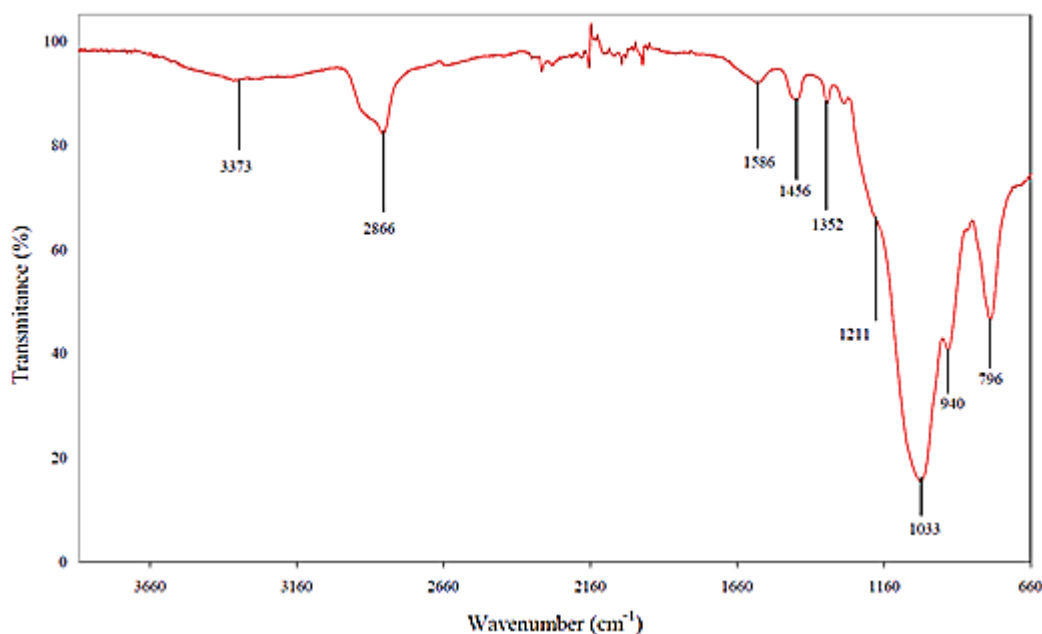


Figure 3.2: The FTIR spectrum of 15-c-5 on silica gel 60 \AA by means of the glymo spacer. This spectrum is representative of 15-c-5 and 18-c-6 on all four supports.

3.4.1.3 Spectra of the immobilised azamacrocycles by means of the glymo spacer

The spectrum in Figure 3.3 is representative of all the glymo immobilised THTD and THTUD ligands on all four different Si supports.

From the spectrum it is clear that the NH signals disappeared. Although the signals are weak, the CH_2 signals are visible in the expected regions. The OH signal is still present at 3366 cm^{-1} while

the CN single bond signal is visible at 1665 cm^{-1} . From the spectrum it was concluded that the attachment of the tri azamacrocycle did in fact take place. The result was verified by means of solid state NMR and will be discussed in the next section.

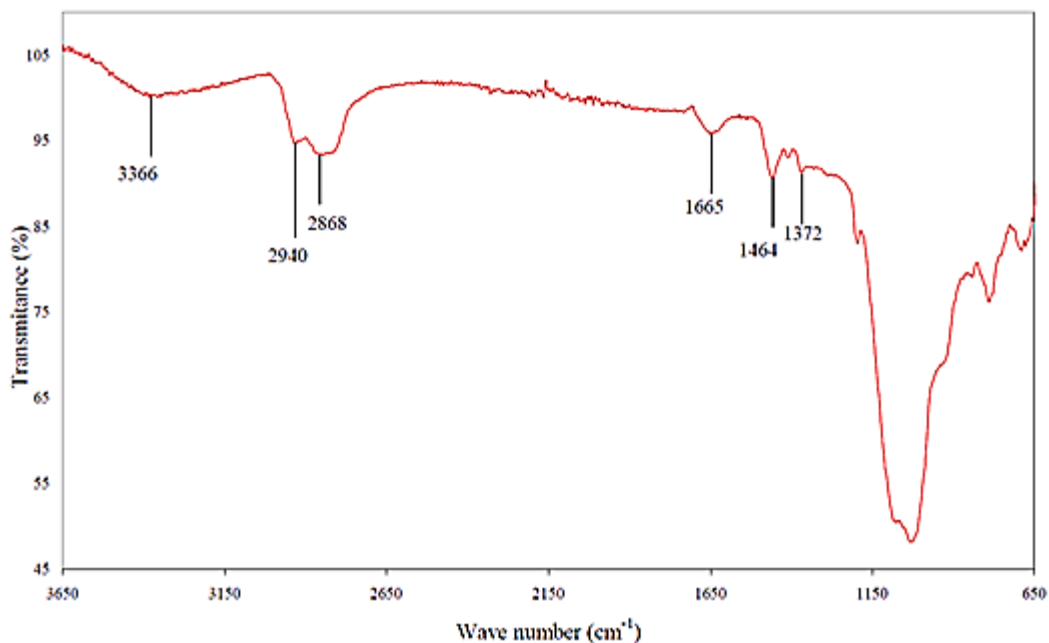


Figure 3.3: The FTIR spectrum of THTD immobilised by the glymo spacer on silica gel (60 Å).

3.4.2 NMR

The NMR data of the intermediate products were compared to that of similar structures found in the literature. The data confirmed that the intermediate products of the ligands were indeed synthesised.

3.4.2.1 *The solid state NMR spectrum of the crown ethers directly immobilised on the silica supports*

As can be seen from Figure 3.4, the CH_2 signal of the crown ether ring is very prominent at 71 ppm. The CH is a small signal at 79 ppm and the CH_2 of the attachment leg next to the amino group is at 41 ppm.

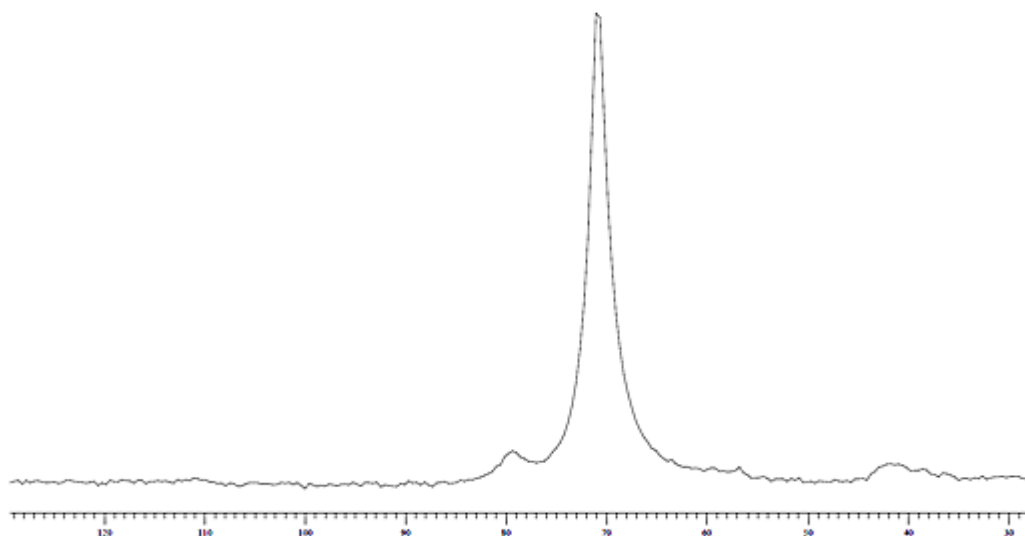


Figure 3.4: The solid state ^{13}C NMR spectrum of 18-c-6 directly immobilised on a silica support. This spectrum is also representative of 15-c-5 immobilised directly onto the silica support.

From the spectrum it is clear that the crown ether must have attached itself to the support. The reference NMR of the silica supports showed that there is an overlap of two very broad signals. After immobilisation these overlapping peaks were still present, but a very distinct third peak appeared (Figure 3.5), indicating that the amino group of the crown ether has attached itself to the silanol groups of the support. Hence, from the data obtained, it can be deduced that the immobilisation did take place because of the change in the surface of the silica supports.

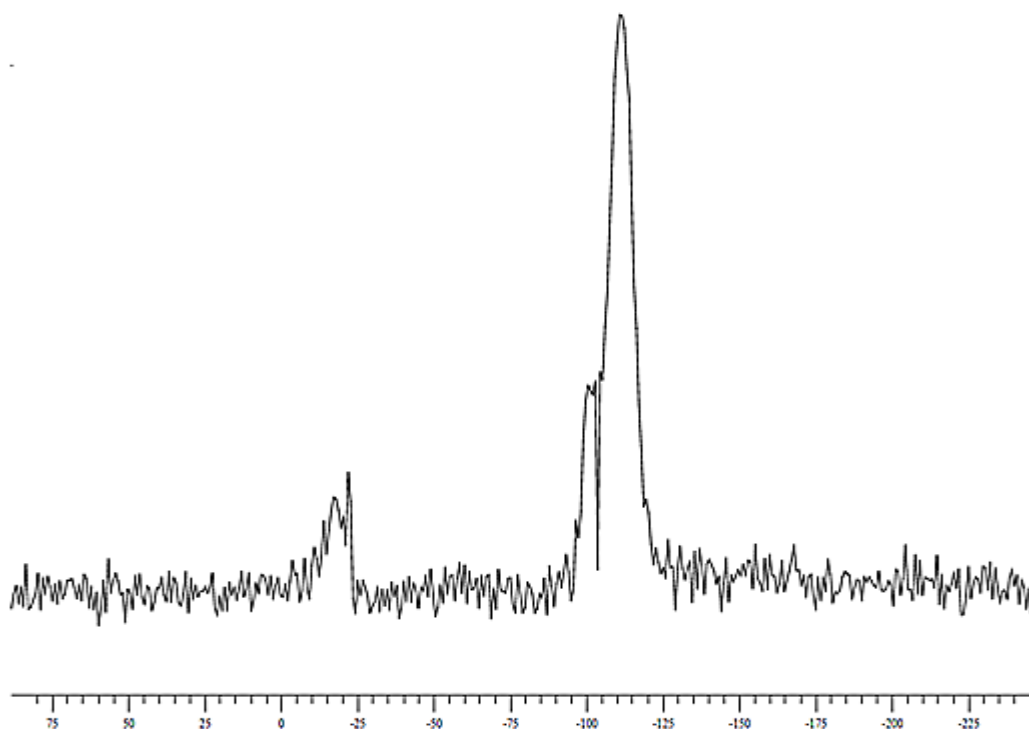


Figure 3.5: The solid state NMR spectrum shows the direct immobilisation of the crown ethers on the silica supports. This spectrum is representative of both crown ethers immobilised on all four supports.

3.4.2.2 *The solid state NMR spectrum of the glymo spacer, immobilized on the silica supports*

The solid state ^{13}C NMR spectrum of the immobilised glymo spacer on silica gel is shown in Figure 3.6. The split in the signal at 72 ppm are the carbon atoms of the $\text{CH}_2 - \text{O} - \text{CH}_2$ (no.3 & 4). The two singlets at 44 and 50 ppm are the carbon atoms of the epoxide (no.1 & 2). The three remaining signals are the CH_3 (no. 7) at 25 ppm and the two CH_2 's at 8 ppm (no. 5 & 6).

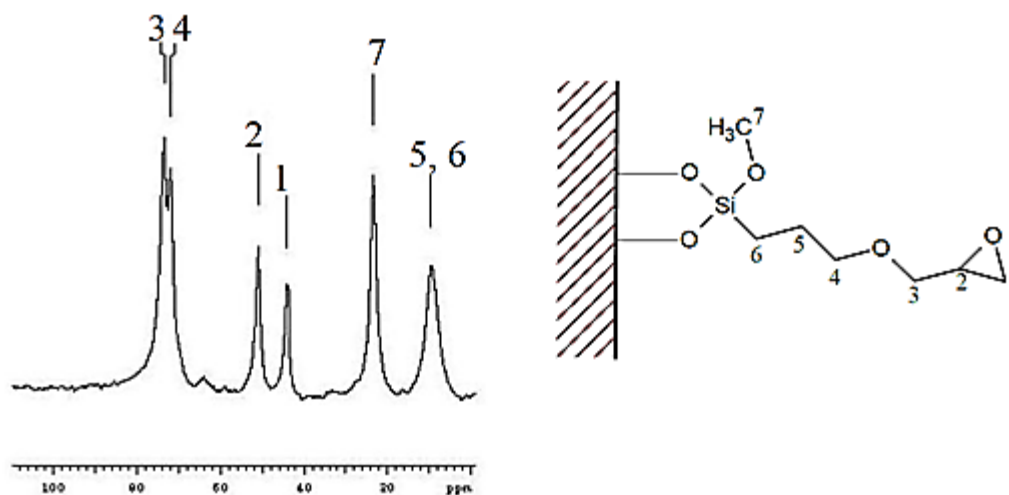


Figure 3.6: The spectrum is a representation of the immobilised glymo spacer on the silica.

3.4.2.3 *The solid state NMR spectra of the crown ethers immobilized on the silica supports with the glymo spacer*

The solid state ^{13}C NMR spectrum of 15-c-5, immobilised with a glymo spacer on silica gel, is shown in Figure 3.7. The signals of carbon atoms no.5 and 6 of the glymo spacer can still be seen at 8 ppm and the methyl signal of carbon no.7 can be observed at 25 ppm. There is a slight shoulder at 78 ppm on the main signal at 70 ppm, representing the carbon (no. 9) where the amino arm attaches to the crown ether. The other carbon atoms are all incorporated in the huge signal at 70 ppm.

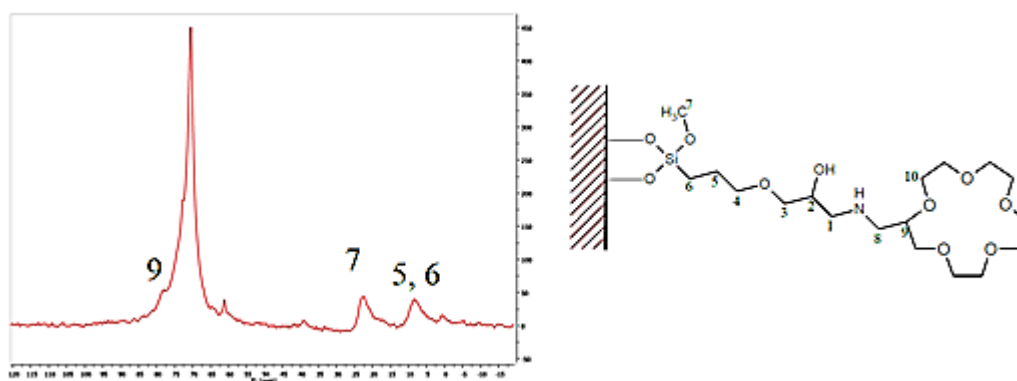


Figure 3.7: The solid state spectrum ^{13}C -NMR is representative of the immobilisation of the crown ethers onto the silica supports by means of the glymo spacer.

3.4.2.4 *The solid state NMR spectra of the aza crown ethers immobilized on the silica supports with the glymo spacer*

The signals from the glymo (no's. 5, 6 &7) can still be observed in both spectra (Figure 3.8). The top spectrum shows the azamacrocycle, without the pendant arms, immobilised with the glymo spacer. The bottom spectrum shows the azamacrocycle, with the pendant arms attached, immobilised with the glymo spacer. The remainder of the top spectrum integrates to the amount of carbon atoms that are left in the rest of the glymo chain as well as the amount of the carbon atoms in the aza-crown macrocycle. In the bottom spectrum, the integration of signals between 45 and 80 ppm increased to the amount of the carbon atoms that was added as the pendant arms.

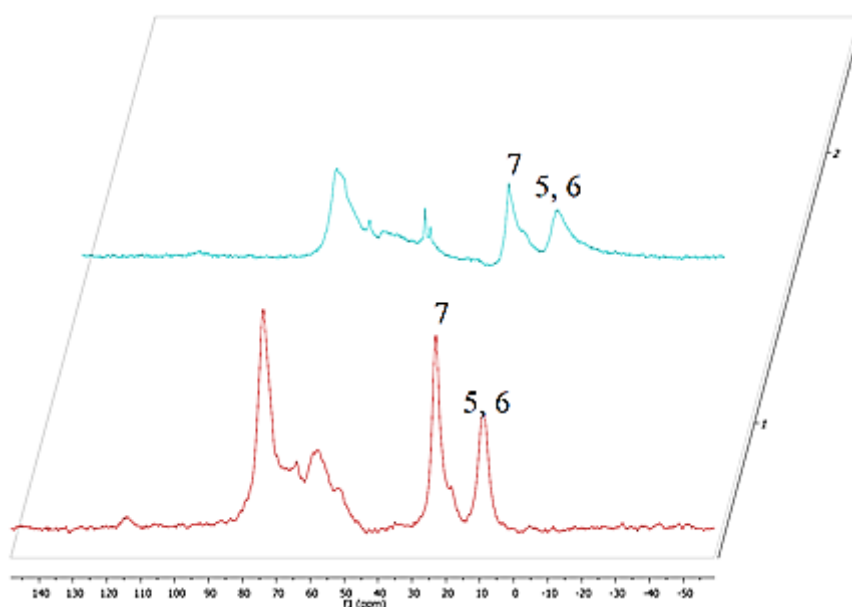


Figure 3.8: The solid state ^{13}C NMR spectrum is representative of the immobilisation via the glymo spacer, of the aza-crown ethers onto the silica supports.

3.4.3 Brunauer-Emmett-Teller (BET) results

The supports were all subjected to BET experiments to determine the surface areas, pore volumes and pore diameters.

3.4.3.1 Surface area determination and comparison of the four silica supports

From the data (Table 3.3 and 3.4) it can be seen that MCM-41 had the highest surface area (1020.0 m²/g), followed by SBA-15 (758.0 m²/g), Si-gel 60 Å (469.0 m²/g) and HMS (466.1 m²/g). It is likely that MCM-41 may be the best support, but other factors also need to be considered such as the active silanol sites for instance.

Table 3.3: The surface areas of Si-gel 60 Å and MCM-41

	Si-Gel (60Å)	MCM-41
Single Point Surface Area at P/Po 0.2039	451.0 m ² /g	981.8 m ² /g
BET Surface Area	469.0 m ² /g	1020.0 m ² /g
BJH Adsorption Cumulative Surface Area of Pores between 17.0 and 3000.0 Å Diameter	517.1 m ² /g	1021.3 m ² /g
BJH Desorption Cumulative Surface Area of Pores between 17.0 and 3000.0 Å Diameter	629.2 m ² /g	1343.5 m ² /g

Table 3.4: The surface areas of SBA-15 and HMS

	SBA-15	HMS
Single Point Surface Area at P/Po 0.2039	729.3 m ² /g	453.0 m ² /g
BET Surface Area	758.0 m ² /g	466.0 m ² /g
BJH Adsorption Cumulative Surface Area of Pores between 17.0 and 3000.0 Å Diameter	605.3 m ² /g	78.6 m ² /g
BJH Desorption Cumulative Surface Area of Pores between 17.0 and 3000.0 Å Diameter	851.5 m ² /g	158.9 m ² /g

The average pore volumes of MCM-41 are larger than those of Si gel 60 Å and SBA-15. Hexagonal mesoporous silica (HMS) has by far the smallest pore volumes in comparison with the other three supports (Tables 3.5 and 3.6).

Table 3.5: The average size of the pore diameters and average pore volumes for MCM- 41 and Si-gel (60 Å) are shown in the table below.

	MCM-41	Si-Gel (60Å)
Single Point Total Pore Volume of pores less than 1027.5 Å Diameter at P/Po 0.9808	0.9 cm ³ /g	0.7 cm ³ /g
BJH Adsorption Cumulative Pore Volume of pores between 17.0 and 3000.0 Å Diameter	0.8 cm ³ /g	0.6 cm ³ /g
BJH Desorption Cumulative Pore Volume of pores between 17.0 and 3000.0 Å Diameter	1.0 cm ³ /g	0.7 cm ³ /g

Table 3.6: The average size of the pore diameters and average pore volumes for HMS and SBA-15 are shown in the table below.

	HMS	SBA-15
Single Point Total Pore Volume of pore less than 1027.5 Å Diameter at P/Po 0.9808	0.3 cm ³ /g	0.8 cm ³ /g
BJH Adsorption Cumulative Pore Volume pores between 17.0 and 3000.0 Å Diameter	0.1 cm ³ /g	0.7 cm ³ /g
BJH Desorption Cumulative Pore Volume of pores between 17.0 and 3000.0 Å Diameter	0.2 cm ³ /g	0.9 cm ³ /g

The average pore diameter for each of the silica supports are summarised in Tables 3.7 and 3.8.

Table 3.7: The average pore diameter for Si-gel 60 Å and MCM-41 was determined by BET and is shown in the table below.

	Si-Gel (60Å)	MCM-41
Average Pore Diameter (4V/A by BET):	61.4 Å	35.8 Å
BJH Adsorption Average Pore Diameter (4V/A):	50.1 Å	29.5 Å
BJH Desorption Average Pore Diameter (4V/A):	46.9 Å	30.8 Å

Table 3.8: The average pore diameter for HMS and SBA-15 was determined by BET and is shown in the table below.

	HMS	SBA-15
Average Pore Diameter (4V/A by BET):	22.4 Å	42.3 Å
BJH Adsorption Average Pore Diameter (4V/A):	57.1 Å	43.2 Å
BJH Desorption Average Pore Diameter (4V/A):	38.2 Å	41.0 Å

On average, it appears that the Si gel is the obvious choice as a support considering the surface area, the average pore diameter and average pore volume. On the other hand, it is necessary to see whether the active sites (the areas where the spacers will attach) of the other supports will increase on activation and also whether the pore diameters and pore volumes will have an influence on the total available surface area for immobilisation.

3.5 Extraction of Toxic Elements using Silica supported ligands

Metal ion solutions were prepared from the various metal ion salts. The aqueous source phase consisted first, of single metal ion solutions (Table 3.9 – solutions 1-6). Next, an equi-molar mixture of four different metal ion solutions (Table 3.0 – solutions 1-4) were made up as one solution, as well as a solution containing the other two metal ions (Table 3.9 – solutions 5, 6) to determine the selectivity of the ligands on the different supports. The two mixed metal ion solutions were split due to their very different acidic properties. Hg^{2+} and U^{6+} must first be dissolved in glacial acetic acid after which it had to be adjusted to the desired pH. The other metal salts were dissolved directly in the buffer solution.

Table 3.9: The metal salts that were used for the preparation of the different solutions

	1	2	3	4	5	6
Metal salt	CrO_3	As_2O_5	$\text{Sr}(\text{NO}_3)_2$	$\text{Cd}(\text{NO}_3)_2$	$\text{Hg}(\text{NO}_3)_2$	$\text{UO}_2(\text{CH}_3\text{COO})_2$
Metal ions	Cr^{6+}	As^{5+}	Sr^{2+}	Cd^{2+}	Hg^{2+}	UO_2^{2+}

All the solutions for the first series of extraction experiments were buffered with an acetic acid/sodium acetate buffer solution at pH 4.5. The solutions for the second series of extraction experiments were buffered at pH of 5.9. Again the buffer solutions consisted of an acetic acid/sodium acetate buffer. It must be stressed that pH 5.9 is right on the border for an acetic acid/acetate buffer. All solutions were made up to as close to $1.000 \times 10^{-3} \text{ mol.L}^{-1}$ as possible with their exact concentrations recorded. Equal weights of ligand per substrate were weighed off and 10 mL of each metal ion solution were added for the extraction.

The extractions were carried out over a period of 24 hours at a constant temperature of 25 °C. After this period of time, equilibrium is assumed to have been established. The solutions were

shaken on an automatic shaker at a tempo of 220 rev.min⁻¹. Thereafter, the solutions were filtered using normal filter paper. The solutions were then analysed before and after extraction, using ICP to determine the quantities of metal ions remaining in aqueous phase, hence the effectiveness of the extraction capabilities of the different ligands.

3.5.1 Results and Discussion

To explain the extraction yields, it is important to have a look at the speciation of the different metal ions in aqueous solution. It must be mentioned that all extraction values below 2.5%, falls within instrumental error that was reported by the instrument operator, and can be considered to be zero.

3.5.1.1 Extraction of As(V) with various ligands immobilized on four different silica supports

Arsenic is present in aqueous solutions as two species: as HAsO_4^{2-} or H_2AsO_4^- . The average extraction of H_nAsO^x at a pH of 4.5 with the various ligands immobilised on any of the four supports were less than 2.5% and are therefore considered to be zero (Figure 3.9). Even with the pH raised to 5.9, the average extraction with the ligands immobilised on the various supports remained less than 2.5%. It is therefore clear that no extraction was obtained with any of the ligands immobilised on the various supports with the pH level at 4.5. The results indicate that no extraction took place. This is due to the fact that there are lone pairs of electrons on the donor atoms that are trying to coordinate to the already negatively charged arsenic ions resulting in no extraction.

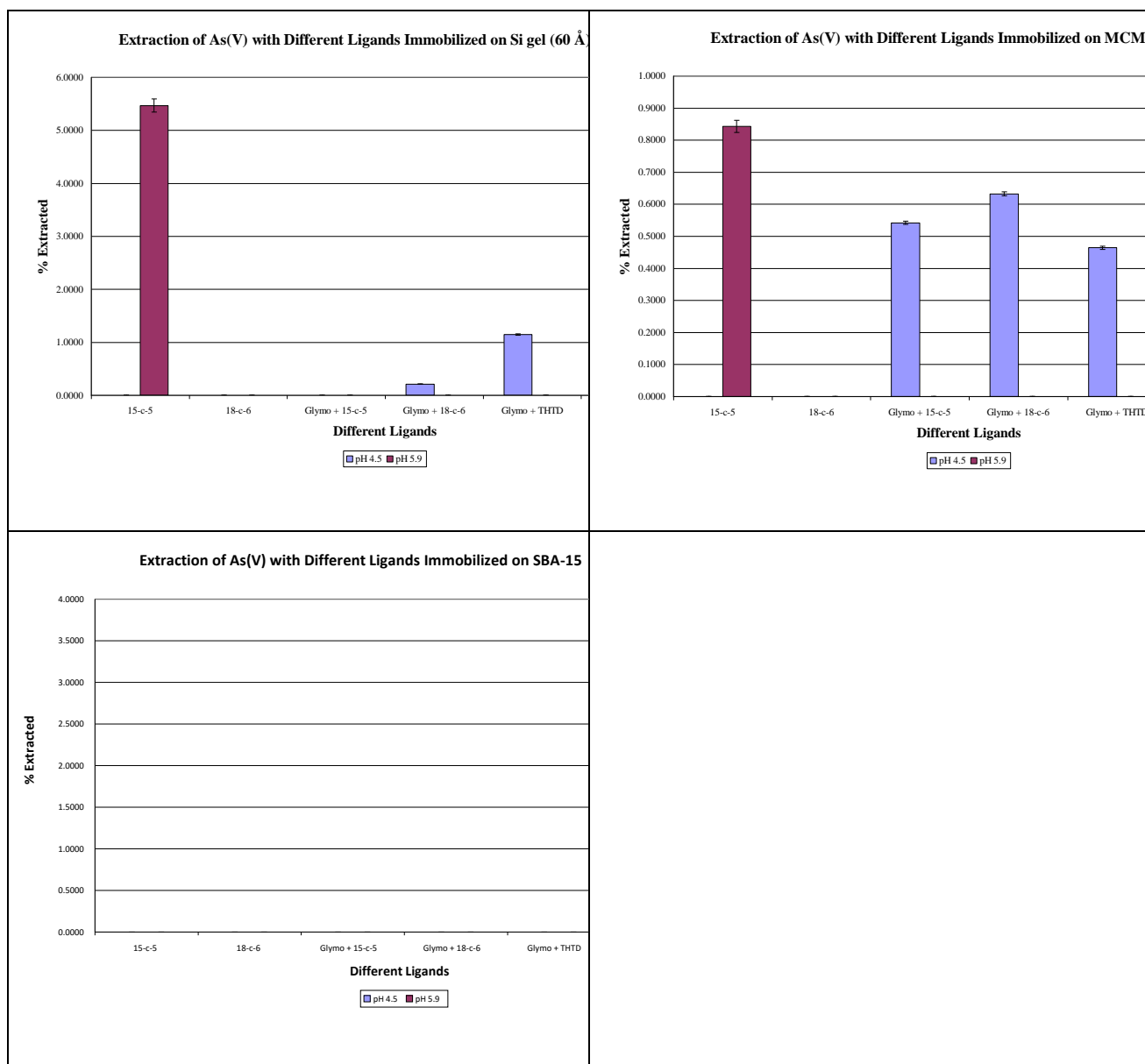


Figure 3.9: The extraction of As(V) with various ligands immobilised on four different silica supports

3.5.1.2 Extraction of Cd(II) with various ligands immobilised on four different silica supports

The decision for immobilising THTD and THTUD as ligands on the silica supports, was based on their unusually high formation constants with Cd^{2+} , as can be seen in Table 3.10.

Table 3.10: The comparison between the stability constants ($\log K$) of THPTD, THPTUD, [10]-ane-N₃, THETAC and TETA are shown (Barnard, 2008)

	THPTD	THPTUD	[10]-ane-N ₃	THETAC	TETA
Cd(II)	19.38	18.05	9.1	10.6	18.25

1,4,7-tris[2(S)-hydroxypropyl]-1,4,7-triazacyclodecane (THPTD) has the highest formation constant – 19.38 while THPTUD (Barnard, 2008) and TETA have almost the same value. Since THPTD and THPTUD have the same design and basic structure, it was decided to use these two similar ligands to immobilize on the silica substrates.

Table 3.11: The pK_a values of the two free azamacrocyclic ligands are shown (Barnard, 2008)

	pK_1	pK_2
THPTD	9.18	4.26
THPTUD	11.32	5.87

The pK_a values in Table 3.11 indicate that the free ligands are deprotonated at the pH values that are being used for the extractions. It is anticipated though that the electronic structure and behaviour of the ligands will change slightly once they are immobilised on the silica substrates due to the influence of the supports as well as the influence of the spacer. These changes should not be so drastic that it would change the behaviour of the ligands after immobilisation.

The average extraction of Cd²⁺ at a pH of 4.5 with the various ligands immobilized on Si gel (60 Å), was less than 2.5%. Although THPTD showed some extraction with Cd²⁺, it was still less than 2.5% and is therefore considered to have zero extraction with Cd²⁺ (Figure 3.10). The other ligands did not extract any Cd²⁺ at all. All the values fall within the experimental error.

With the pH raised to 5.9, the average extraction with the immobilized ligands on Si gel (60 Å) increased to 15.2% (ligands are 45% effective). With the exception of 18-c-6 and 15-c-5 with glymo, the other ligands all participated in the extraction (figure 4.2). The only support that failed to extract any of the Cd²⁺ was HMS. The ligands on this support showed no extraction at all.

The average extraction increased significantly with the various supports with the exception of HMS at the higher pH of 5.9. At the lower pH, no extraction with any of the ligands immobilised on any of the

supports was possible. It appears that extraction with THTD, although slightly lower than the crown ether, is more selective towards the Cd^{2+} at the two pH values since it shows extraction with all the supports except with HMS, while the crown ethers only extracted with Si gel (60 Å) and SBA-15.

Cd^{2+} is considered to be a fairly soft metal ion and it has a radius of 0.95 Å (Luckay et al., 1996). The Cd^{2+} metal ions should therefore not favour the oxygen donors of the crown ethers, but rather that of the softer nitrogen donors. The cavity sizes of the azamacrocycles are smaller than that of the crown ethers and this should then lead to the azamacrocycles being more selective towards the Cd^{2+} metal ions. It is interesting to note that 18-c-6 on SBA-15 (35.9%) and the glymo 18-c-6 (37.7%) on Si gel (60 Å) show almost the same extraction for Cd^{2+} . It might be because the crown ether can fold itself around the smaller Cd^{2+} , much the way it does with K^+ , since Cd^{2+} is smaller than K^+ . Also, because of the presence of the N atoms which are used as an anchor point to the glymo spacer, Cd^{2+} can perhaps be incorporated between the N atom of the “anchor”, the O atom of the hydroxyl group and an O atom of the crown ether.

For comparison purposes we have looked at other work involving Cd^{2+} extraction. Kumbasar studied the extraction of Cd in detail. The extraction depended on surfactant concentration, acid concentration, solute concentration and time. At optimum conditions, Kumbasar achieved 96% extraction using selective membranes. Cadmium iodide anions were targeted by using an Amberlite LA-2 exchanger (Kumbasar, 2010; Kumbasar, 2013). Mahmoud and Al-bishri worked at a pH of 1 using $\text{Emim}^+\text{Tf}_2\text{N}^-$ and $\text{Omim}^+\text{Tf}_2\text{N}^-$ on nano-silica. The adsorption capacities obtained ranged between 1.2 and 1.3 mmol g^{-1} (97.25 -99.30%).

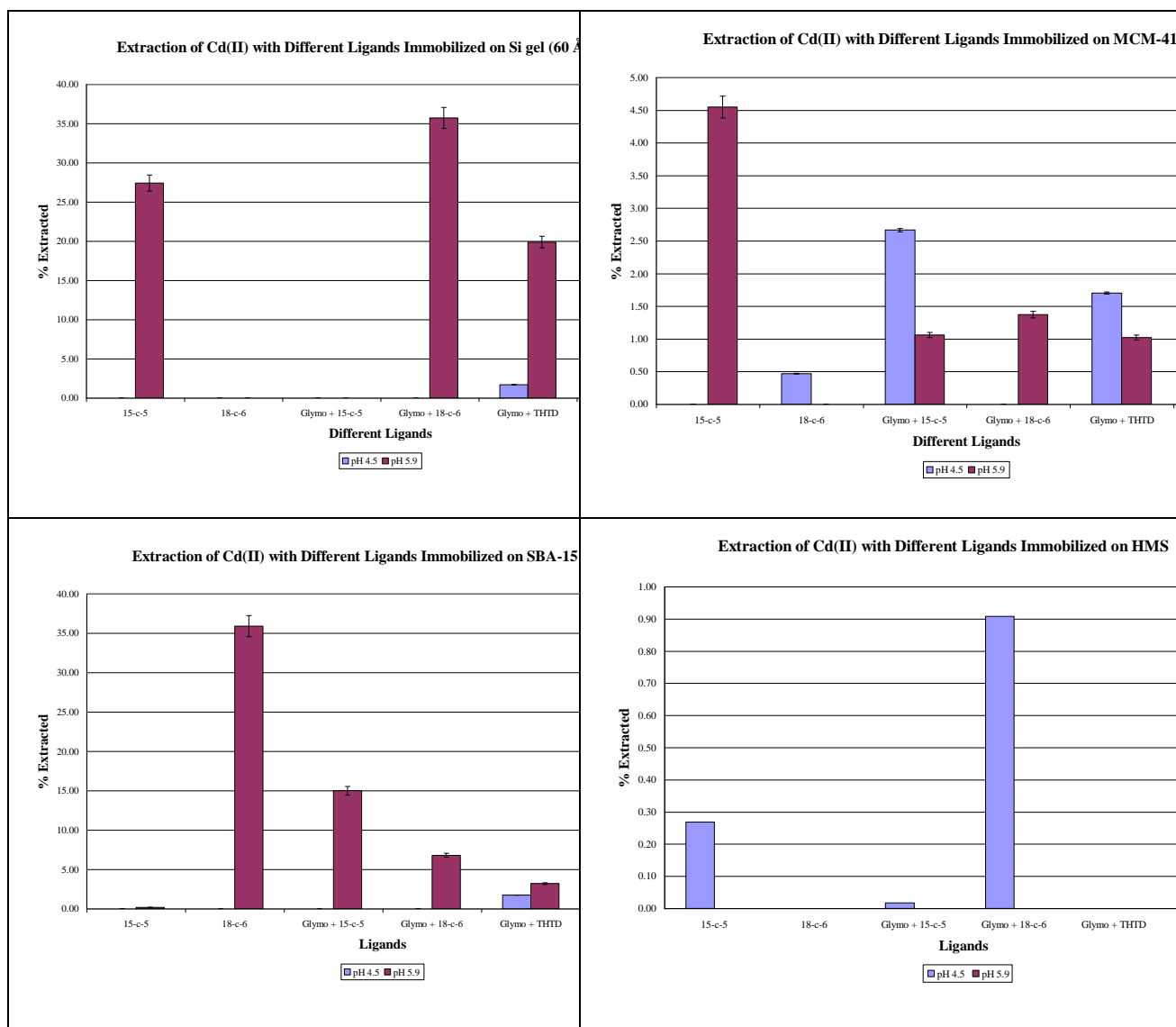


Figure 3.10: The extraction of Cd(II) with various ligands immobilised on four different Si supports

Equilibrium constants ($\log K$) have been determined by Wassink and co-workers 2000 for the extraction of Cd^{2+} chloride complexes with Aliquat 336 in benzene from LiCl solutions and were found to be 8.17. In chloroform, the extraction from HCl was lower with a value of 5.66. This means that Cd^{2+} is strongly extracted from chloride solutions by Aliquat 336 (Wassink et al., 2000).

3.5.1.3 Extraction of Cr(VI) with various ligands immobilised on four different silica supports

Chromium is normally found as one of the following species: $\text{Cr}_2\text{O}_7^{2-}$, CrO_4^{2-} or HCrO_4^- . It appears that the ligands have the right configuration to accommodate the metal ions. The extraction was carried out in an acidic medium, which means that the ligands were partially protonated. The ligands could be positively charged. The ligands could thus coordinate the negatively charged chromium species.

With the solution buffered at 4.5, the average extraction for the different ligands, immobilised on Si gel (60 Å) were 11.7% (ligands are 34% effective), of which THTD (21.4-64% effective) and THTUD (23.9-90% effective) were the best performing ligands (Figure 3.11).

With the pH raised to 5.9, the average extraction increased dramatically, as expected, to 25.8%. The THTD (33.8% -90% effective) and THTUD (33.7% -95% effective) were again the most effective ligands to use.

With the pH at 4.5, MCM-41 was the least effective support to use. SBA-15 and HMS were almost the same with an average extraction of $\pm 10\%$ (ligands are 40% effective). THTD was the best ligand to use. With the pH at 5.9, even the other supports showed a dramatic increase in the extraction capabilities with the various ligands. THTD again proved the most selective ligand of the “six” to use when extracting $H_xCr_yO_z^{-n}$.

With the Si gel (60 Å), it is interesting to note that the extraction increased as the length of the spacer increased. With the MCM-41 and SBA-15, the extraction stayed almost constant, but there was a slight decline when HMS was used as a support. 15-c-5 was the least effective ligand with an average extraction of 18.7% (52% effective). 1,4,7-tris[2(S)-hydroxypropyl]-1,4,7-triazacyclodecane (THTD) performed the best on all supports and it had an average extraction capability of 33.1% (90% effective). 18-c-6 immobilised with glymo and THTUD were very close to each other with an average extraction of $\pm 25\%$.

The increase in the extraction when a spacer is used with the ligand on the Si gel (60 Å), is most probably because there is more freedom for the ligands to move about in the solution. When a shorter spacer is used, the ligand is very close to the support and the metal ions may find it harder to get close to the ligand.

$H_xCr_yO_z^{-n}$ is known as a hard acid, and the ligands that were used contain hard oxygen and borderline/hard nitrogen donors. Therefore it is quite a reasonable assumption that the hard donors and the hard acid will complex very well in the case of $H_xCr_yO_z^{-n}$.

It does not look like the different surface areas of the silica supports had any influence on the working of the ligands because with the higher pH, the extraction was also high. The only factor that had a profound influence on the degree of extraction was the difference in the pH. With all the different ligands attached to the different supports, it is clear that there is a dramatic increase in the extraction as the pH increased from 4.5 to 5.9.

A number of experiments were conducted by various groups to find the best and most efficient way for the removal of chromium from waste solutions. Agrawal, Pal and Sahu used cyanex 923 and obtained very high yield of up to 99% under optimum conditions which included an initial feed of 1 g/L. The only

metal to interfere with their results was Zn (Agrawal et al., 2008). Hossain used non-traditional solvents such as sunflower oil and lubricant oil in conjunction with Aliquat 336 to remove hexavalent chromium from ground water and industrial water. Extraction of 50-96% was achieved at a pH of between 6 and 8 (Hossain, 2013).

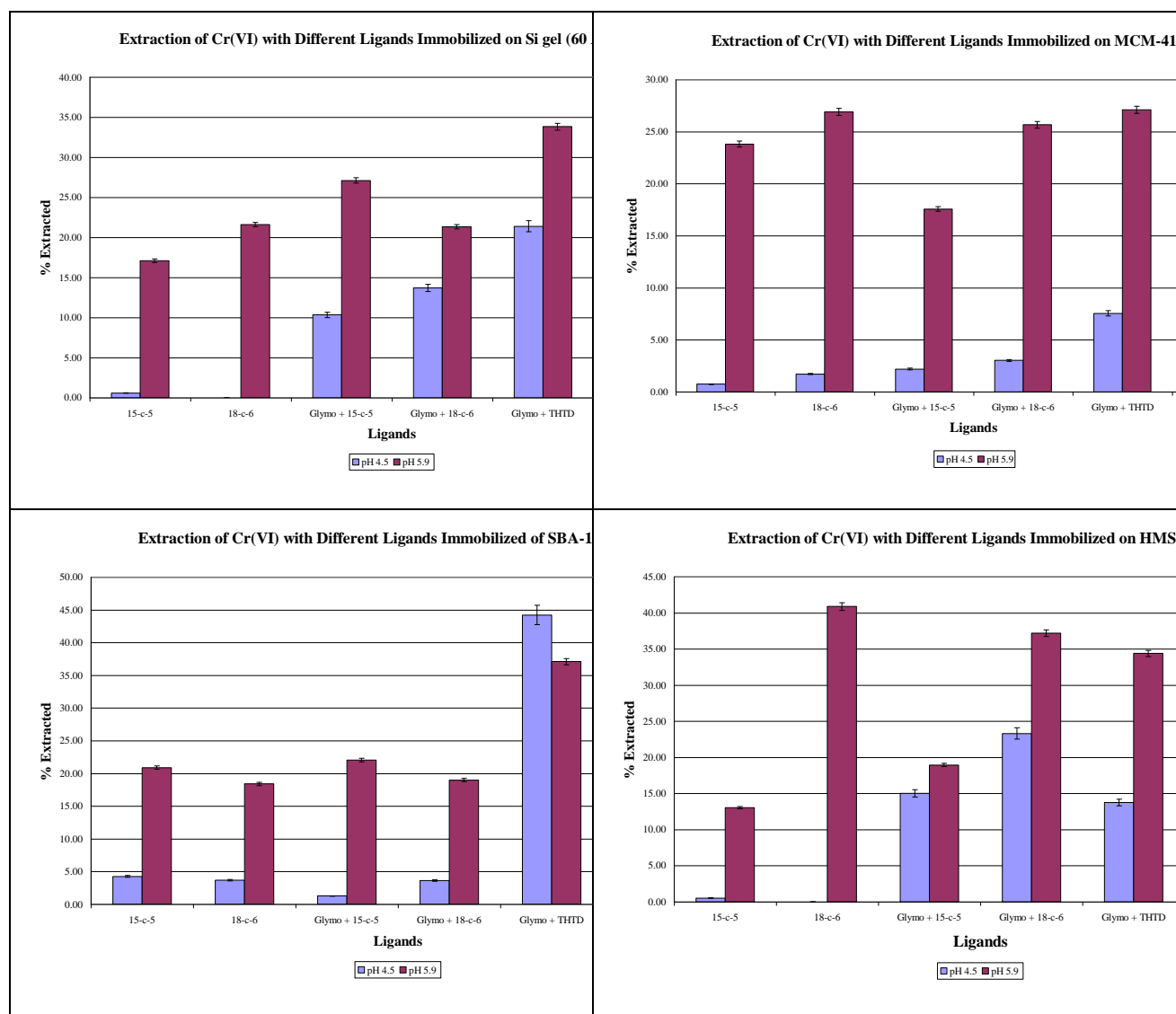


Figure 3.11: The extraction of Cr(VI) with various ligands immobilised on four different Si supports.

The average extraction of $H_xCr_yO_z^{-n}$ for Si gel (60 Å) with each of the different ligands immobilised increased from approximately 11.46% to 25.79%. For MCM-41 there was an increase from 2.70% to 24.14%. There was an increase from 9.40% to 24.13% for SBA-15 and finally for HMS the increase was from 10.62% to 25.76%. It appears that Si gel (60 Å) is the best support for immobilisation of each of the ligands when used for the extraction of $H_xCr_yO_z^{-n}$. A reason for this observation is that the Si gel (60

Å) could have a much more even distribution of the immobilised ligands on the surface. This even distribution would give a larger contact surface for the $H_xCr_yO_z^{-n}$ ions to coordinate to the ligands.

3.5.1.4 Extraction of Sr(II) with various ligands immobilised on four different silica supports

With the pH at 4.5, it was found that no Sr^{2+} was extracted with any of the ligands immobilised on any of the supports (figure 3.12). There was a remarkable improvement in the extraction when the pH was increased to 5.9. The average extraction with all the ligands immobilised on Si gel (60 Å) was 10.0% (ligands are 30% effective) and with MCM-41 as a support the average extraction was 9.0% (ligands are 27% effective). The extraction with SBA-15 as support was less than 1%.

As expected, the best extraction was obtained using the crown ethers. The 15-c-5 immobilised with the glymo spacer on Si gel (60 Å) gave an extraction of 25.4% (ligand is 75% effective) while 18-c-6 immobilised with the glymo spacer on MCM-41 yielded 24.5%. With the exception of 18-c-6 immobilised directly on HMS (30.2%), it is clear that the better extraction was obtained as the spacer was introduced. THPTD and THPTUD did not perform as well with the extraction of the Sr^{2+} , as was expected. There is an unusual occurrence with the THPTD and THPTUD immobilised on MCM-41. The nitrogen donating ligands performed better than the crown ethers with the exception of 18-c-6 immobilised with the glymo to the support. It is also interesting to note that 15-c-5 immobilised with a spacer on Si gel (60 Å) performed the same as the 18-c-6 immobilised with the spacer on MCM-41. Both 15-c-5 and 18-c-6 immobilised with spacers on SBA-15 extracted Sr^{2+} equally well. It was found that the best average extraction was obtained by using the 18-c-6 ligand (11.0%) and the best support is the Si gel (60 Å). The 15-c-5 and 18-c-6 ligands that were immobilised with the glymo spacer yielded an average extraction of 9.3% and 9.3% respectively (Figure 3.12).

Wood et al., 1997 used DtBuCH18C6 for the removal of ^{90}Sr and Pb (>99%) in batch solvent extraction experiments. It was found that this method was more selective towards Pb. The extraction was very much dependent on the nitric acid concentration of the solutions (Wood et al., 1997).

Wai et al. (1999) reported that Sr^{2+} is selectively extracted from aqueous solutions into supercritical fluid CO_2 by DC18C6. They also reported that any of the 18-membered crown ethers with a radius in the range of 1.3-1.4 Å are most suitable as hosts for Sr^{2+} which has a radius of 1.13 Å (Wai et al., 1999). Izatt et al. (1976) determined the $\log K$ value for Sr^{2+} with the free ligand 18-c-6, to be 2.72 (Hancock et al., 2007). Hancock et al. (2007), reported the radius of Sr^{2+} as 1.18 Å. 18-c-6 has an estimated radius of 1.38 Å. This means that Sr^{2+} should fit very well into the cavity of this crown ether. It may therefore appear that

size match selectivity plays a role in the extraction process. Sr^{2+} is considered to be a hard acid. The crown ethers contain hard oxygen donors that prefer to coordinate with hard acids. This may be another reason why there is better selectivity when the crown ethers are used. The azamacrocycles have two slight drawbacks. Firstly, the radii are much smaller than that of the crown ethers and secondly, the nitrogen donor atoms are not as hard as the oxygen donors. The nitrogen donors are considered to be borderline/hard in their soft/hard properties. With regards to the better extraction when a spacer is introduced, it could well mean that there is better interaction between the metal ions and the ligands. The influence of the supports are minimised, and the longer spacer gives more freedom to the ligands to move around in solution as not constrained by the spacer.

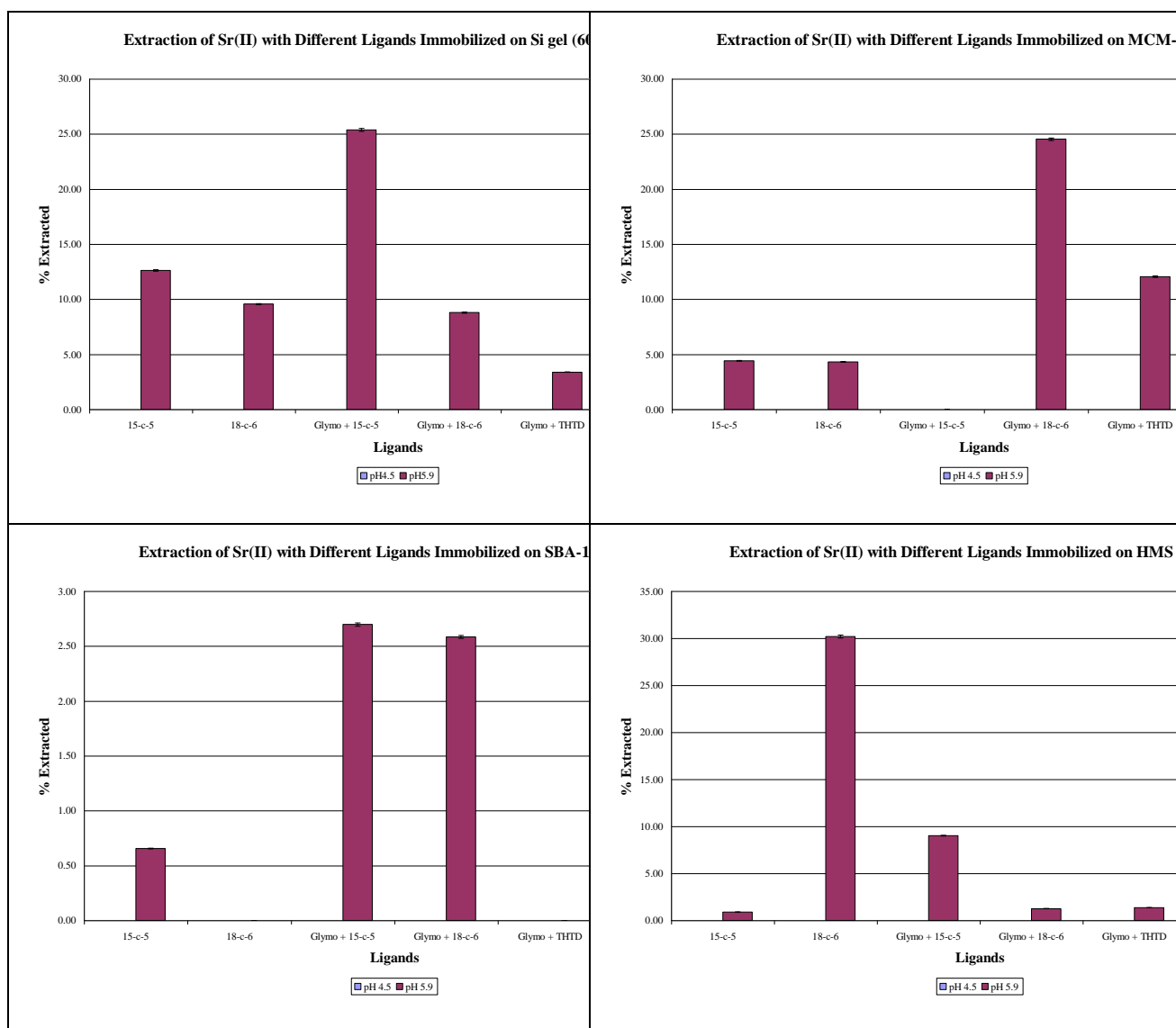


Figure 3.12: The extraction of Sr(II) with various ligands immobilised on four different Si supports

3.5.1.5 Extraction of Hg(II) with various ligands immobilised on four different silica supports

No extraction of Hg^{2+} occurred at a pH of 5.9 when using any of the ligands in any combination with the supports. Since no extraction was possible at the higher pH, it was decided not to do the extraction at pH 4.5.

Hg^{2+} is considered to be a soft acid. The ligands that were used for the extraction are all hard or borderline. Although Hg^{2+} has a radius of 1.1 Å, and can fit into the cavities of the crown ethers, the size match selectivity cannot overcome the hardness of the ligands and thus no extraction was possible.

Since Hg^{2+} is very acidic, this means that other species may be present to prevent complexation with the crown ethers. With the free ligands, the $\log K$ value for Hg^{2+} with 18-C-6 is 2.42 and for 15-C-5 it is 1.68 according to Izatt et al. (1976). The $\log K$ values are very low, so complexations with the crown ethers are not all that favourable.

3.5.1.6 Extraction of U(VI) with various ligands immobilised on four different silica supports

The average extraction of U(VI) for the different ligands on the various supports ranged between 13% and 16.5%. HMS was the best support (16.5%) and MCM-41 was the worst (13%). All the ligands showed extraction of the uranyl. The best ligand for the extraction was 15-c-5 (17.5% -ligand is 50% effective) which was directly immobilised on the supports. The second best was the 18-c-6 (15.0%), also directly immobilised on the supports. When the spacer was introduced, the extraction of the uranyl decreased. This trend was observed for the crown ethers on all the supports. This confirmed the findings of Szigethy and Raymond (1999). The chelator orientation about the uranyl strongly depends on the length of the spacer and it was found that ligands that were immobilised with short flexible spacers coordinate better to the uranyl than the same ligand with a longer spacer. The best extraction was achieved with 15-c-5 (25.7% ligand is 70% effective), immobilised directly on HMS (Figure 3.13).

THTD (14.7%) and THTUD (13.6%) performed better than the crown ethers that were immobilised with the spacers. Because UO_2^{2+} is so acidic, it was decided that the extraction at pH 4.5 would not provide better results since all other extraction showed that a higher extraction is obtained at the higher pH.

Yuan et al. (2012) compared various supports and found that the results between SBA-15 and MCM-41 were similar (Yuan et al., 2012).

Sadeghi and Sheikhzadeh adjusted their pH to 5.5. It was proven that hydrolysis of the APMS system was resistant to a pH range between 3 and 8. It was also shown that a lowering of the pH decreased the uptake

capacity of the sorbent. A maximum extraction of 1.13 mmol g^{-1} was achieved (Sadeghi and Sheikhzadeh, 2009). Yuan et al. (2012) showed that the maximum sorption of U(VI) with DIMS (dihydroimidazole functionalised SBA-15) was 268 mg g^{-1} at pH 5.0. (Yuan et al., 2012) The extraction of UO_2^{2+} was therefore done only at pH 5.9. Gruner and co-workers also reported that only very weak complexation with UO_2^{2+} occurs at pH 4.5-5 (Gruner et al., 2002; Aydeef et al., 1978).

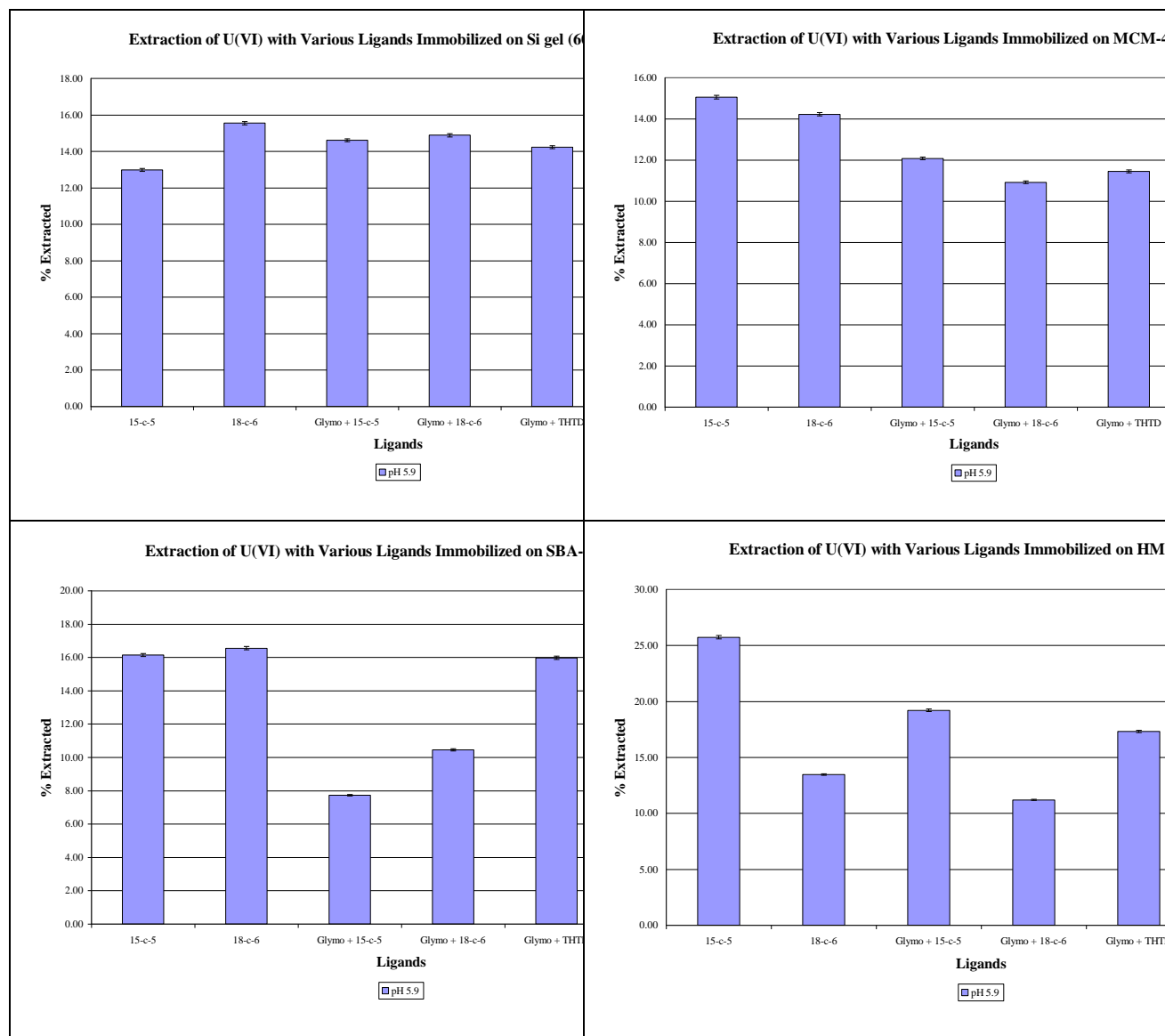


Figure 3.13: The extraction of UO_2^{2+} with various ligands immobilised on four different Si supports

The uranyl ion is considered to be a hard Lewis acid. This means that the uranyl ion will have a greater affinity for hard donors. Szigethy and Raymond (1999) found that there was a profound affinity between uranyl and the crown ethers. Since the crown ethers contain only hard oxygen donors, it is understandable that the crown ether should have a great affinity for the uranyl ion according to the Irving-Williams classification system. The tri-azamacrocycles are borderline/hard donors and it is thus not strange that there would be some affinity for the uranyl. The nitrogen may not be as hard as the oxygen donors in the ring, but there are oxygen donors on the pendant arms that will show affinity towards the uranyl ion.

Uranyl is a big molecule and cannot fit into the cavities of the crown ethers and definitely not in the azamacrocycles. It is therefore clear that the uranyl must be situated on the outside of the cavities of the macrocycles. It was found by Szigethy and Raymond that the uranyl ion definitely coordinates to form the preferred pentagon. Even when there was considerable strain when the ideal angle changed from 72° to 65.2° , the preferred structure was still the pentagon (Szigethy and Raymond, 1999).

3.5.1.7 The extraction of two metal ions with various ligands immobilised on four different silica supports

The competitive extraction of Hg^{2+} and UO_2^{2+} was executed at pH 5.9 since the extraction at pH 4.5 was very weak. There was high selectivity in the extraction between Hg^{2+} and UO_2^{2+} since no Hg^{2+} was extracted. Only UO_2^{2+} was extracted.

Again it was clear that the crown ethers that were immobilised directly onto the support extracted the UO_2^{2+} better than the crown ethers that were immobilised with the glymo spacer. On average, the ligands that are supported on the Si gel (60 Å) produced the best results (9.2% - ligands are 27% effective). 18-c-6 (13.6%) and THTUD (14.4% ligand is 56% effective) were the best ligands for the extraction (Figure 3.14).

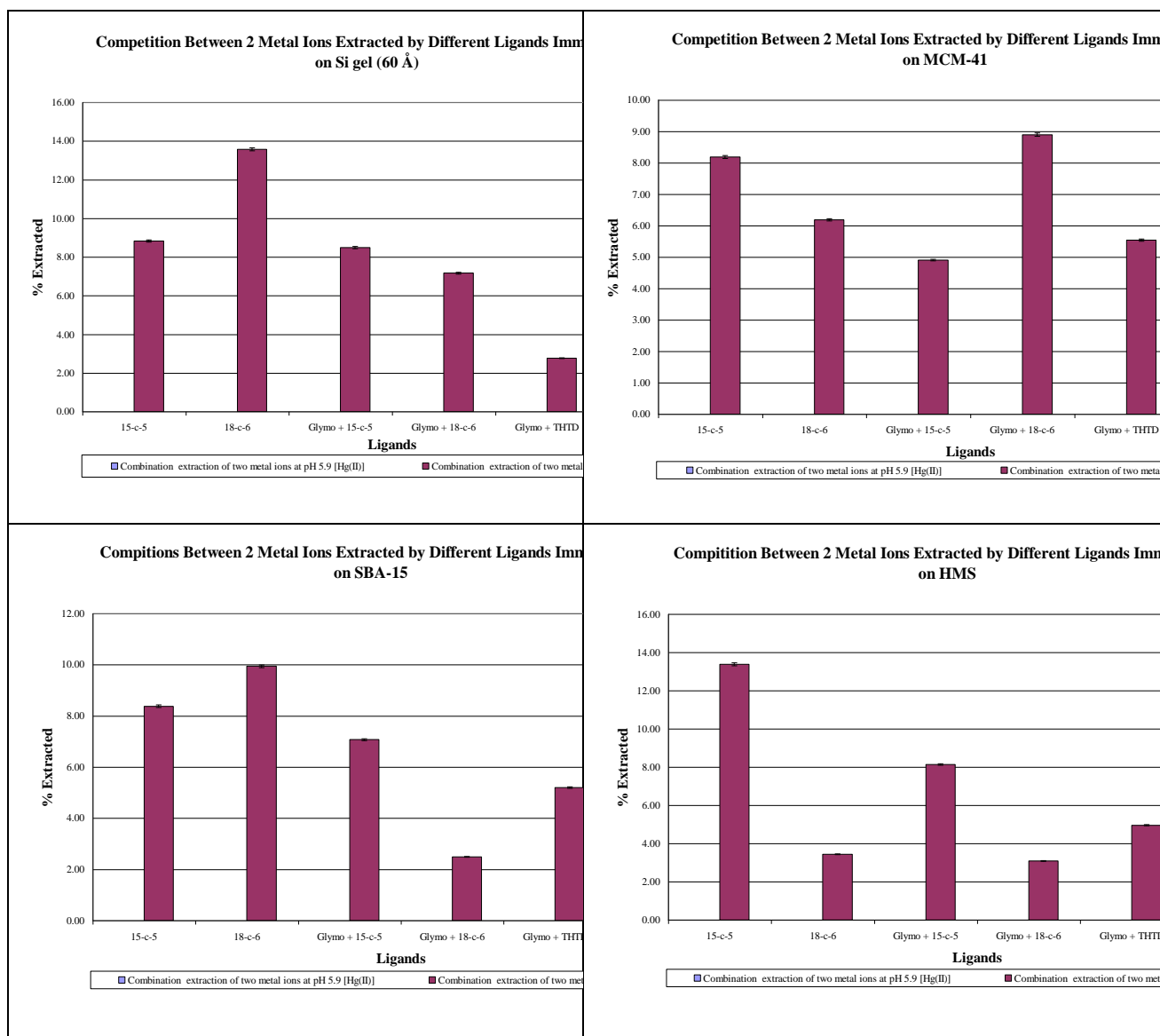


Figure 3.14: The extraction of 2 metal ions with various ligands immobilised on four different Si supports

The average extraction of Hg^{2+} and UO_2^{2+} with 15-c-5, directly immobilised on the supports is 9.7% (ligand is 30% effective). Of the crown ethers, the highest extraction was achieved with 18-c-6 (13.6%), directly immobilised on Si gel (60 Å). The best extraction though was achieved with THTD (14.4% - ligand is 56% effective) immobilised on Si gel (60 Å).

There is a slight decline in the extraction capacity when two metal ions are in competition with each other. Both uranyl and the mercury ions are very big ions and one reason could thus be that there is a lot of shielding by the Hg^{2+} which means that the UO_2^{2+} cannot get close to the ligands for extraction in the time that was allowed. It appears therefore that the immobilised ligands are so overwhelmed by the sheer amount of metal ions, that the time allowed for extraction was just not enough. Since there is less contact between the UO_2^{2+} and the ligands in the extraction time period, the extraction will not be as efficient as

was the case when only UO_2^{2+} was extracted. The extraction trend with the single metal ion and that of the combination with two metal ions are similar in almost all respects, except for the extraction percentage that was achieved.

3.5.1.8 The extraction of four different metal ions with various ligands immobilised on four different silica supports.

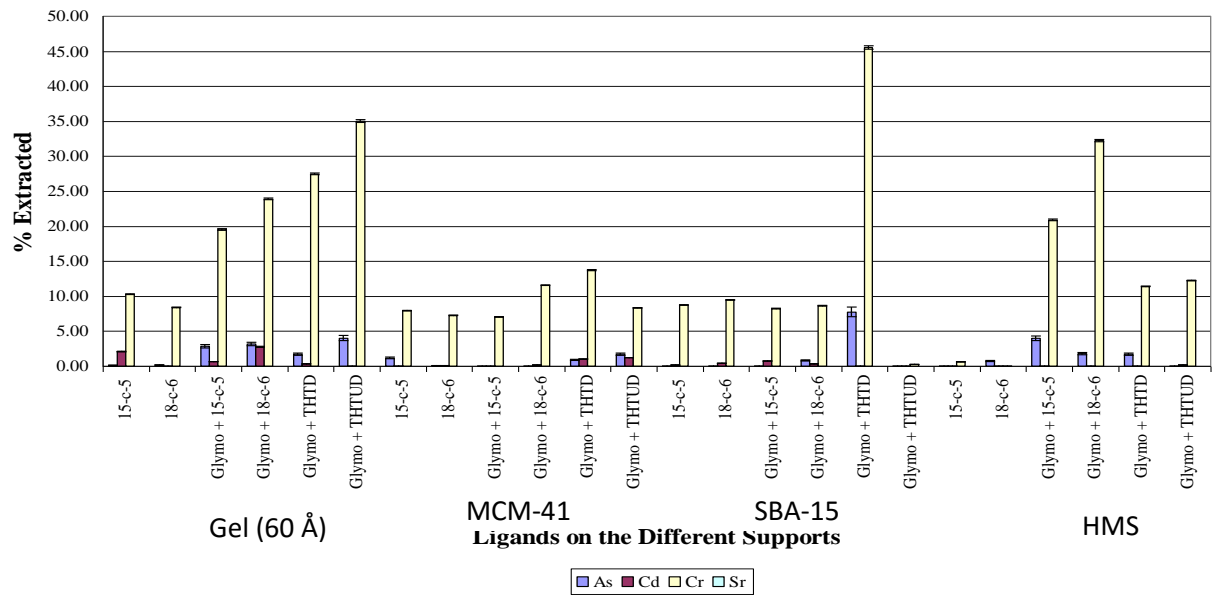
With the pH at 4.5, it can be seen that the only extraction occurred with $\text{H}_x\text{Cr}_y\text{O}_z^{-n}$. The overall extraction of the $\text{H}_x\text{Cr}_y\text{O}_z^{-n}$ is 7.0%. The other metal ions had an extraction of less than 2.3%. With the pH increased to 5.9, the overall percentage of the extraction of metal ions decreased. The interesting fact is actually that more metal ions now get extracted and the extraction is not limited to the $\text{H}_x\text{Cr}_y\text{O}_z^{-n}$ alone. Although more metal ions get extracted, it can be seen that the $\text{H}_x\text{Cr}_y\text{O}_z^{-n}$ is preferred in the competition extraction (Figure 3.15).

The ligand that is more selective towards $\text{H}_x\text{Cr}_y\text{O}_z^{-n}$ with this combination of metal ions, is the THTD. It appears that the hardness of the ligand and that of the metal ion is the major driving force for the extraction. Size match selectivity is therefore a secondary contributing factor.

The two supports that yielded the best results with the immobilised ligands in the competitive extraction with four metal ions were Si gel (60 Å) and HMS. It would appear that the surface area, pore volume and pore diameters distribute the immobilised ligands more evenly. This gives the ligands, attached to their supports, the freedom to move about in the solution. The metal ions in the solution on the other hand also move about the solution easier and can get closer to the ligands. The other supports have smaller surface areas, pore diameter and pore volumes. This influences the total surface areas of the supports that can be used for immobilisation. Because of the “smaller” surface area that is available for immobilisation, the ligands are forced closer to each other. This hampers the free movement of the ligands on their supports. The metal ions can also not get into close proximity of the ligands and thus less metal ions can be extracted.

The slight decline in the extraction capacities can be attributed to the amount of metal ions that were introduced to the solution. In this instance, it could be a matter of “first come first served”. Once a metal ion is complexed to the ligand, there is little chance that another metal will replace it. There is also the $\text{H}_n\text{AsO}^{-x}$ that might act in a kind of shielding manner, preventing other metal ions from coming into contact with the ligands in the time that was allowed.

Competition Between 4 Metal Ions with Varians Ligands Immobilized on Different Supports (pH 4.5)



Competition between 4 Metal Ions Extracted by Various Ligands Immobilized on Different Supports (pH 5.9)

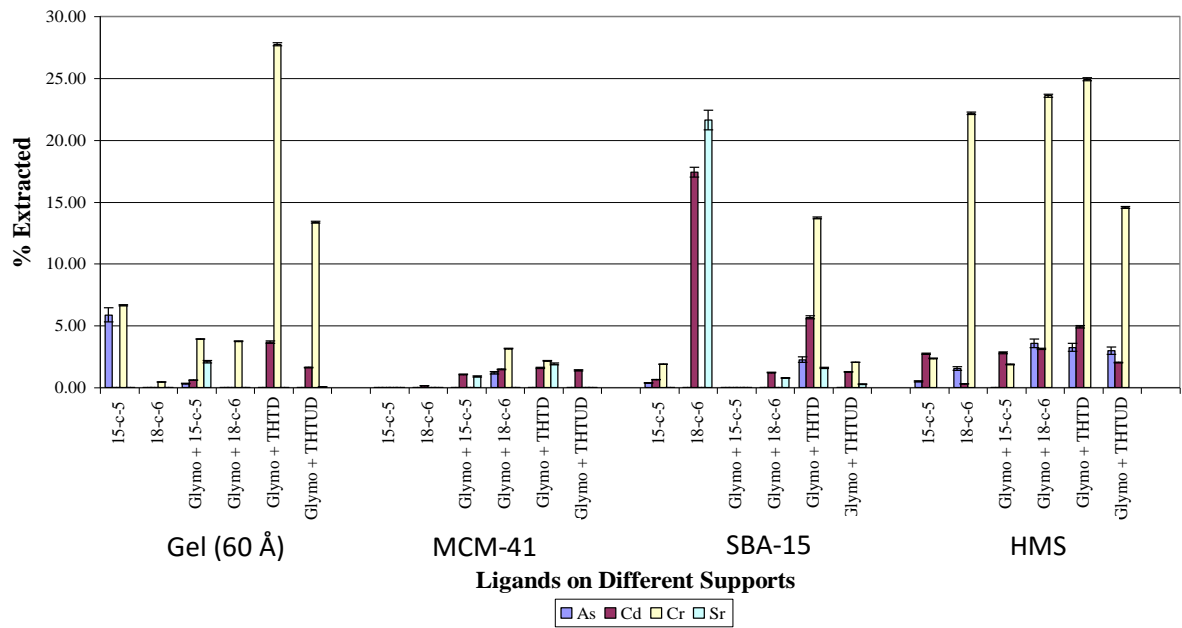


Figure 3.15: The extraction of metal ions with various ligands immobilised on four different Si supports.

3.5.1.9 The extraction of various metal ions with 15-c-5 directly immobilised on different silica supports.

At a pH of 4.5 there was very little extraction of any metal ions with the exception of a small amount of $H_xCr_yO_z^{-n}$. With the pH at 5.9, the extraction of $H_xCr_yO_z^{-n}$ increased to more than 20%. It was also found that UO_2^{2+} was extracted in significant amount. With the ligand supported on HMS, the extraction of uranyl increased to 25.7%. From Figure 3.16, it is clear that the best support though, is Si gel (60 Å). More metal ions are extracted with 15-c-5 immobilized on this particular support than with any of the other ligands and supports. It is proposed that the overall surface area is more accessible than the other supports due to the fact that the pore diameter and pore volume is also available while with the other supports, the pore opening is so small, the ligands cannot enter the cavity, leaving just the outside surface to be used for immobilisation.

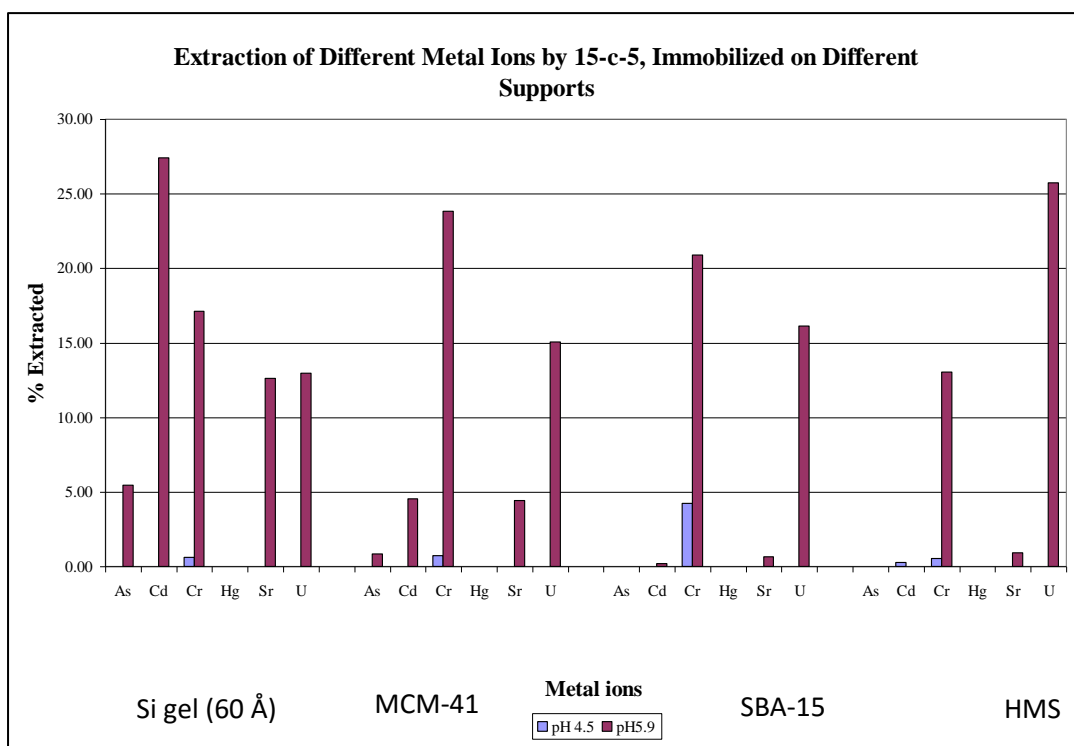


Figure 3.16: The extraction of various metal ions with 15-c-5, directly immobilised on different silica supports. It is proposed that there is crowding of the ligands on the surface of the support, and the metal ions cannot get in between the ligands to be extracted.

3.5.1.10 The extraction of various metal ions with 18-c-6 directly immobilised on different silica supports.

With the pH at 4.5, there was no extraction of any of the metal ions with the exception of a small amount of $H_xCr_yO_z^{-n}$ in conjunction with the supports MCM-41 and SBA-15. With the pH raised to 5.9, the extraction of $H_xCr_yO_z^{-n}$ increased remarkably, especially with HMS as support (40.9%). It can also be seen that the extraction of Cr^{6+} increased as the length of the spacer increased. As expected, the extraction of UO_2^{2+} also increased with all 18-c-6 immobilised on the different supports. The extraction of Sr^{2+} shows a significant increase with HMS as the support. Only with SBA-15 no extraction of Sr^{2+} was achieved (Figure 3.17).

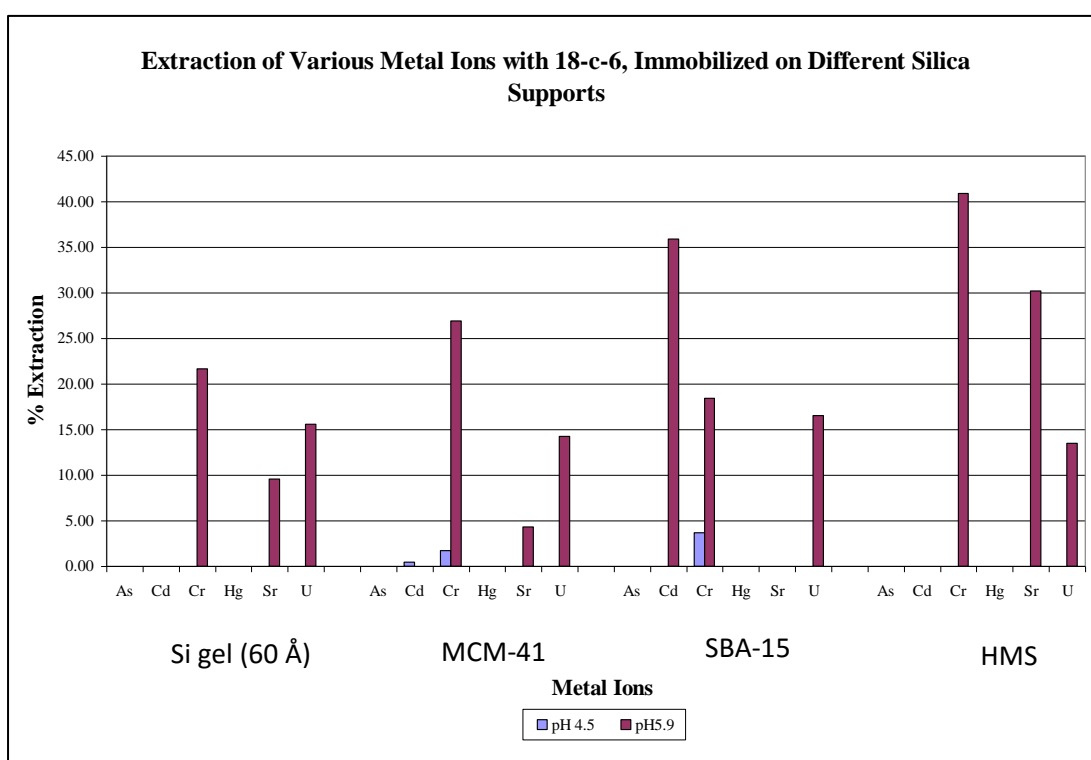


Figure 3.17: The extraction of various metal ions with 18-c-6, directly immobilised on different silica supports.

The fact that Cd^{2+} is extracted by 18-c-6 on SBA-15 is perhaps due to synergism. It is quite strange that no other support showed the same enhanced cooperation.

3.5.1.11 The extraction of various metal ions with 15-c-5 immobilised with a glymo spacer on different silica supports.

$H_xCr_yO_z^{-n}$ showed a fairly low extraction by the two supports, Si gel (60 Å) and HMS with the pH at 4.5. When the pH was increased to 5.9, the extraction of $H_xCr_yO_z^{-n}$, Sr^{2+} and UO_2^{2+} increased significantly (Figure 3.18). With Si gel (60 Å) as support, the percentage extraction was considerably higher.

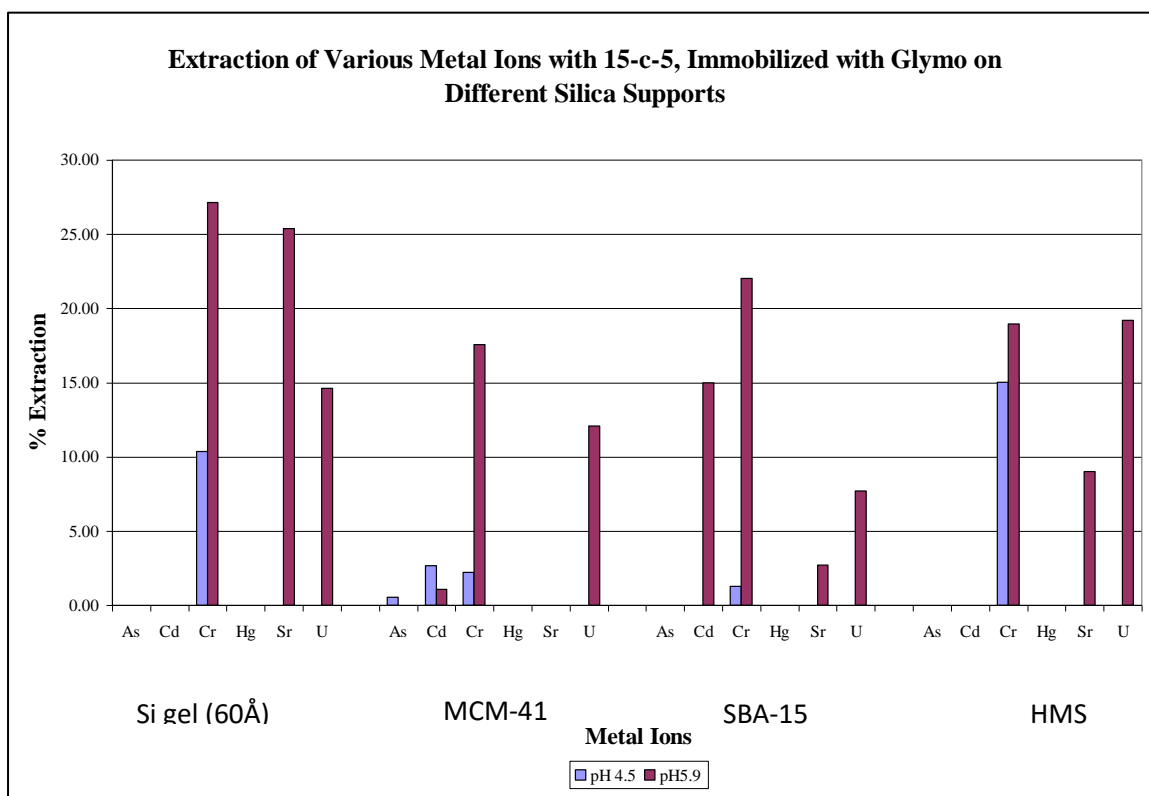


Figure 3.18: The extraction of various metal ions with 15-c-5, immobilised with a glymo spacer on different silica supports.

The extraction decreased with the use of MCM-41 and was even lower with SBA-15, and the worst support was HMS (Figure 3.18). From the data (Figure 3.18) it can be seen that 15-c-5, immobilised with a glymo spacer is more selective towards $H_xCr_yO_z^{-n}$, Sr^{2+} and UO_2^{2+} , irrespective of the silica support that was used.

3.5.1.12 The extraction of various metal ions with 18-c-6, immobilised with a glymo spacer on different silica supports.

Only $H_xCr_yO_z^{-n}$ showed any extraction at all with the pH at 4.5. At pH 5.9 there is quite a substantial increase in the extraction of all the metal ions, especially Sr^{2+} with the MCM-41 as support. Cd^{2+} shows good extraction (36%) with the ligand supported on Si gel (60 Å).

This is extraordinary considering that no Cd^{2+} is extracted with the ligands supported directly onto the support. It appears that the ligand has more flexibility to move about in the solution to coordinate to the metal ion. Sr^{2+} and UO_2^{2+} are being extracted in more significant quantities as is expected. Si gel (60 Å) again is the best support to use, since it can be seen that the extractions of all the metal ions, with the exception of the extraction of Cr^{6+} (HMS), is much higher than that of any of the other supports (Figure 3.19).

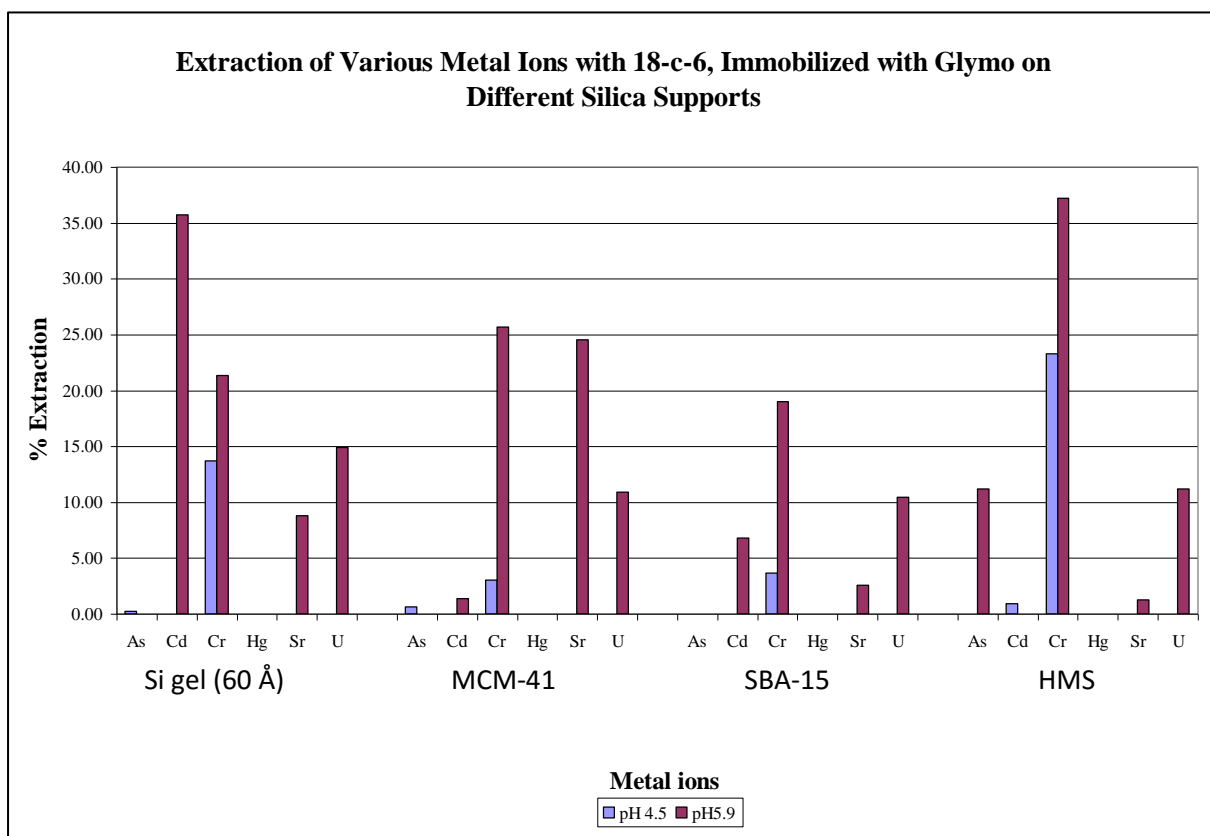


Figure 3.19: The extraction of various metal ions with 18-c-6, immobilised with a glymo spacer on different supports.

3.5.1.13 The extraction of various metal ions with THTD, immobilized with a glymo spacer on different silica supports.

At the lower pH of 4.5, there was a small extraction of Cd^{2+} and $\text{H}_x\text{Cr}_y\text{O}_z^{-n}$ (Figure 3.20).

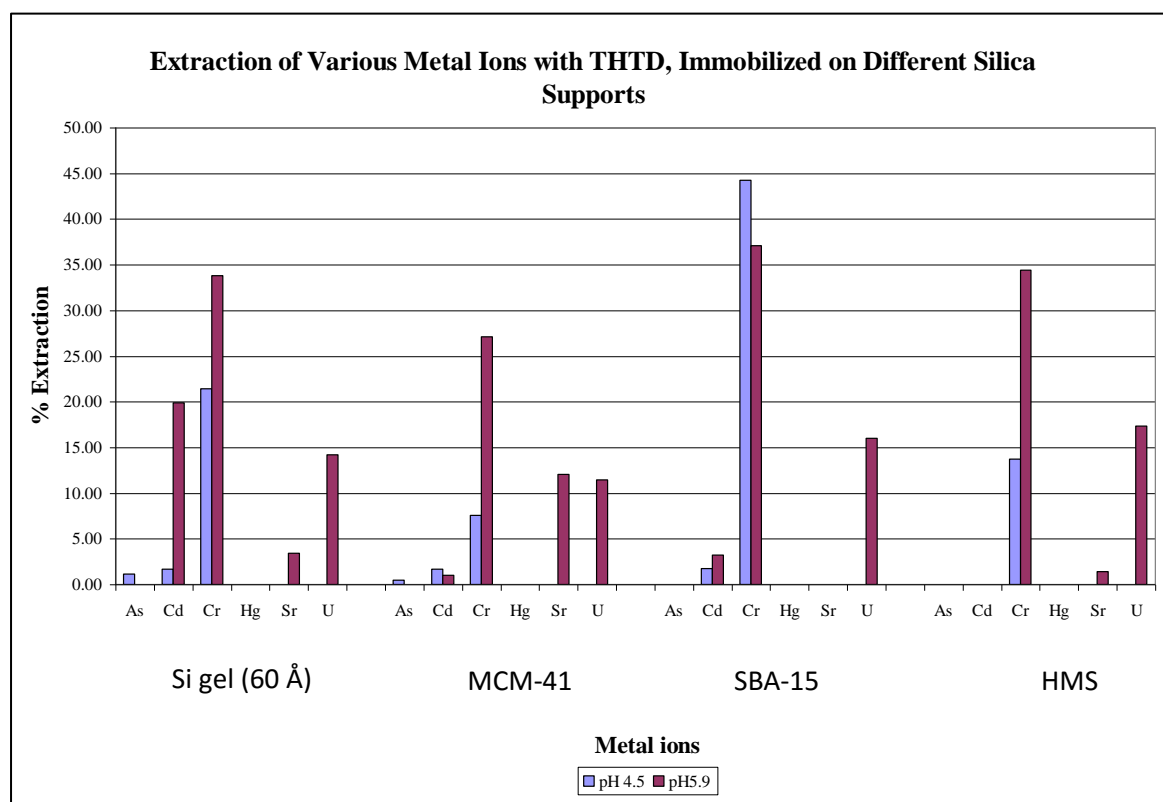


Figure 3.20: The extraction of various metal ions with THTD, immobilised with a glymo spacer on different silica supports.

The extraction of $\text{H}_x\text{Cr}_y\text{O}_z^{-n}$ at the pH value of 4.5 is quite prominent, especially when Si gel (60 Å) and SBA-15 were used as supports. There is the unusual result of the extraction being better at pH 4.5 rather than 5.9. As expected, with the increase in the pH to 5.9, the average extraction also increased. Cd^{2+} shows an improvement in extraction with Si gel (60 Å) as a support. The % extraction of $\text{H}_x\text{Cr}_y\text{O}_z^{-n}$ also increased significantly. Previously, no Sr^{2+} was extracted, but with the higher pH, all the supports except SBA-15 show a slight extraction. THTD extracted significant amounts of uranyl on all the supports. Si gel (60 Å) is again better to use as a support with this ligand (Figure 3.20).

3.5.1.14 The extraction of various metal ions with THTUD, immobilised with a glymo spacer on different silica supports.

The only notable extraction at pH 4.5 was that of $H_xCr_yO_z^{-n}$ with the Si gel (60 Å) as support (Figure 3.21). As expected, the extraction increased with the pH at 5.9. Cd^{2+} shows extraction when Si gel (60 Å) is used as a support and to a much lesser extent, with the MCM-41 as well. The $H_xCr_yO_z^{-n}$ is extracted in the range of 10-34% with this ligand anchored on any of the 4 supports. THTUD extracted the UO_2^{2+} in quite significant amounts (11-17.5%) with any of the supports that were used (Figure 3.21).

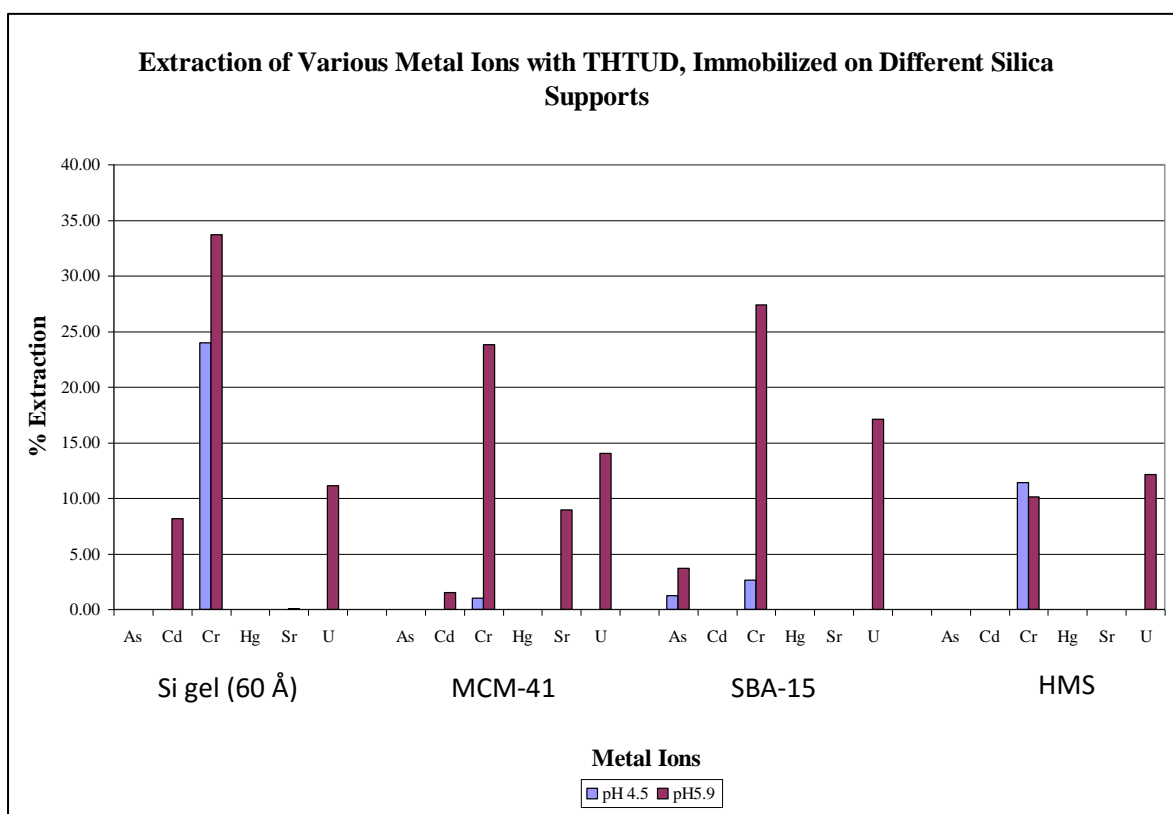


Figure 3.21: The extraction of various metal ions with THTUD, immobilised with a glymo spacer on different silica supports.

Si gel (60 Å) is best support to use, while the other supports show a definite decline in the extraction of the various metal ions. The higher extraction percentage of $H_xCr_yO_z^{-n}$ at a pH value of 4.5 when HMS was used, showed a negligible difference as HMS is the lowest in terms of surface area, pore size and pore volume of the four supports. Throughout the extraction experiments, its performance was the least effective as support.

3.5.1.15 Discussion of the Protonation Constants: Influence of the pH on the Extraction

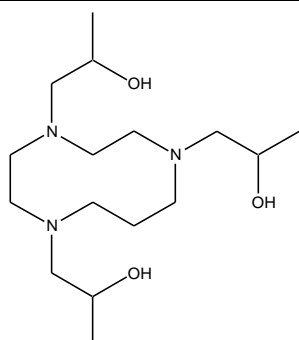
There is competition between the protons and the metal ion for the ligand. For coordination of the ligand to the metal ion to take place, the ligand and/or the metal ion must be deprotonated. As the solution becomes more basic, the metal ions can form hydroxide complexes because of the excess OH^- . Other species may also be found when the species distribution is investigated.

For the tri-azamacrocycles, it is possible to determine protonation constants, for this will give an indication of the competition that can arise during the complexation with metal ions when extraction experiments are conducted at various pH levels. These protonation constants for the free ligands, THTD and THTUD (Figure 3.22), are shown in Table 3.13 along with the parent and other similar ligands. These protonation constants are determined for the free ligands, however, when the ligands are attached (via spacers) to the supports, the protonation constants could be different, because electronically, the immobilised ligands are now different from the free ligands.

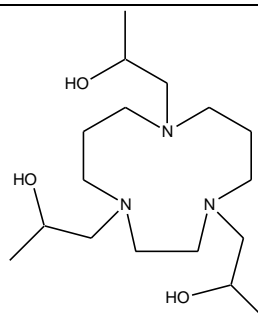
At the lower pH of 4.5 THTD will be protonated. THTUD has 2 protons on the nitrogen atoms. One of these protons is held in position in the cavity by the two nitrogen donor atoms. The occupation of the macrocyclic cavity, and the fact that the donor atoms are already attached to the protons, will prevent the complexation with the metal ions. In order to achieve complexation, it is necessary to work at a higher pH to prevent the ligands from being protonated. There are no protonation constants for the crown ethers.

Table 3.12: The log(K) values of ligands with similar structures to THTD and THTUD.

No.		Log(K_1)	Log(K_2)	Log(K_3)
1	1,4,7-tris[2-(<i>S</i>)-hydroxypropyl]-1,4,7-triazacyclodecane (THTD) Barnard, 2008	9.18	4.20	
2	1,4,8-tris[2-(<i>S</i>)-hydroxypropyl]-1,4,8-triazacycloundecane (THTUD) Barnard, 2008	11.32	5.87	
3	1,4,7-tris(2-hydroxyethyl)-1,4,7-triazacyclononane (THETAC) Smith et al., 2009; Sayer et al., 1983	11.50	3.42	
4	1,4,7-triazacyclononane (9-ane-N ₃) Martell and R.J. Motekaites, 1988	10.44	6.81	
5	1,4,7-triazacyclodecane (10-ane-N ₃) Sayer et al., 1983	12.00	6.61	
6	1,4,8-triazacycloundecane (11-ane-N ₃) Sayer et al., 1983	12.00	7.61	
7	1,4,7-triazacyclononane-N,N',N''-triacetic acid (NOTA)	11.60	5.70	3.17
8	1,4,7-triazacyclodecane-N,N',N''-triacetic acid (DETA)	N/A	6.12	3.69
9	1,4,8-triazacyclodecane-N,N',N''-triacetic acid	N/A	7.20	3.40



THTD



THTUD

Figure 3.22: Structures of the neutral, free ligands, THTD and THTUD.

3.6 Conclusions

Extraction experiments with just the supports were conducted. The amount of metal ions extracted was below 2.5% and can be considered to be negligible.

It is evident that a better extraction is achieved at a higher pH, in this particular study, a pH-value of 5.9, compared to 4.5. The reason may well be because the ligands are less protonated at the higher pH. This leaves the cavity as well as the donating atoms exposed, and complexation can take place.

It was found that Si gel (60 Å) is the most effective support to use. It does not always have the highest yields, but in all the extraction experiments, some extraction was obtained when Si gel (60 Å) was used as the support. A reason for this result may be because of the more favourable BET results concerning the surface area of Si gel (60 Å). The area of the Si gel (60 Å) is more accessible and can be modified more easily. MCM-41 is also a very good and easy support to use, but it is very expensive, even more than Si gel (60 Å) and the pore openings are very small which might prevent the ligands and metal ions from entering. This leads to crowding of the ligands on the surface of MCM-41 which in turn leads to less contact area for the metal ions. SBA-15 and HMS showed the least effective results as supports with all of the ligands. Their BET results showed that the usable surface areas were much lower than that of Si gel (60 Å) or that of MCM-41.

There was no affinity for As^{5+} or Hg^{2+} at either of the two pH levels. There is slight selectivity for Cd^{2+} extraction by 18-c-6, THTD and THTUD. Cr^{6+} is selectively extracted by all the ligands, independent of the support that was used. Sr^{2+} is selectively extracted by 15-c-5 and to a lesser extent by 18-c-6. Uranyl showed the same preferential affinity towards 18-c-6 and 15-c-5.

It was shown that the extraction increased for the same ligands as soon as a spacer was introduced except for the extraction of the uranyl. As the length of the spacer increased, the extraction of the immobilised ligands increased as well, except for the uranyl extraction. The reason is that the metal ions generally can come into better contact with the ligands because the ligands have more flexibility to move about in the solution, and that there is less interference from the Si supports.

4 Synthesis of ligand and immobilisation on polymer nanofibers

In this section the synthesis of a selective ligand and its immobilisation on an electrospun nanofiber mat are detailed, where after the ligand's use for selective metal extraction is presented.

4.1 Electrospinning process

Electrospinning is the method used for the production of nanofibres. The beadless nanofibres were achieved by only the concentration of the polymer. Figure 4.1 is the schematic set-up the process.

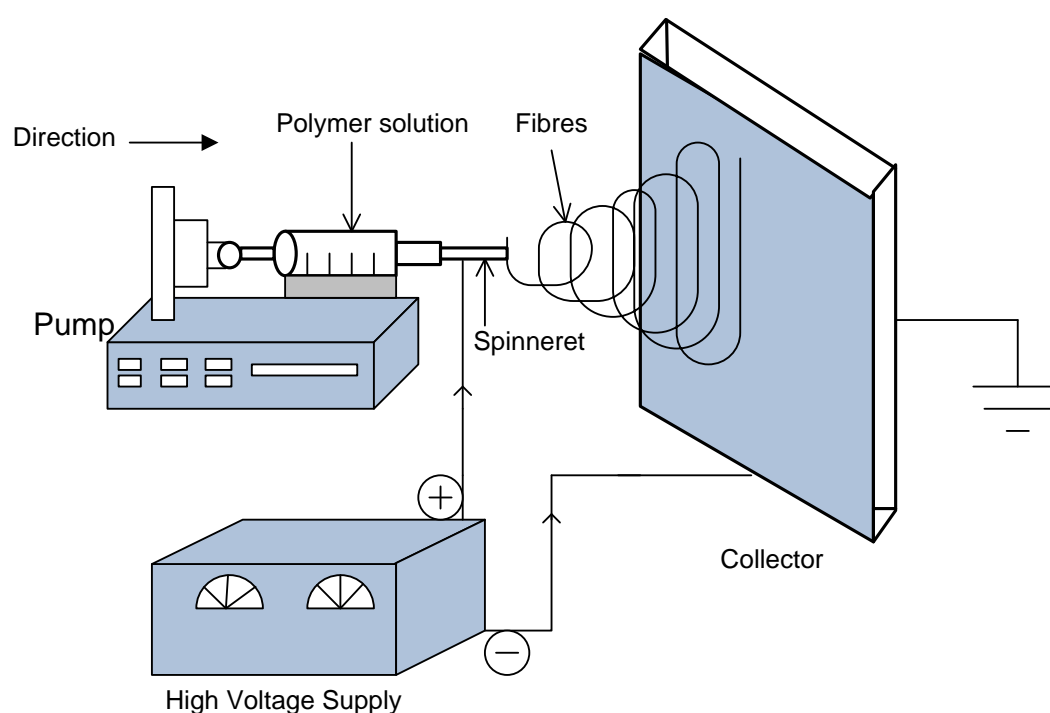


Figure 4.1: Electrospinning set-up.

4.1.1 Electrospinning of PAN solution

The electrospinning procedure was adapted from the previously conducted studies with little modification (Horzum et al., 2012; Neghlani et al., 2011). This experiment was carried out to optimise the electrospinning concentration for PAN. The following PAN concentrations were prepared in DMF (4 wt%, 6 wt%, 8 wt%, 10 wt% and 12 wt%). Each concentration was electrospun by introducing the polymer solution into a 20 mL syringe with 0.2 mm inner diameter iron needle. The syringe was fitted into a metering syringe pump (Figure 4.1). A stationary collector covered with A4 size Al foil was used. The process parameters were: applied voltage= 25 kV, flow rate= 0.4 mL/hr, collection distance= 15 cm and

the room temperature = 28°C, all were kept constant for all the concentrations during electrospinning process that lasted for 4 hours. The nanofibres from the respective 6 concentrations were mechanically collected from the Al foil and transferred into wax wraps labelled with code names; 4 wt%, 6 wt%, 8 wt%, 10 wt% and 12 wt% respectively and stored in a cupboard. Each nanofibre was characterised using HRSEM, ATR-FTIR and TGA techniques. The average fibre diameter of nanofibres from respective concentration was measured from the HRSEM image using image J software.

4.2 Synthesis of 2-pyridine amidoxime (PyAMI)

The synthesis of 2-pyridine amidoxime was adapted from Bernasek (1957) with little modification. A solution containing 2.1 g (0.030 moles) of hydroxylamine hydrochloride and 1.845 g (0.015 moles) of sodium carbonate monohydrate in 10 mL of deionised water was heated to 60°C in a closed container. 3.0 g (0.029 moles) of 2-pyridine carbonitrile was added in one portion to the solution above, followed by the addition of sufficient ethanol (approximately 10 mL) to dissolve the 2-pyridine carbonitrile. The temperature of the resultant mixture was raised to 90°C and maintained for 3 hours. The resultant product was cooled to zero degrees. The crystalline solid was filtered, washed twice with ice-cold water, transferred into a schott bottle, dried in a vacuum desiccator over calcium chloride. The dried PyAMI weighed 3.79 g. NMR, ATR-FTIR and TGA techniques were used to characterise PyAMI.

4.3 Immobilisation of 2-pyridine amidoxime on PAN-nfs (PAN-PyAMI)

For effective immobilisation of a ligand on a support, it is imperative to investigate the proper reaction pathways that can bring the two together. For the case of 2-pyridine amidoxime (PyAMI) ligand and PAN-nfs (support), the first step is to identify the reactive functional groups on the two materials. The functional group on the PAN-nfs is a nitrile group which is fairly electrophilic while the functional groups on the PyAMI are hydroxide and primary amine which are nucleophilic. However it might still be difficult to immobilise any ligands on PAN-nfs unless the nitrile group is made more electrophilic. This can be done via electrophilic assistance using a brønsted acid such as $\text{AlCl}_3 \cdot 6\text{H}_2\text{O}$ (Figure 4.2) (Kampalanonwat and Supaphol, 2014). A carbocation is thus generated on the carbon of the nitrile and this is susceptible to nucleophilic attack (Figure 4.3).

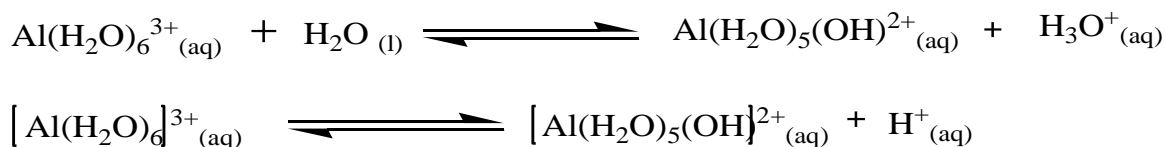


Figure 4.2: Brønsted acidity of $\text{AlCl}_3 \cdot 6\text{H}_2\text{O}$.

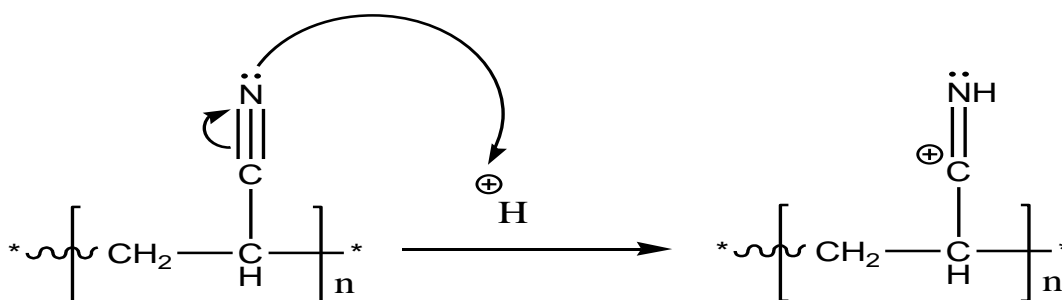


Figure 4.3: Formation of carbocation on PAN-nfs in acidic medium.

The ligand PyAMI can be immobilised either by direct or in a deprotonated form. The former can perform a nucleophilic addition using either the electron pair on neutral nucleophile nitrogen or oxygen (Figure 4.4 and Figure 4.5).

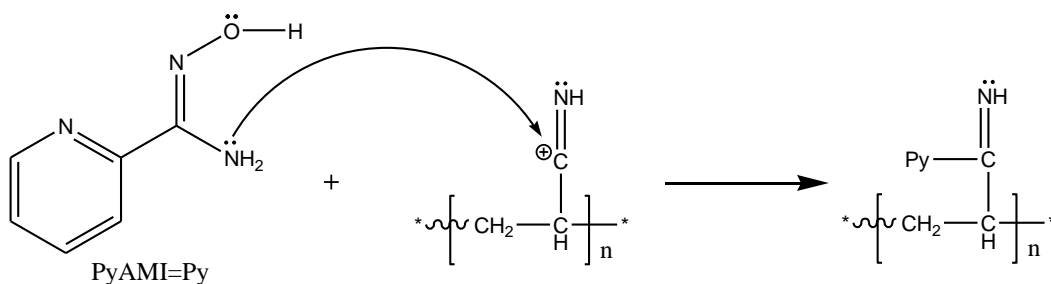


Figure 4.4: Reaction of PyAMI using nitrogen with PAN-nfs from Figure 3.3.

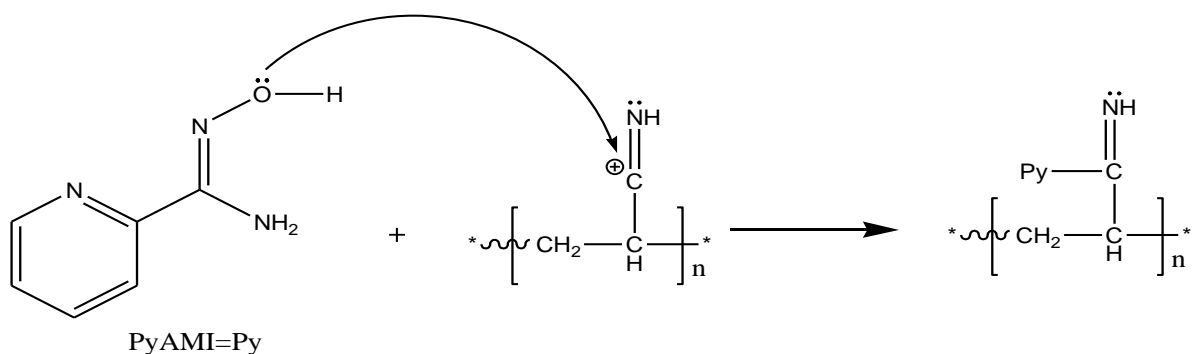


Figure 4.5: Reaction of PyAMI using oxygen with PAN-nfs from Figure 3.3.

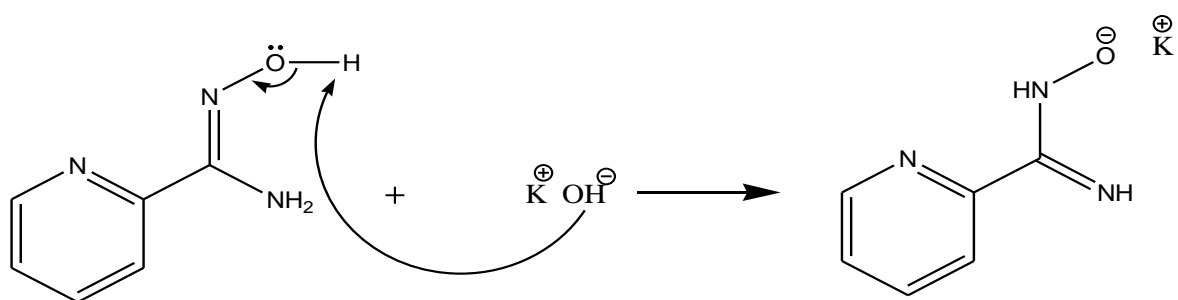


Figure 4.6: De-protonation of PyAMI on the hydroxide.

De-protonation can also occur on the hydrogen of OH from PyAMI in basic medium (Ndayambaje et al., 2016) (Figure 4.6), thereby suggesting the reaction with PAN-nfs according to Figure 4.7.

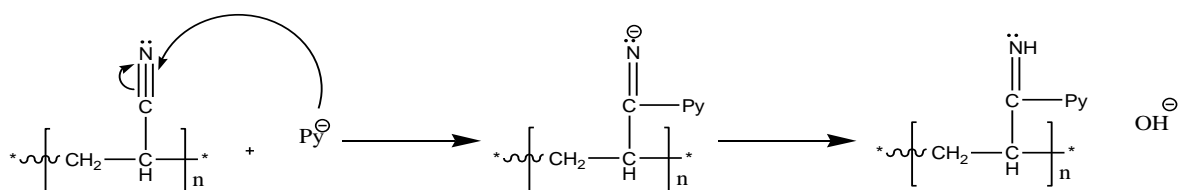


Figure 4.7: Reaction of PyAMI from Figure 3.6 with PAN-nfs.

4.3.1 Acid-catalysed immobilisation of PyAMI on PAN-nfs

6.8 g (0.05 moles) of 2-pyridine amidoxime and 4.8 g (0.02 moles) of $\text{AlCl}_3 \cdot 6\text{H}_2\text{O}$ (Kampalanonwat and Supaphol, 2014), were transferred into 50 mL deionised water in a 200 mL glass container and stirred for 15 mins at 60°C until PyAMI completely dissolved. Afterwards, 0.545 g of PAN-nfs was transferred into the solution. The reaction was carried out at different times (20, 40, 60 and 90 minutes) at 60°C . Upon the completion of the reaction, the resultant nanofibres were washed with deionised water to remove the

unreacted PyAMI and then dried in a vacuum over night at 40°C to constant weight. The resultant nanofibres were characterised using ATR-FTIR, HRSEM and TGA analysis.

4.3.2 Stability of PAN-PyAMI in EDTA & HNO₃ solutions

This experiment was carried out in order to determine the stability of PAN-PyAMI synthesised in section 4.3.1 in the metal sequestering medium. This investigation is important in order to study the possible regeneration of PAN-PyAMI. The experiments were carried out by shaking 0.1 g of PAN-PyAMI in 10 mL of 0.01 or 0.1 or 1 M EDTA and 0.01 or 0.1 or 1 M HNO₃ at 25°C for 1 hour. The nanofibre samples were then washed with deionised water, dried in a vacuum oven at 40°C for 1 hour. The resultant nanofibres were characterised using ATR-FTIR analysis.

4.4 Results and discussion

4.4.1 Polyacrylonitrile nanofibres (PAN-nfs)

From the electrospinning experiments of PAN in dimethyl formamide (section 4.1.1), PAN-nfs of different average fibre diameters (AFD) were obtained by varying the concentration (4, 6, 8, 10 and 12 wt%) of PAN in dimethyl formamide and fixing other electrospinning process parameters at; applied voltage= 25 kV, flow rate= 0.4 mL/hr and collection distance= 15 cm. The resultants PAN-nfs were characterised using HRSEM, ATR-FTIR and TGA techniques. The results are presented in the following sub-sections.

4.4.2 (High resonance scanning electron microscope (HRSEM) of PAN-nfs

HRSEM was used to observe the surface morphology of various concentrations (4, 6, 8, 10 and 12 wt%) of electrospun PAN-nfs under high magnifications. Each sample of PAN-nfs was coated with Au prior to imaging and was observed at different magnifications under HRSEM. Figure 4.8 and Figure 4.9 is the HRSEM images of PAN-nfs at different polymer concentrations in dimethyl formamide with their average fibre diameter (AFD). The images for 4 wt%, 6 wt% and 8 wt% show smooth nanofibre surfaces without beads. However, at a concentration 10 wt% and 12 wt% (Figure 4.9), there is the appearance of beads, which are conspicuous at 1000 magnification. The appearance of beads can be attributed to the higher concentration, resulting in higher surface tension, which invariably caused the polymer to clog at the end of the tip (preventing the easy ejection of the polymer fluid from the needle) thereby preventing the formation of a Taylor cone (Bhardwaj and Kundu, 2010). Therefore, instead of spinning, there was forceful ejection of polymer to the collector.

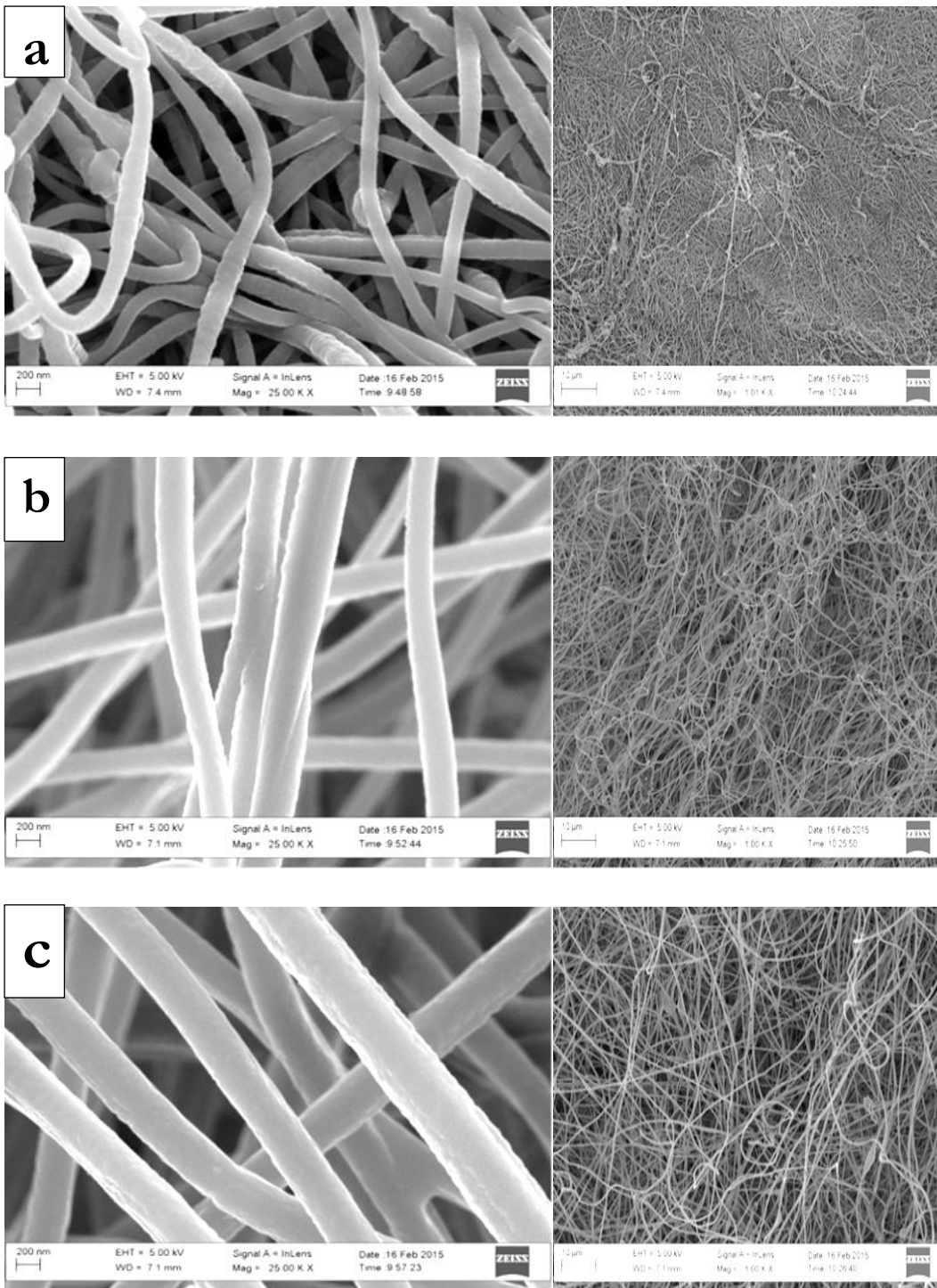


Figure 4.8: HRSEM images of PAN-nfs at (a) 4 wt% (b) 6 wt% and (c) 8 wt% concentrations in dimethyl formamide.

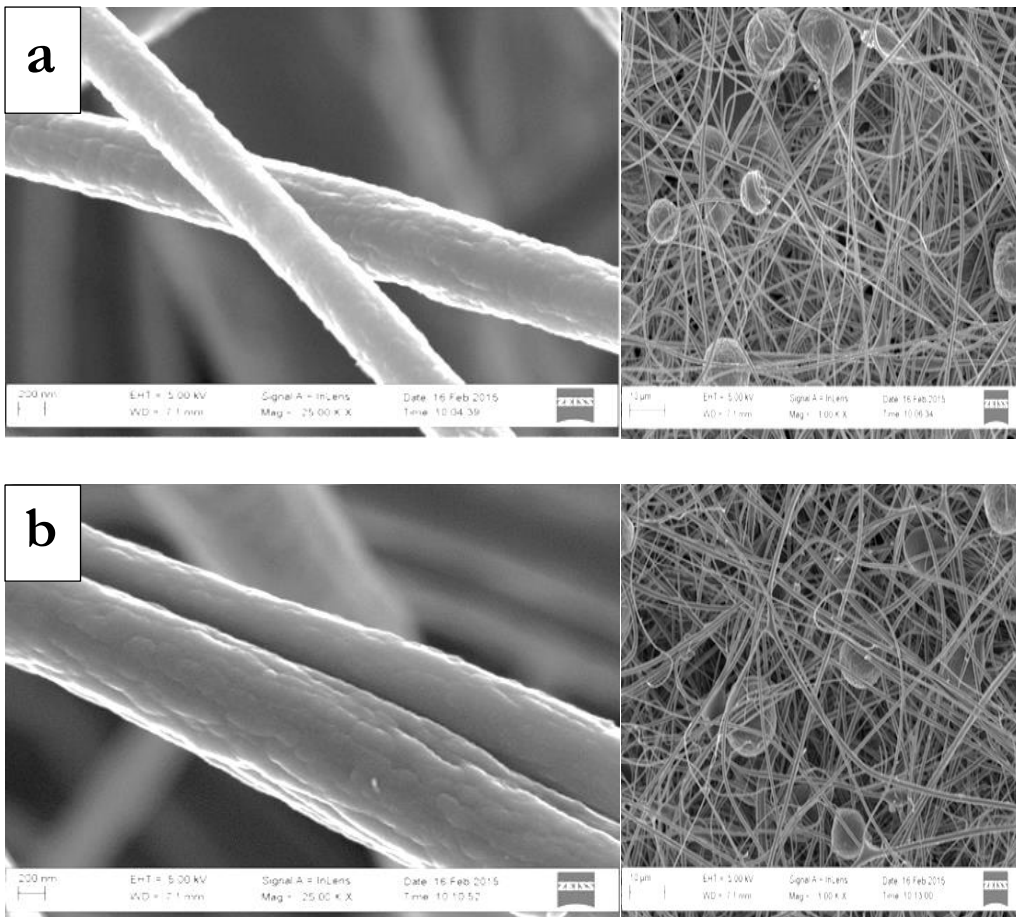


Figure 4.9: HRSEM images of PAN-nfs at (a) 10 wt% and (b) 12 wt% concentrations in dimethyl formamide.

Furthermore, to determine the average fibre diameter, image J software was used to measure the nanofibre diameter of at least 20 nanofibre strands from the HRSEM images. Figure 4.10 shows that the fibre diameter of PA6-nfs was directly proportional to polymer concentration (Bhardwaj and Kundu, 2010).

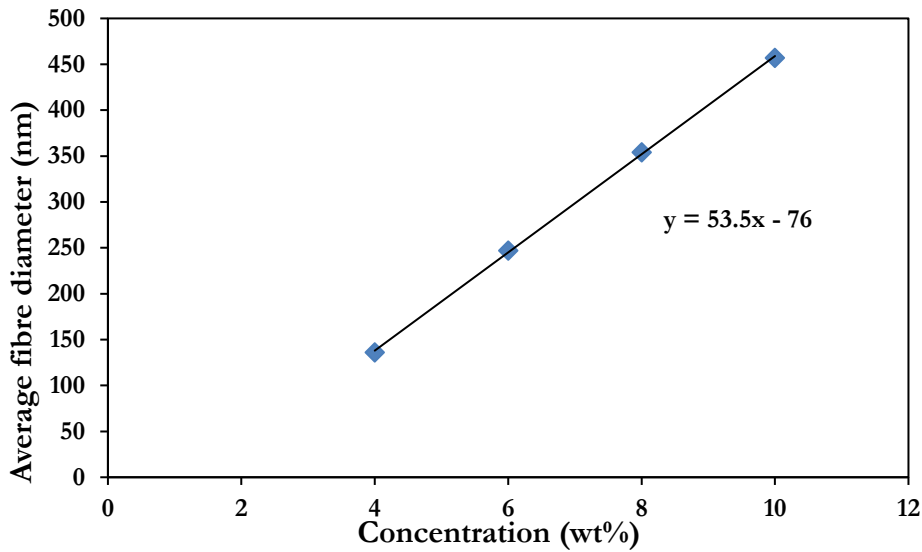


Figure 4.10: The relationship between the average fibre diameters of PAN-nfs and the polymer concentration.

Figure 4.11 shows the fibre diameter distributions of different concentrations. The average fibre diameters of 136, 247, 357, 457 and 893 nm were determined for 4, 6, 8, 10 and 12 wt% respectively, thus, confirming that the polymer concentration is directly proportional to the nanofibre diameter. This trend has also been reported for PAN in DMF by Horzum et al. (2012) and Neghlani et al. (2011).

For this study, 8 wt% was therefore chosen as the optimum concentration at electrospinning process parameters of; applied voltage= 25 kV, flow rate= 0.4 mL/hr, collection distance= 15 cm and the room temperature=28°C as 4 wt% and 6 wt% nanofibres were fragile and mechanically not strong enough because the number of entanglements of polymer chains in the polymer solution was not enough (Bhardwaj and Kundu, 2010).

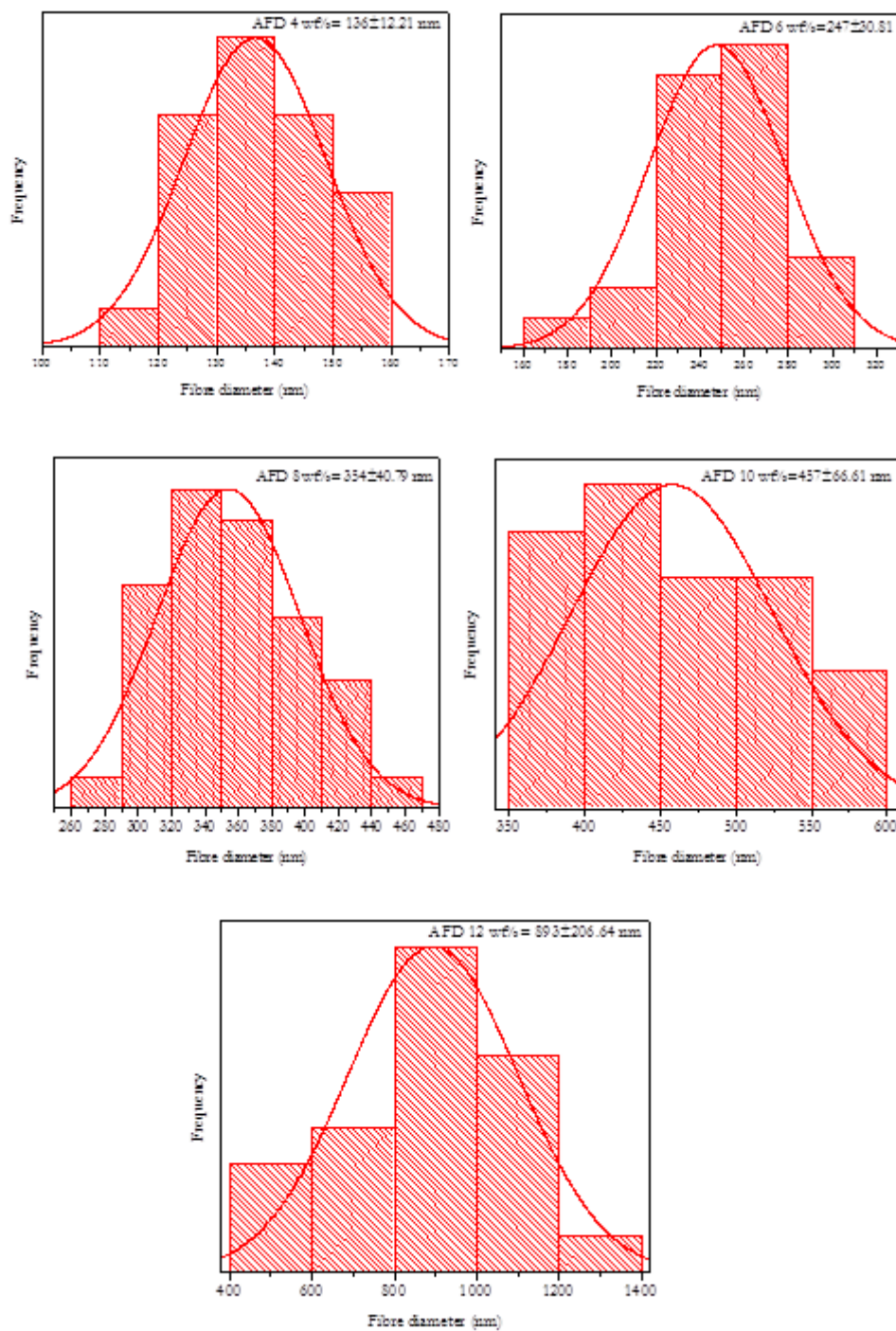


Figure 4.11: Fibre diameter distributions of PAN-nfs at different concentrations in dimethyl formamide.

The above optimum conditions were used to electrospin 8 wt% PAN until $\approx 0.5 \text{ mm}$ thickness of PAN-nfs was formed on the collector. The time to reach this thickness was 8 hours 22 minutes.

The above findings show that PAN could be electrospun into nanofibres and beadless nanofibres could be achieved at lower concentration in dimethyl formamide. This is important to this research in order to

know the parameters suitable for preparing PAN-nfs composite membrane for the adsorption of dyes. For further characterisation, ATR-FTIR was used to determine the chemical composition of PAN-nfs.

4.4.3 Attenuated total reflectance-FTIR of PAN-nfs

The ATR-FTIR analysis was carried out to investigate the functional groups on PAN-nfs. This is important to this research as PAN-nfs would be used as support for ligands via chemical reaction. ATR-FTIR was also used to understand and compare the chemical composition of 8 wt% PAN-nfs and PAN powder to check if PAN chemical composition was affected during electrospinning. Figure 4.12 is the ATR-FTIR spectra of 8 wt% PAN-nfs electrospun in DMF and PAN powder that was used to prepared PAN solution in DMF. The ATR-FTIR analysis was performed as described in section 3.3.5 over the wavelength range of 650 to 4000 cm^{-1} .

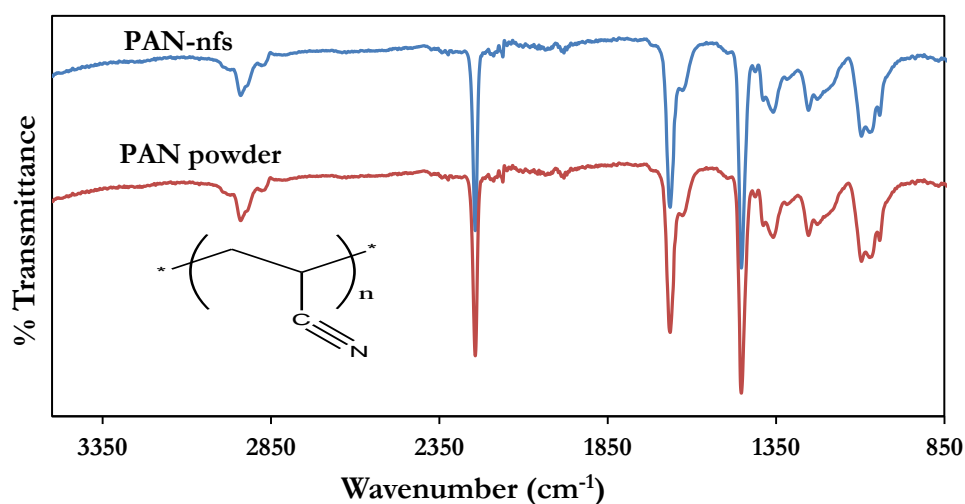


Figure 4.12: ATR-FTIR of 8 wt% PAN-nfs and PAN powder.

The ATR-FTIR spectrum of the PAN powder had the following characteristic peaks that are unique to PAN; the peak at 2930 cm^{-1} is assigned to C-H stretching vibration of CH_2 and the peak at 2241 cm^{-1} corresponded to the $\text{C}\equiv\text{N}$ stretching vibration. The strong bands at 1350 cm^{-1} , 1465 cm^{-1} and 1220 cm^{-1} are assigned to the aliphatic CH group vibrations of CH_2 groups. The appearance of a peak at 1727 cm^{-1} on PAN-nfs which corresponds to the C=O stretching vibration is assumed to have come from the C=O of methylacrylate. This means that PAN is a copolymer of acrylonitrile and methylacrylate (Korobeinyk et al., 2012; Feng et al., 2011; Neghlani et al., 2011; Saeed et al., 2008; Deng et al., 2003). Similarly, the spectrum of PAN-nfs showed the same peaks. The above findings show that the chemical composition of PAN was not affected by electrospinning process. The main reactive site of PAN (nitrile) is present and

could be ready for different chemical reaction such as amination, reduction etc. For further characterisation, TGA analysis was used to determine the thermal properties of PAN-nfs.

4.4.4 TGA profile of PAN-nfs

The TGA analysis was conducted under nitrogen and the heating rate of the sample was set at 1 °C/min up to 250°C and then 5°C /min from 250°C to 800°C. Figure 4.13 represent the thermal profile of PAN-nfs. The profile shows that PAN-nfs have two main weight loss steps. The PAN-nfs start losing their stability at temperature around 270°C to 350°C with about 16% weight loss which is attributed to nitrile oligomerisation, which produced volatile products such as HCN, NH₃ and CH₃CN. The second weight loss of PAN-nfs of about 48% occurred at 350-500°C, which is attributed to the thermal degradation reaction of PAN (Korobeinyk et al., 2012), leaving about 41% carbon residue behind. This high thermal stability is why PAN has been widely used as precursor for carbon nanofibres (CNF) (Nataraj et al., 2012). The above findings indicate that PAN-nfs is stable at temperatures below 270°C and could be used at temperatures below 270°C without causing any damage to its structure.

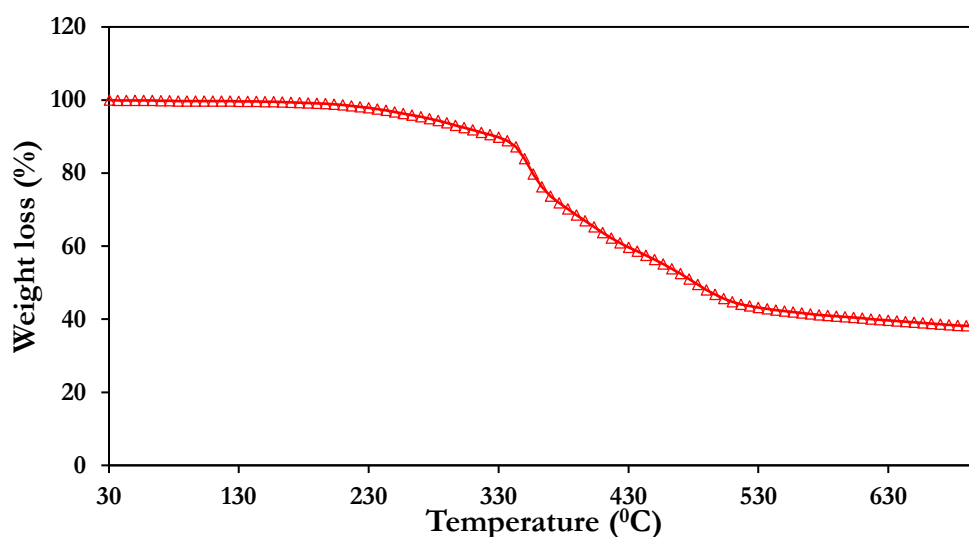


Figure 4.13: TGA profile of 8 wt% PAN-nfs under nitrogen.

4.4.5 Characterisation of PyAMI and PAN-PyAMI

This subsection gives insight into the immobilisation experiments of PyAMI on PAN-nfs. It starts with the characterisation of 2-pyridine amidoxime (PyAMI). 8 wt% PAN-nfs previously electrospun and characterised was chosen as the support for PyAMI. After the immobilisation reaction, PAN-PyAMI is produced and subsequently characterised.

4.4.5.1 NMR analysis of PyAMI

The resultant PyAMI from section 4.2 was characterised using NMR analysis as described in section 3.3.6, to investigate the functional groups on PyAMI and to confirm the structure of the ligand.

Table 4.1 is the NMR data of PyAMI. The spectrum shows the proton of the hydroxide (δ 9.8, H-9), the presence of protons of pyridine (δ 7.4-8.6, H-1, H-2, H-3 and H-4) and protons of the primary amine (δ 5.7, H-10). This confirmed the presence of OH, NH₂ and pyridine ring of PyAMI in deuterated DMSO. Furthermore, the total number of protons from ¹H NMR; 7, conformed to the number of protons on PyAMI.

Table 4.1: Assignment of NMR spectra of PyAMI.

¹³ C NMR		¹ H NMR		
Carbon No.	Chemical shift ppm	Chemical shift ppm	Proton No.	Multiplicity
C-7	150.0	-	-	-
C-5	149.6	-	-	-
C-1	148.3	8.55	H-1	d, 1H
C-2	124.2	7.79	H-2	m, 1H
C-3	136.7	7.86	H-3	m, 1H
C-4	119.5	7.39	H-4	d, 1H
-	-	9.94	H-9	br, 1H
-	-	5.85	H-10	br, 2H

Note: d= doublet, m= multiplet, br= broad

4.4.5.2 ATR-FTIR spectrum of PyAMI

ATR-FTIR analysis was used to investigate the functional groups on PyAMI synthesised in section 4.2. Figure 4.14 is the ATR-FTIR spectrum of PyAMI. The spectra shows the main peaks that could be attributed to pyridine and amidoxime groups. The spectrum shows two sharp peaks at 3490 cm⁻¹ and 3340 cm⁻¹ which could be assigned to N-H and OH stretching bands. The peak at the range of 3100-3010 cm⁻¹ is assigned to CH stretching of pyridine ring. The peak at 1620 cm⁻¹ corresponds to C=N of oximes, while, the band at 1550 cm⁻¹ corresponds to NH bending vibration. The aromatic C-H in-plane bending of aromatics rings are observed in the region 1300-1000 cm⁻¹. The peaks between 996-939 cm⁻¹ is assigned to N-O stretching vibration of the amidoxime group. The ATR-FTIR spectrum of PyAMI also confirms the results from NMR analysis.

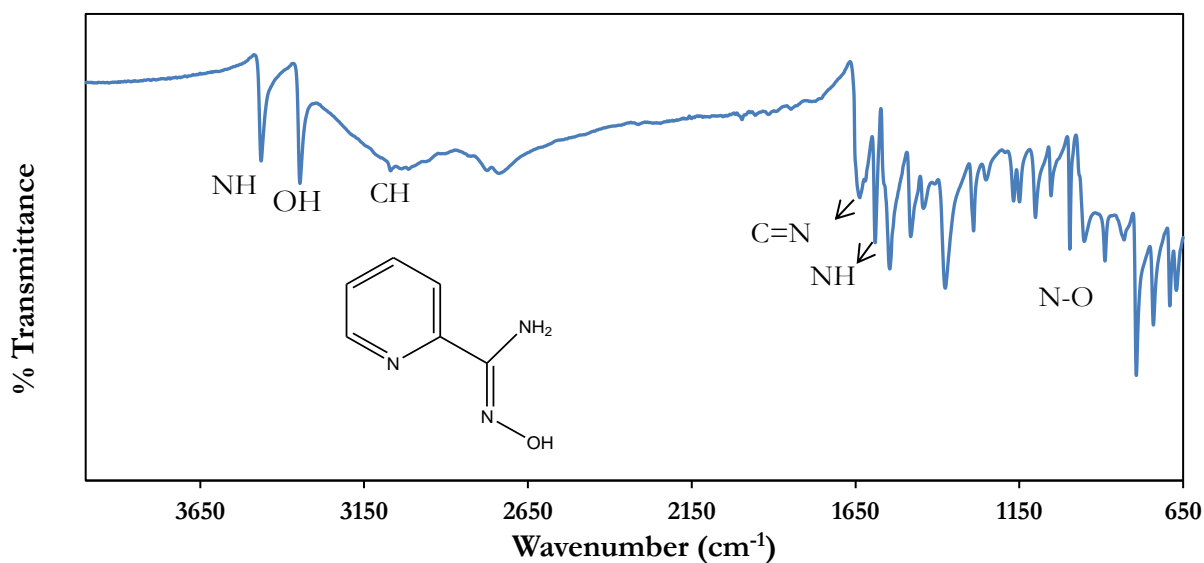


Figure 4.14: ATR-FTIR spectrum of synthesised PyAMI.

4.4.5.3 TGA profile of PyAMI

The thermal gravimetry analysis was used to investigate the thermal profile of PyAMI as set out in section 4.2. The TGA analysis was conducted under nitrogen and the heating rate of the sample was set at 1°C/min up to 250°C and then 5°C/min from 250°C to 800°C. Figure 4.15 represents the thermal gravimetry profile of PyAMI. The result shows that PyAMI underwent single stage decomposition. PyAMI was fairly stable in the 30°C to 200°C temperature range and thereafter degraded completely at 270°C, leaving no residue behind. This shows that PyAMI is a pure single organic compound.

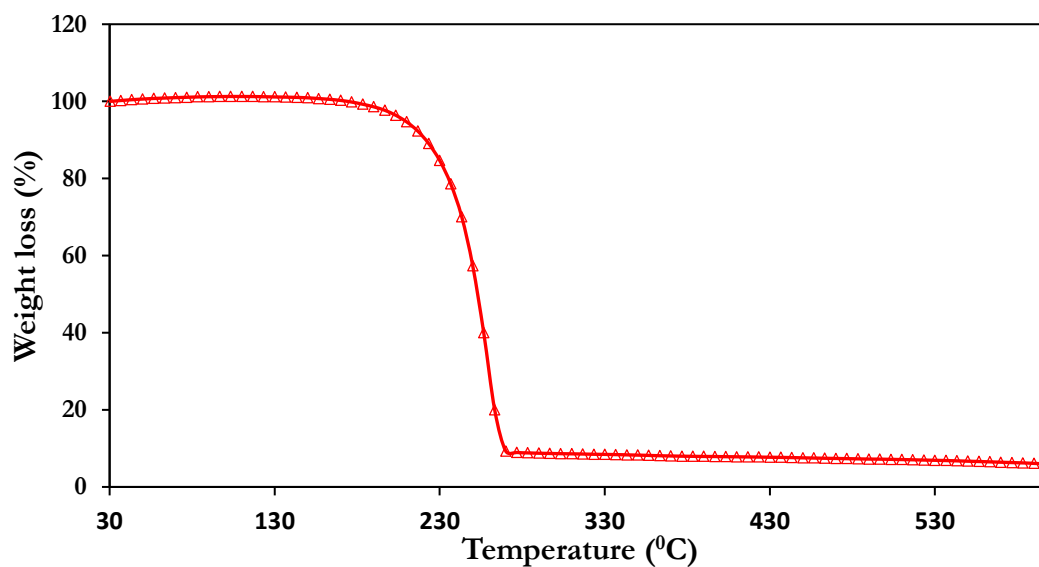


Figure 4.15: TGA profile of PyAMI under nitrogen.

4.4.6 Preparation of PAN-PyAMI

The immobilisation of PyAMI on PAN-nfs was investigated by various experiments as described in section 4.2. The resultant PAN-PyAMI nanofibres of each experiment were characterised using ATR-FTIR, HRSEM and TGA techniques.

4.4.6.1 Acid-catalysed immobilisation of PyAMI on PAN-nfs

This experiment was carried out to immobilise PyAMI on PAN-nfs in acidic medium as described (Kampalanonwat and Supaphol, 2014) in section 4.6.1. The preparation of PAN-PyAMI with $\text{AlCl}_3 \cdot 6\text{H}_2\text{O}$ catalyst was carried out with respect to time (20, 40, 60, and 90 minutes) at 60°C . The experiment was first monitored using ATR-FTIR technique before other techniques. The ATR-FTIR analysis was performed as described in section 3.3.5 over the wavelength range of 850 to 4000 cm^{-1} .

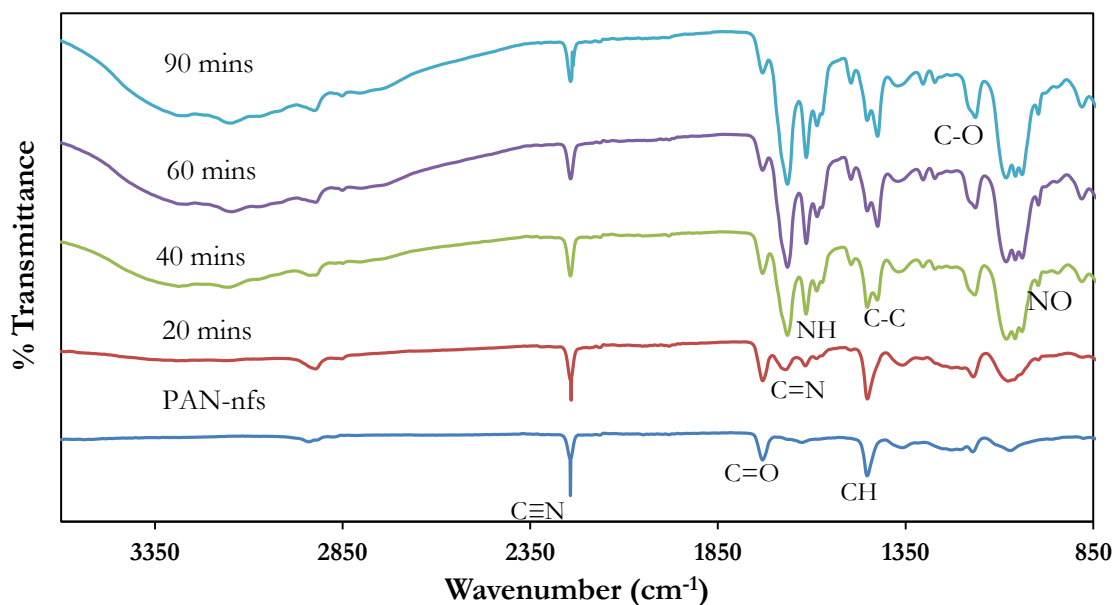


Figure 4.16: ATR-FTIR spectra of acid-catalysed immobilisation of PyAMI on PAN-nfs as function of reaction time.

The results from ATR-FTIR spectra of acid-catalysed immobilisation of PyAMI on PAN-nfs (Figure 4.16) shows some interesting peaks as the reaction time increased from 20 minutes to 90 minutes. At 20 minutes, 1654 cm^{-1} ($\text{C}=\text{N}$) started to appear.

However at 40 minutes, other peaks such as 1605 cm^{-1} (N-H bending vibration), and 968 cm^{-1} (N-O) also appeared. Also a peak at 1145 cm^{-1} which is suspected to be the new bond formed is attributed to C-O. The peak at the range of $3181\text{-}3030\text{ cm}^{-1}$ is assigned to CH stretching of pyridine ring. These peaks are

indicating the presence of PyAMI on PAN-nfs when compared to pristine PAN-nfs (Figure 4.16). The intensity of these peaks increased as the reaction time increased. All the aforementioned peaks appeared at 60 mins with more intensity. However at 90 mins, the intensity of these peaks remained the same as 60 mins. There was also the reduction of the carbonyl ester peak (1720 cm^{-1}) with as the reaction time increased, which also indicates the disappearance of the methylacrylate group as a result of hydrolysis. The peak associated with the nitrile group of the PAN-nfs at 2240 cm^{-1} also decreased in its intensity as the conversion time increased. The ATR-FTIR results of PAN-PyAMI shows that PyAMI was immobilised on PAN-nfs because of the presence of PyAMI FTIR peaks on PAN-nfs.

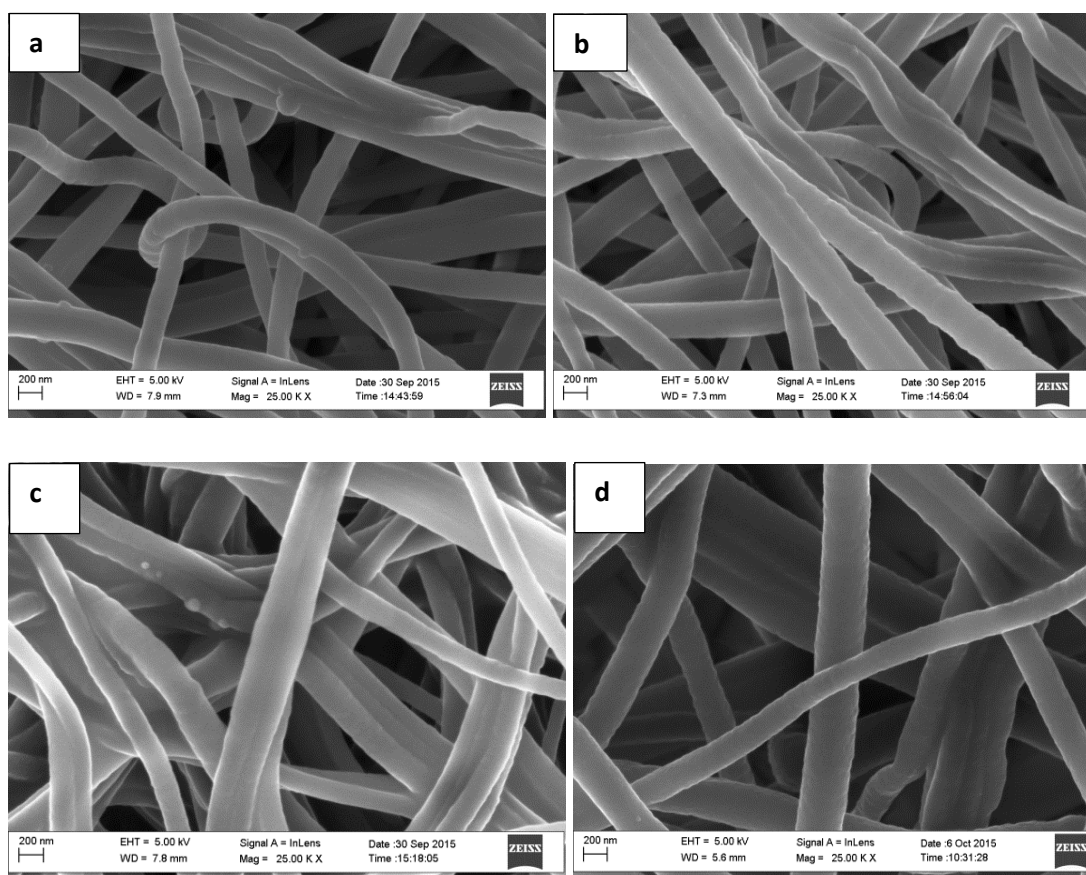


Figure 4.17: HRSEM images of (a) pristine PAN-nfs (b) PAN-PyAMI 20 mins (c) PAN-PyAMI 40 mins and (d) PAN-PyAMI 60 mins.

The HRSEM images of PAN-PyAMI Figure 4.17 (b) 20 mins, Figure 4.17 (c) 40 mins and Figure 4.17 (d) 60 mins when compared with pristine PAN-nfs (Figure 4.17 (a)) shows that the immobilisation of PyAMI on PAN-nfs in acidic medium did not significantly affected the surface morphology of PAN-nfs with respect to time. The HRSEM images show that the surface morphology of the functionalised PAN-nfs showed no degradation as the reaction time increased.

Further investigation on immobilisation was carried out using TGA. The TGA analysis was conducted on PAN-PyAMI under nitrogen and the heating rate of the sample was set at 1 °C/min up to 250°C and then 5°C/min from 250°C to 800°C.

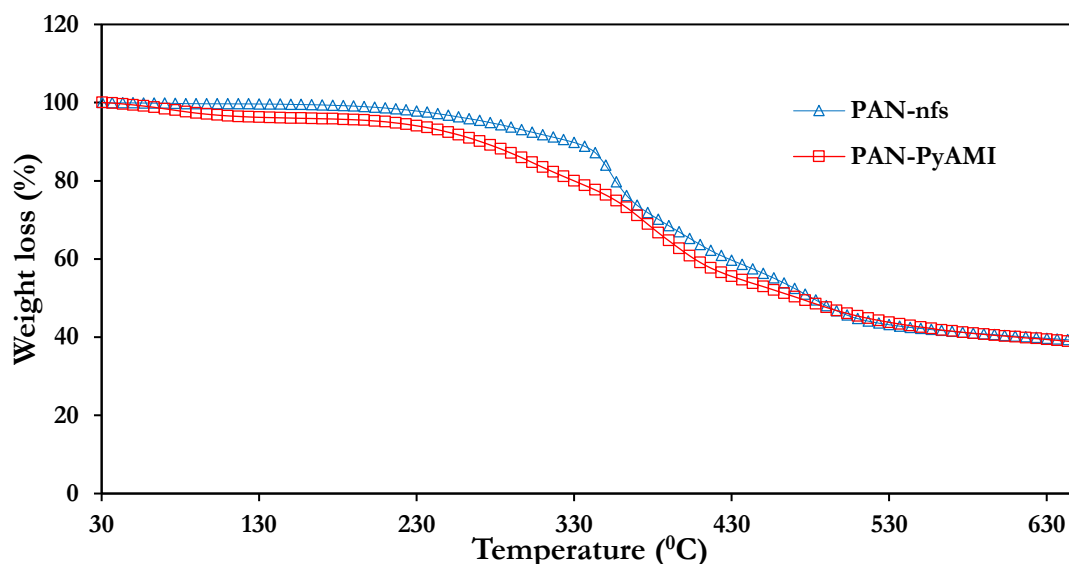


Figure 4.18: Thermal profile of pristine PAN-nfs and PAN-PyAMI under nitrogen.

The thermal profile shows that PAN-PyAMI (Figure 4.18) started losing volatiles at temperature of around 240°C. The loss in stability above that temperature might be due to the loss of organic ligands on the nanofibres. The thermal profile of the PAN-PyAMI and PAN-nfs followed similar trends at about 360°C. The TGA results show that the residue (39%) was only as a result of PAN-nfs and no ligand remained. Hence the PAN-PyAMI material was sufficiently thermally stable for service as an adsorbent.

4.4.6.2 Stability and regeneration tests

PAN-PyAMI is primarily synthesised for adsorption studies, therefore, it is important to test its stability in different pH solutions. This will give an idea at which pH PAN-PyAMI will work best. So, also for the purpose of regeneration of PAN-PyAMI after adsorption, a preliminary test was carried out to understand the best solutions for stripping off the adsorbed metals from PAN-PyAMI without losing the ligand, for the sake of reusability.

4.4.6.3 Regeneration study of PAN-PyAMI

Most studies on the regeneration of functionalised nanofibres are carried out in acidic medium. However, most of these studies never went ahead to reuse the nanofibres or even re-characterised the nanofibres after the acid regeneration.

For this study, regeneration was carried on PAN-PyAMI using 0.1 M EDTA or 0.1 M HNO₃ at 25°C for 1 hour as described in section 3.2.3.6. The resultant PAN-PyAMI was characterised using ATR-FTIR. The ATR-FTIR analysis was performed as described in section 3.3.5 over the wavelength range of 650 to 4000 cm⁻¹. From the ATR-FTIR spectra of the acid regeneration of PAN-PyAMI (Figure 4.19), the acid medium of 0.1 M HNO₃ removed all the immobilised PyAMI from PAN-nfs surfaces.

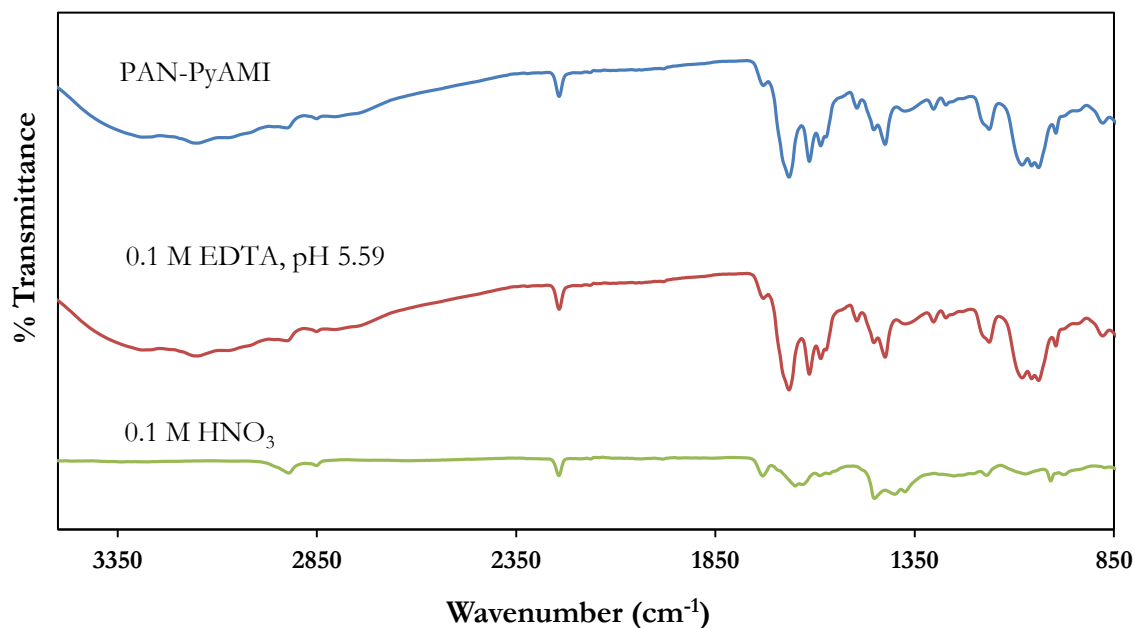


Figure 4.19: ATR-FTIR spectra of PAN-PyAMI showing regeneration studies in EDTA or HNO₃.

Figure 4.19 shows that the acid regeneration was not suitable. This might be the challenge other authors have been facing without reporting it. However, when weak acid such as EDTA (pH 5.59) was considered, the spectrum shows that PyAMI moieties were stable and not lost. Apart from the fact that the pH (5.59) was in the correct range for PAN-PyAMI application, EDTA is considered as one of the best metal chelate solution. Therefore, for this study, EDTA will be used for the regeneration of PAN-PyAMI.

4.5 Extraction of metals using polymer supported ligand

4.5.1 Adsorption experiments

The adsorption experiments were carried out in batch mode as set out in section 3.2.4.3. The adsorption experiments were carried out in triplicate (as indicated with error bars) by investigating parameters such as the effect of pH, the initial adsorbate concentration and the effect of contact time on the adsorption of Pb²⁺ in aqueous solution. All the concentrations of Pb²⁺ for the adsorption process were prepared from

the 1000 mg/L stock solution of Pb^{2+} and stored in a fridge at a temperature of 10°C . The results for each set of parameters are discussed in the following sub-sections.

4.5.2 Effect of solution pH

The effect of pH on the adsorption of Pb^{2+} was carried out in batch mode and in triplicate. The pH was investigated to determine the adsorption capacity of PAN-PyAMI or PAN-nfs at different pH solutions. 10 mL of aqueous solutions of pH 2.2, 3.1, 4.2, 4.9 or 6.1 containing 200 mg/L of Pb^{2+} were prepared and were shaken with 0.1 g of PAN-nfs or PAN-PyAMI at a stirrer speed of 120 rpm for 1 hour at 25°C . The adsorption capacities (q_e) and the percentage adsorption (R) of PAN-nfs or PAN-PyAMI were calculated.

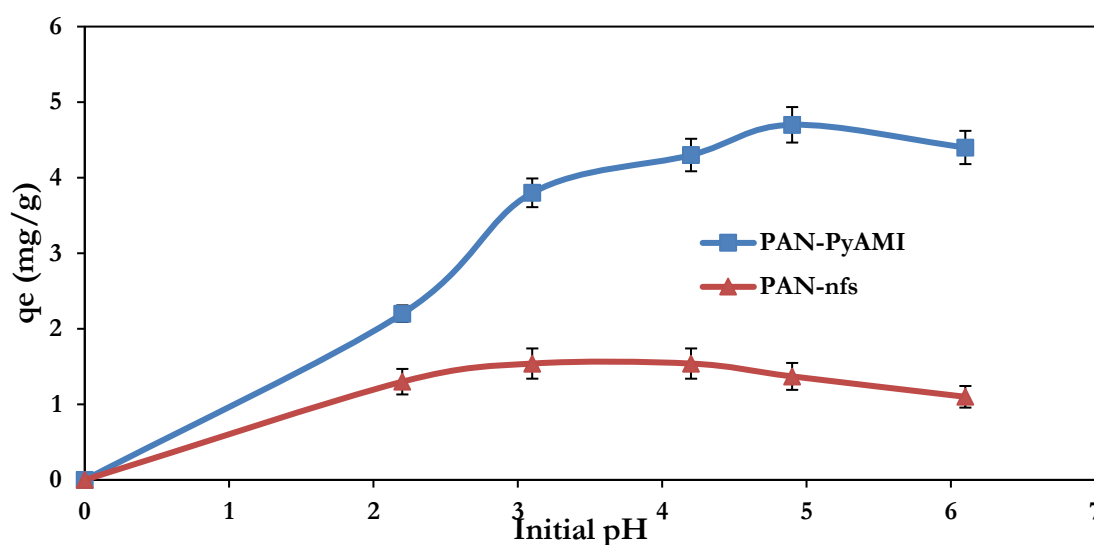


Figure 4.20: Effect of initial pH on quantity adsorbed of Pb^{2+} (initial concentration; 200 mg/L, weight of adsorbent; 0.1 g, contact time; 1 hour).

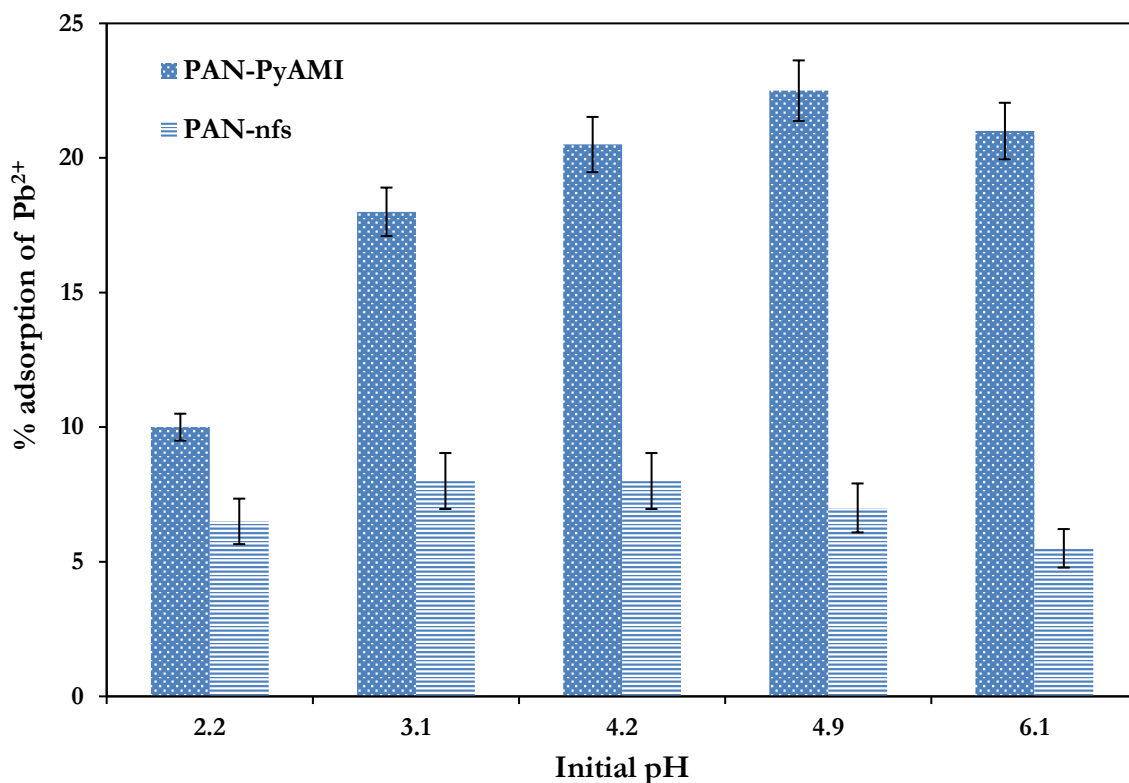


Figure 4.21: Effect of initial pH on the percentage adsorption of Pb^{2+} by PAN-PyAMI and PAN-nfs (initial concentration; 200 mg/L, weight of adsorbent; 0.1 g, contact time; 1 hour).

Figure 4.20 and Figure 4.21 present the quantity of Pb^{2+} adsorbed and the percentage Pb^{2+} adsorbed on PAN-nfs or PAN-PyAMI respectively at different initial pH. The results showed that the adsorption capacity increased as the pH increased from 2.2 to 4.9, and decreased after 4.9. The results revealed that the adsorption capacity of PAN-nfs or PAN-PyAMI adsorbents varied significantly dependent upon the initial pH of the Pb^{2+} aqueous solution. At lower pH, the active sites of the adsorbent are less available for metal ions due to protonation of the active sites at higher H^+ concentration leading to electrostatic repulsive effects between the surface of the adsorbent and Pb^{2+} in the solution. However, as the pH increased, the number of H^+ decreased and the degree of protonation of the surface functional groups was gradually reduced, which increased the adsorption capacity of the adsorbent. The adsorption capacity of PAN-PyAMI gradually increased as the pH increased from 2.2 to 4.9 and the maximum adsorption capacity for Pb^{2+} (4.70 mg/g or 22.5%) was achieved at pH 4.9. The results for PAN-nfs showed that a maximum adsorption capacity of 1.54 mg/g or 8% was achieved at a pH of 3.1. The difference in adsorption capacity between PAN-nfs and PAN-PyAMI is obviously due to the presence of the chelating ligand (PyAMI) on PAN-PyAMI. This confirmed two facts; the surface of PAN-nfs is passive and needs to be functionalised for adsorption of metal ions, and that PyAMI ligand has been successfully immobilised on PAN-nfs, hence creating active adsorption sites on PAN-nfs. Meanwhile, the adsorption capacity of

PAN-PyAMI decreased as the pH increased further from 4.9 to 6.1. This was due to the formation of hydrated lead (II) ions at a pH above 4.9 resulting in the decrease binding capability of Pb^{2+} . This is a common trend for adsorption of Pb metal as has been reported by several authors (Hong et al., 2015; Musyoka et al., 2011; Powell et al., 2009). Therefore, to prevent the metal ions from precipitation, a pH of greater than 7.0 was not studied. Thus, the initial solution pH of 4.9 was chosen for subsequent adsorption experiments on PAN-PyAMI and further adsorption experiments on PAN-nfs was discontinued due to its low adsorption capacity.

4.5.3 The effect of initial concentration

The effect of initial adsorbate concentration on the adsorption of Pb^{2+} was investigated in order to determine the optimum Pb^{2+} concentration for 0.1 g of PAN-PyAMI. 10 mL of 50, 100, 150, 200 and 250 mg/L of Pb^{2+} of pH 4.9 were prepared. 0.1 g of PAN-PyAMI was shaken with each solution for 1 hour at 25°C at a stirrer speed of 120 rpm. The resultant solution was filtered and analysed using ICP-OES and the adsorption capacity (q_e) and the percentage adsorption (R) were calculated.

Figure 4.22 and Figure 4.23 present the quantity of Pb^{2+} adsorbed and the percentage adsorbed on PAN-PyAMI at different initial concentrations respectively. The results show that the adsorption capacity increased as the initial concentration increased from 50 mg/L to 150 mg/L. At 150 mg/L, the equilibrium capacity of PAN-PyAMI of 3.17 mg/g (21%) was achieved and thereafter saturation was reached and the adsorption of Pb^{2+} was no longer increasing. This may be due to the fact that at lower concentration, sufficient adsorption sites were available; hence Figure 4.22 shows that the percentage adsorption decreased as the initial concentration increased.

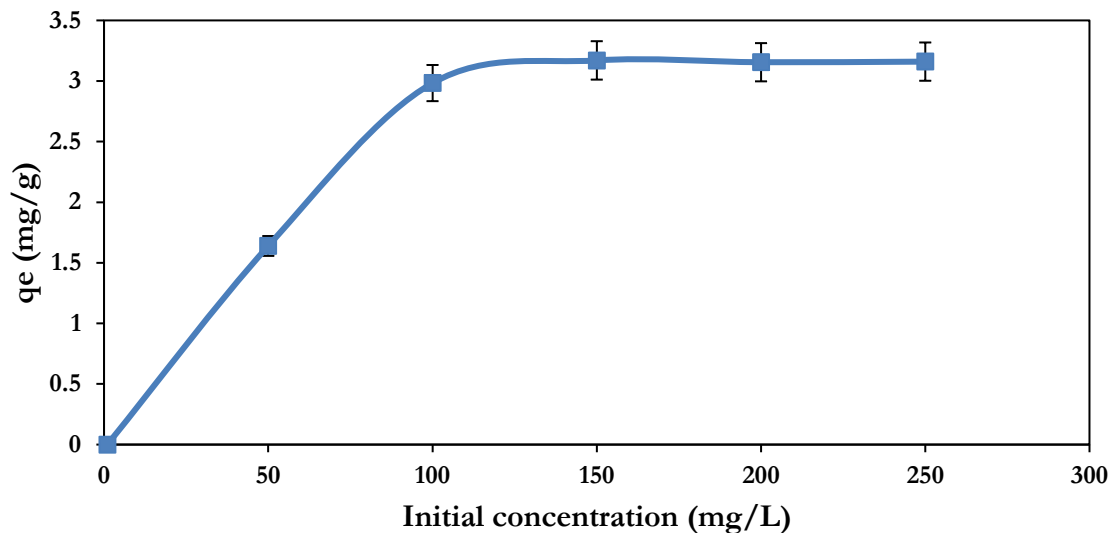


Figure 4.22: Effect of initial concentration on quantity adsorbed of Pb^{2+} on PAN-PyAMI at pH; 4.9, weight of adsorbent; 0.1 g, contact time; 1 hour.

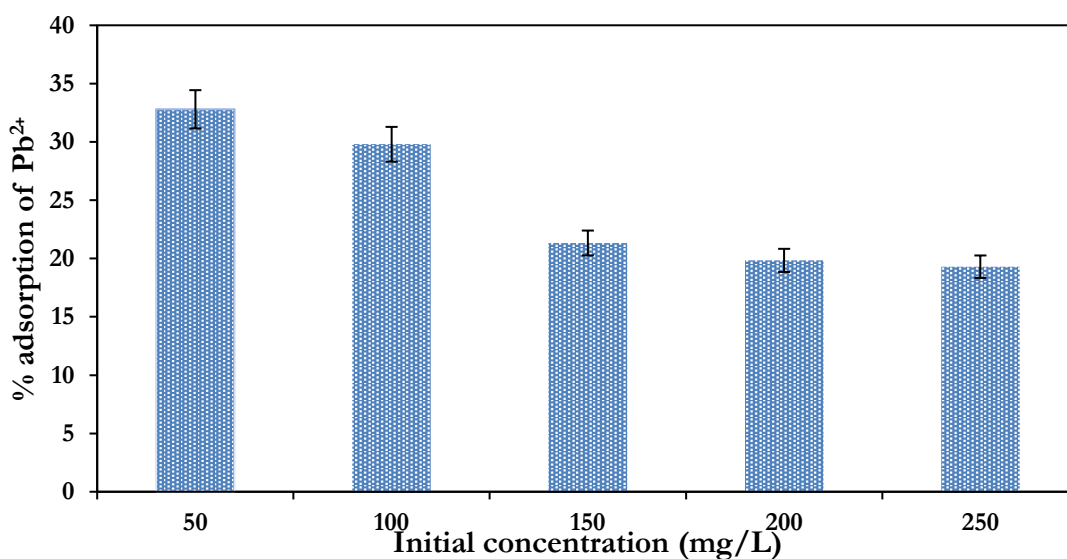


Figure 4.23: Effect of initial concentration on percentage adsorption of Pb^{2+} on PAN-PyAMI at pH; 4.9, weight of adsorbent; 0.1 g, contact time; 1 hour.

The adsorbent could take up to 33% of 50 mg/L of Pb^{2+} . As the initial concentration increased, the adsorption sites were completely filled and could no longer adsorb Pb^{2+} from the solution. Adsorption isotherm models were applied in the next sub-section to model the adsorption process.

4.5.4 The effect of contact time

Contact time is an important parameter in determining the performance of adsorbents. In order to study the adsorption kinetics, the effect of contact time on adsorption of Pb^{2+} on PAN-PyAMI was investigated. Seven samples containing 10 mL of 200 mg/L of Pb^{2+} at pH 4.9 were shaken with 0.1 g PAN-PyAMI for 10, 20, 40, 60, 80, 100 or 120 minutes respectively at 120 rpm. The resultant solutions were filtered and analysed using ICP-OES. The adsorption capacity (q_e) and the percentage adsorption (R) were calculated.

Figure 4.24 and Figure 4.25 present the quantity and the percentage of Pb^{2+} adsorbed on PAN-PyAMI at different contact times respectively. It was found that the rate of adsorption of Pb^{2+} on PAN-PyAMI increased steadily from 10 to 60 minutes, and thereafter, the adsorption rate slowed down after 60 minutes, and increase no further after 80 minutes indicating that the adsorbent was saturated for Pb^{2+} . The steady increase in the adsorption rate in the first 60 minutes could be due to the availability of many adsorption sites on the surface of PAN-PyAMI and as the contact time increased further, the amount of Pb^{2+} adsorbed gradually reached a maximum when there was no more significant metal ion removal taking place because all the active sites on PAN-PyAMI had been occupied by metal ions. The adsorption capacity at equilibrium time (80 minutes) was calculated to be 3.29 mg/g, (32.9%).

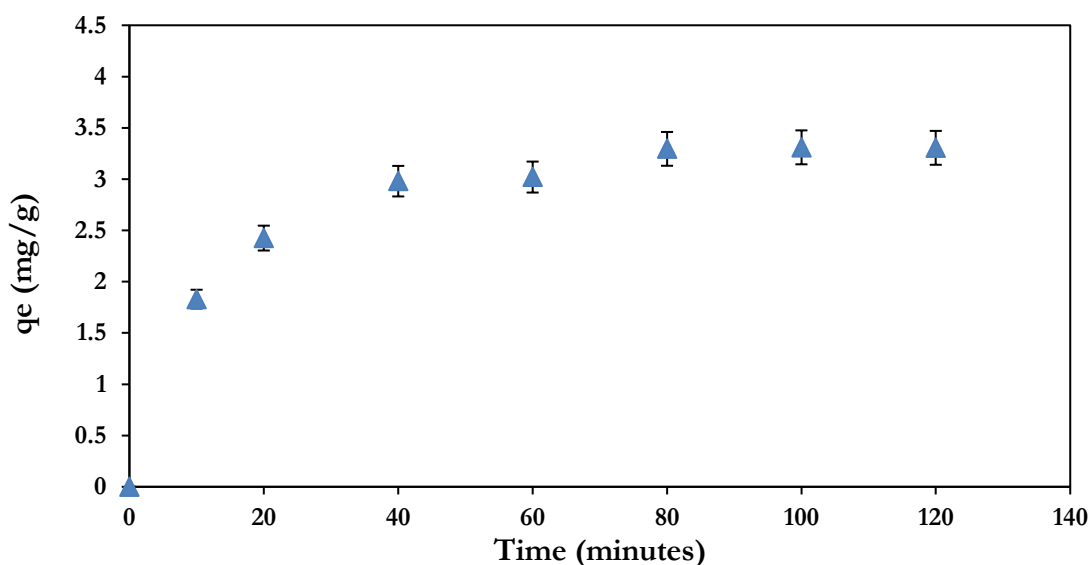


Figure 4.24: Effect of contact time on quantity of Pb^{2+} adsorbed using PAN-PyAMI (initial concentration; 200 mg/L, weight of adsorbent; 0.1 g, initial pH; 4.9).

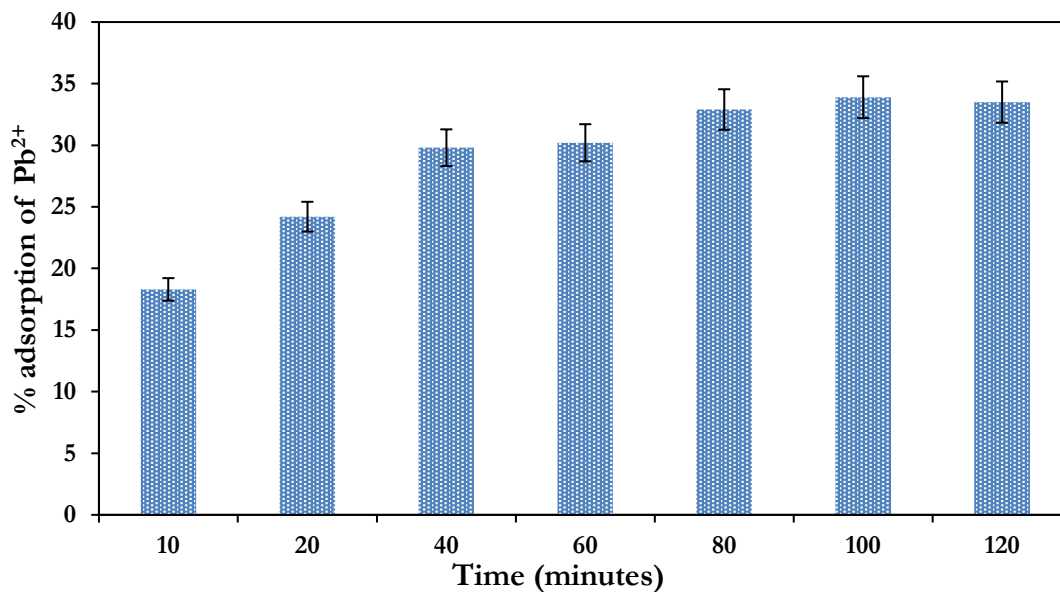


Figure 4.25: Effect of contact time on percentage adsorption of Pb²⁺ using PAN-PyAMI (initial concentration; 200 mg/L, weight of adsorbent; 0.1 g, initial pH; 4.9).

4.5.5 Desorption and reusability experiments

Desorption experiments were carried out in order to regenerate 0.1 g PAN-PyAMI previously used for adsorption of Pb²⁺ at variables; pH 4.9, initial concentration 200 mg/L at 1 hour contact time, at 25°C. The adsorbent PAN-PyAMI was regenerated by desorbing Pb²⁺ from the mat using 10 mL of 1 M, 0.1 M or 0.01 M EDTA (Note; for this study, acid was not used to regenerate PAN-PyAMI because of the functional ligands instability at solution pH of less than 4.5 (recall from section 4.4.6.3). The resultant solution was filtered and analysed using ICP-OES and the percentage desorbed was calculated. The regenerated PAN-PyAMI was reused to adsorb Pb²⁺ following the same procedure and variables pH 4.9, initial concentration 200 mg/L at 1 hour contact time, at 25°C.

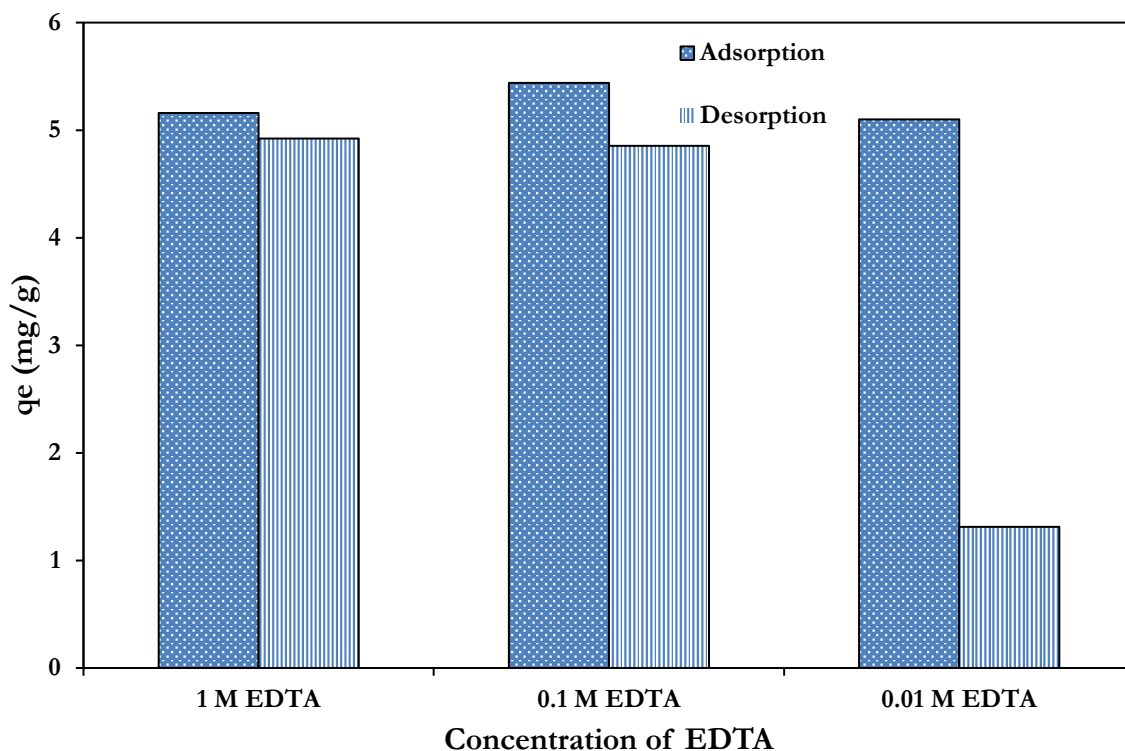


Figure 4.26: Regeneration of 0.1 g PAN-PyAMI loaded with Pb^{2+} using different concentrations of EDTA.

Figure 4.26 presents the regeneration of PAN-PyAMI loaded with Pb^{2+} using 10 mL of 1 M, 0.1 M or 0.01 M EDTA. The results show that regeneration of PAN-PyAMI varies depended on the concentration of EDTA. 1 M EDTA gave the highest desorption of 95% (4.92 mg/g) out of 5.16 mg/g previously adsorbed. 0.1 M EDTA desorbed 89% (4.85 mg/g) out of 5.44 mg/g while 0.01 M EDTA gave the lowest result, desorbing 25% (1.31 mg/g) out of 5.10 mg/g previously adsorbed on PAN-PyAMI. However, after desorption using 1 M EDTA at first cycle of regeneration, PAN-PyAMI became brittle and could no longer be re-used. Therefore, further studies were carried out using 0.1 M EDTA to regenerate PAN-PyAMI.

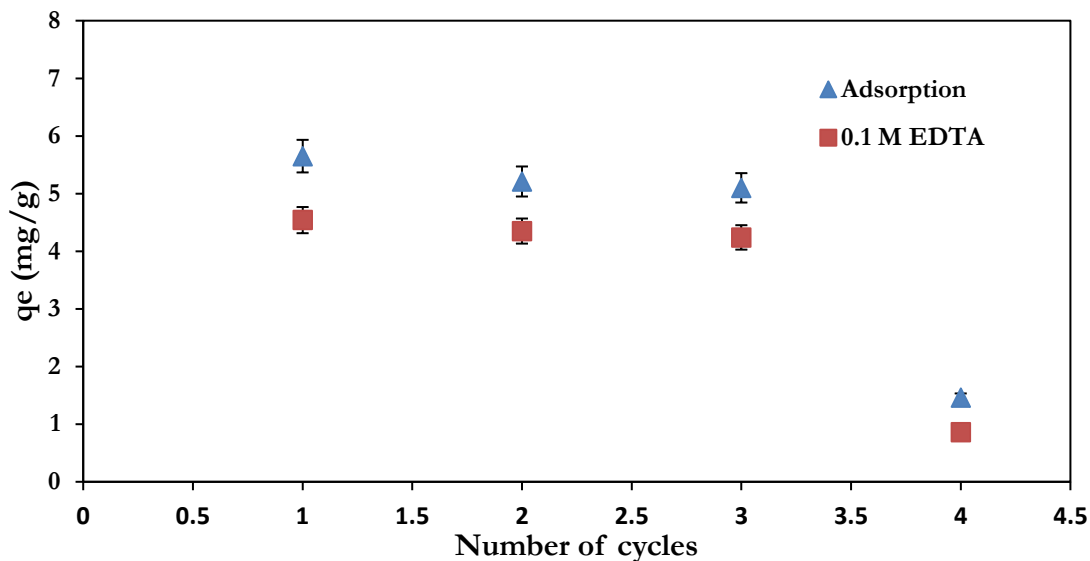


Figure 4.27: Desorption and reusability test of PAN-PyAMI for Pb^{2+} (initial concentration 200 mg/L, weight of adsorbent; 0.1 g, initial pH; 4.9, contact time; 1 hour, 0.1 M EDTA).

Figure 4.27 presents desorption and reusability of PAN-PyAMI after adsorption of Pb^{2+} at conditions; initial concentration; 200 mg/L, pH; 4.9; weight adsorbent; 0.1 g and contact time; 1 hour. The results show that PAN-PyAMI can be regenerated using 0.1 M EDTA after been previously used for adsorption of Pb^{2+} and can be subsequently reused after regeneration for at least four cycles.

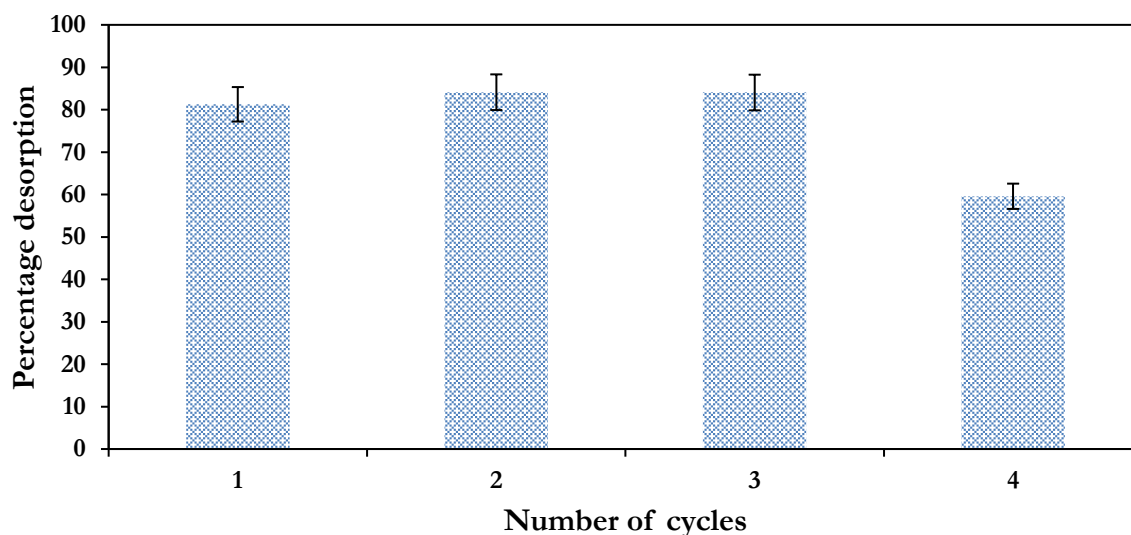


Figure 4.28: Percentage desorption of Pb^{2+} adsorbed onto PAN-PyAMI with respect to number of cycles using 0.1 M EDTA (initial concentration 200 mg/L, weight of adsorbent; 0.1 g, contact time; 1 hour).

For the first cycle, out of 5.65 mg/g previously adsorbed by PAN-PyAMI, 4.54 mg/g, 81% (Figure 4.28) was desorbed. Thereafter, for the Pb^{2+} adsorption cycle with PAN-PyAMI, 84%, 84% and 59% desorption was achieved for second, third and fourth desorption cycles respectively (Figure 4.28). However as the reuse cycles increased from 2 to 4, the adsorption capacities of PAN-PyAMI decreased from 5.26 to 1.46 mg/g. The loss in capacity could be due to the gradual loss of PyAMI on PAN-nfs or due to Pb^{2+} that was irreversibly adsorbed.

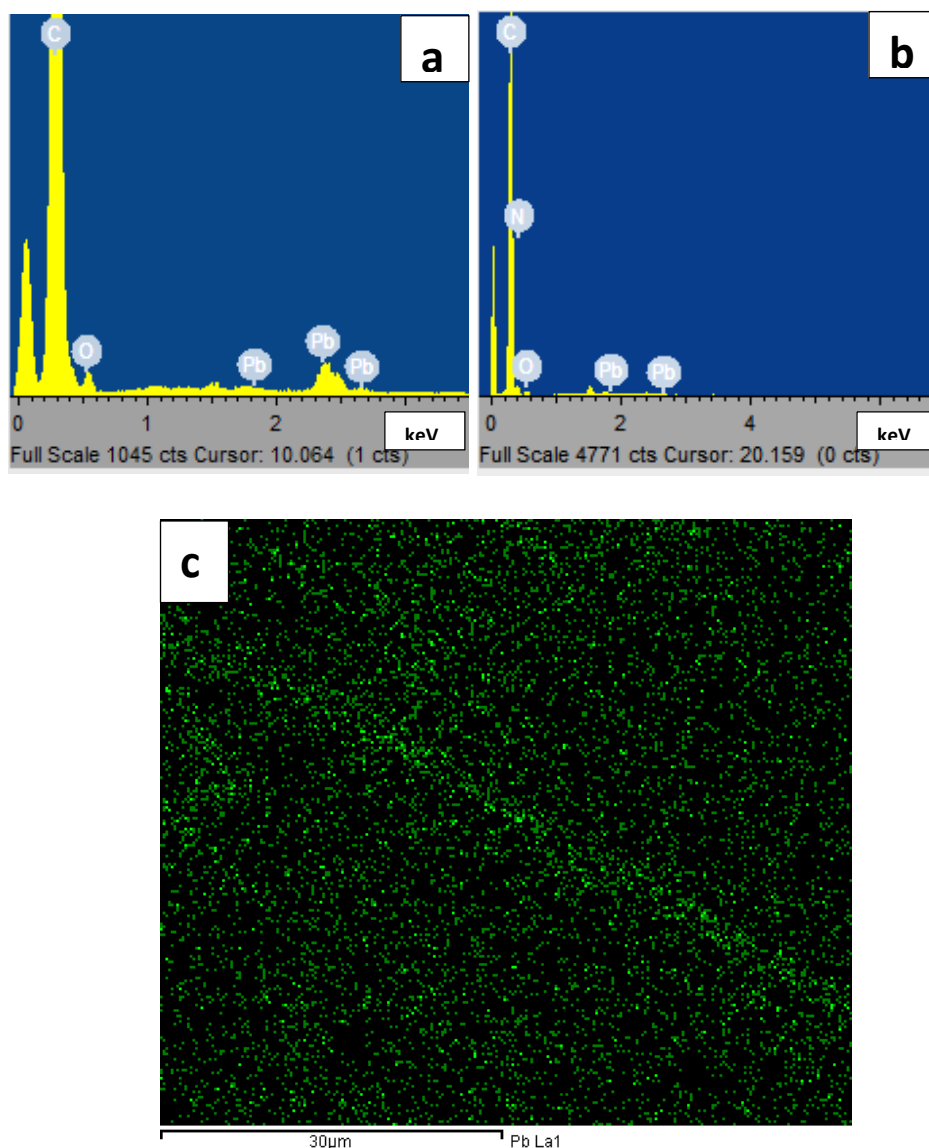


Figure 4.29: SEM-EDS {(a) PAN-PyAMI after 1st adsorption cycle of Pb^{2+} and (b) PAN-PyAMI after 4th adsorption cycle of Pb^{2+} } and (c) SEM-EDS mapping of PAN-PyAMI after 1st adsorption cycle of Pb^{2+} .

To ascertain which of the two possibilities (or both) mentioned earlier was responsible for the reduction in adsorption capacities of PAN-PyAMI, SEM-EDS, SEM-EDS mapping and ATR-FTIR techniques

were employed. SEM-EDS and SEM-EDS mapping were used to check the availability of Pb^{2+} on PAN-PyAMI after the 1st and the 4th adsorption cycles (Figure 6.14). The results show that PAN-PyAMI adsorbed to its surface Pb^{2+} (Figure 4.29 (a)) after the first adsorption, however, the presence of Pb^{2+} was reduced significantly after the 4th adsorption (Figure 4.29 (b)). The reduction in adsorption capacity could be due to the reduction in active adsorption sites as a result of loss of ligands on PAN-PyAMI. Meanwhile, SEM-EDS mapping shows (Figure 4.29 (c)) that the entire surface of the PAN-PyAMI was covered with Pb^{2+} (green spots) after the 1st adsorption, which implies that the surface of PAN-PyAMI was uniformly active for adsorption of lead at 1st adsorption cycle.

For further confirmation, ATR-FTIR technique was used to check the availability of PyAMI on PAN-nfs after each regeneration cycle.

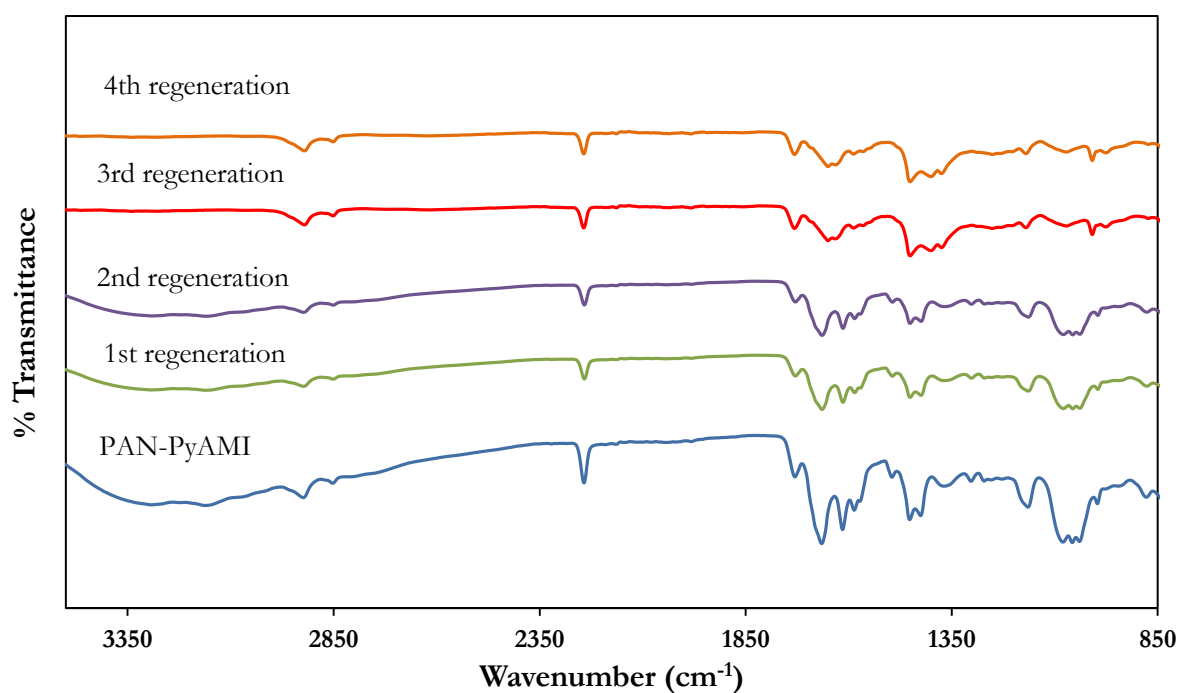


Figure 4.30: ATR-FTIR spectra of regenerated PAN-PyAMI using 0.1 M EDTA.

Figure 4.30 is the ATR-FTIR spectral of PAN-PyAMI as made and after several regeneration cycles. The results show that the peaks from the ligand started to decrease in intensity after the first regeneration using 0.1 M EDTA (1st regeneration). The peaks further decreased as the number of regeneration cycles increased from 2 to 4. After the 4th regeneration, the peaks attributed to PAN-PyAMI such as 1654 cm^{-1} (C=N), 1605 cm^{-1} (N-H bending vibration) and 968 cm^{-1} (N-O) have virtually disappeared. From the SEM-EDS and the ATR-FTIR results, it could be concluded that PAN-PyAMI could not effectively be reused

more than four times after being regenerated with 0.1 M EDTA because of the loss of adsorption sites which leads to reduction in adsorption capacities.

4.5.6 Competitive adsorption

The experiment was designed to show if PAN-PyAMI could be used to separate two metals from the same solution by adsorbing one more and leaving the other behind in the solution. 0.1 g of PAN-PyAMI was applied to separate two toxic metals Pb^{2+} and Sr^{2+} in the same solution. The experiment was set up by varying the concentration of the two metals in the ratio Pb^{2+}/Sr^{2+} 1:1, 1:2.5 or 2.5:1 (250/250; 100/250 and 250/100 mg/L) with the optimised conditions (pH= 4.9, contact time= 1 hour and room temperature= 25°C) for Pb^{2+} adsorption.

Figure 4.31 and Figure 4.32 present the results for the quantity adsorbed in mg/g and in percentage adsorbed for Pb^{2+}/Sr^{2+} respectively. The results showed that at equal concentration (250 mg/L), 3.98 mg/g, or 16% of Pb^{2+} was adsorbed while 0.50 mg/g or 3.08% of Sr^{2+} was adsorbed from the solution. This shows that at an equal concentration, PAN-PyAMI was much more selective for Pb^{2+} adsorption. At concentration ratio 100/250 mg/L, about 2.14 mg/g, or 21.4% of Pb^{2+} was adsorbed while only 1.20 mg/g or 11% of Sr^{2+} was adsorbed. This further confirmed that Pb^{2+} adsorption was preferred even at a higher concentration of Sr^{2+} . Finally, at a concentration of 250/100 mg/L of Pb^{2+}/Sr^{2+} , the trend still remained unchanged as PAN-PyAMI adsorbed 4.20 mg/g or 16.8% of Pb^{2+} only while 0.46 mg/g or 4.2% of Sr^{2+} was adsorbed.

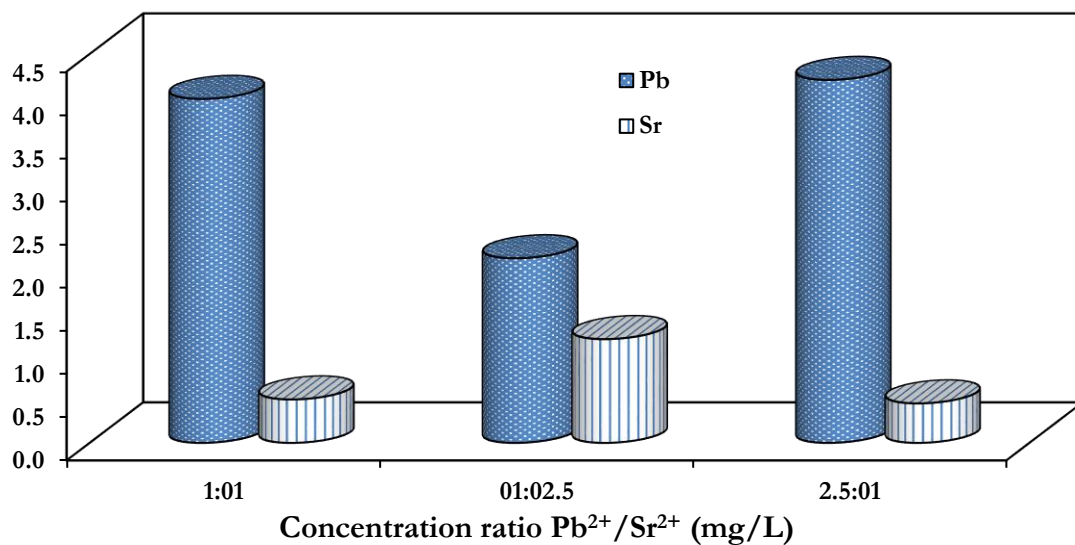


Figure 4.31: Selectivity test of PAN-PyAMI for separating Pb^{2+} and Sr^{2+} in solution (Weight of adsorbent; 0.1 g, pH; 4.9, contact time 1 hour).

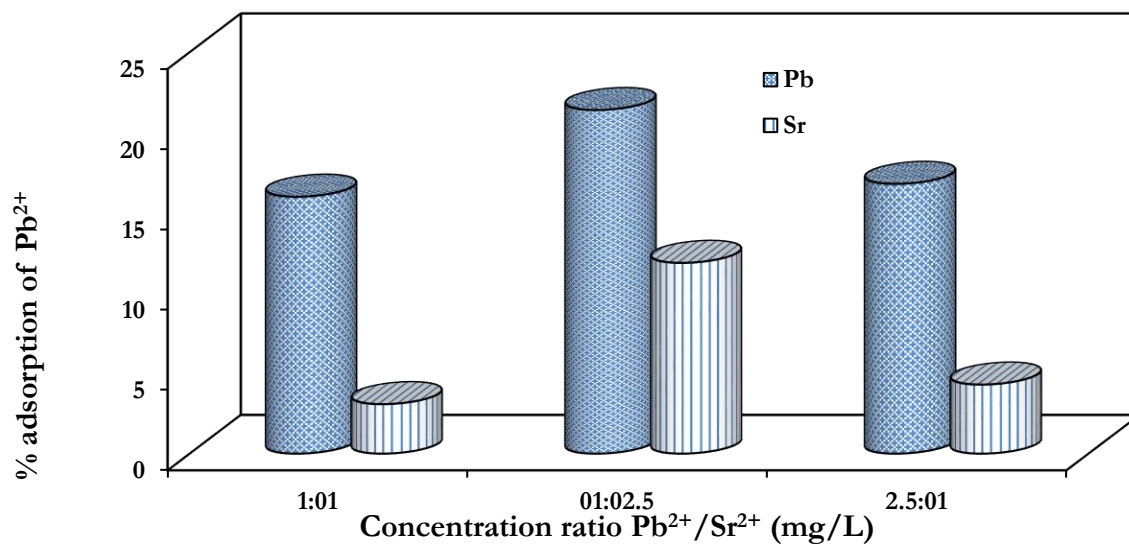


Figure 4.32: Percentage Pb^{2+}/Sr^{2+} adsorbed onto PAN-PyAMI (Weight of adsorbent; 0.1 g, pH; 4.9, contact time; 1 hour).

To check for the factor responsible for the disparity in the adsorption capacities of PAN-PyAMI for Pb^{2+} and Sr^{2+} , the effect of solution pH was performed on the adsorption of Sr^{2+} using PAN-PyAMI.

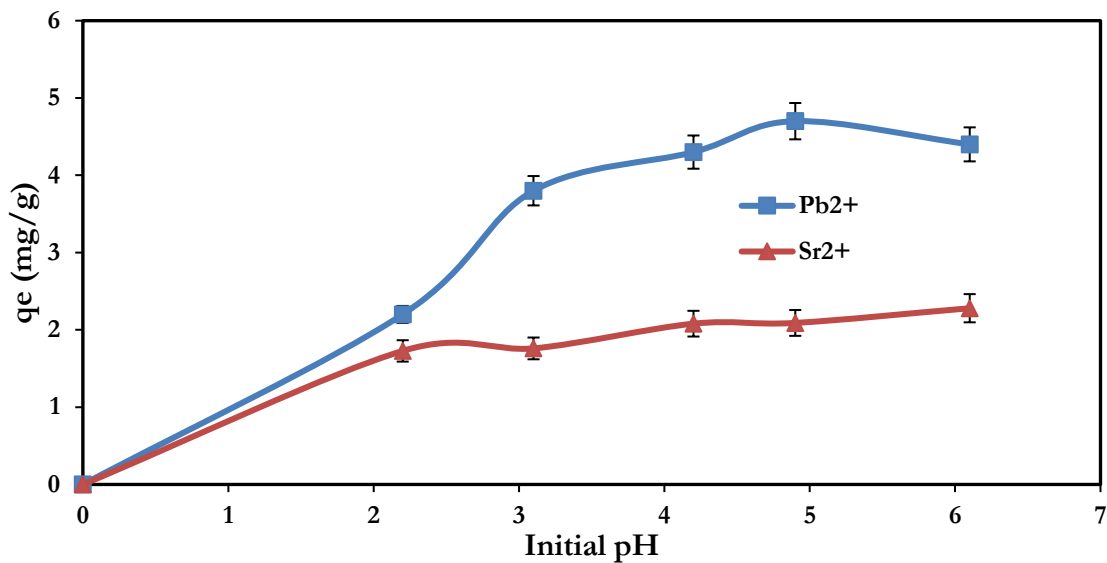


Figure 4.33: Effect of initial pH on the adsorption of Pb²⁺ and Sr²⁺ on PAN-PyAMI (Initial concentration; 200 mg/L, weight of adsorbent; 0.1 g, contact time; 1 hour).

Figure 4.33 presents the comparison of the effect of initial pH on adsorption of Pb²⁺ and that of Sr²⁺ using PAN-PyAMI as adsorbent. The results show that the adsorption of Sr²⁺ was not significantly affected by pH compared to that of Pb²⁺. The maximum adsorption capacity of PAN-PyAMI for Sr²⁺ was 2.28 mg/g at pH 6.1, whereas, for Pb²⁺, it was 4.7 mg/g at pH 4.9. This implies that at the optimum pH for adsorption of Pb²⁺, PAN-PyAMI will perform poorly for the adsorption of Sr²⁺. Therefore, it could be concluded that the selectivity of PAN-PyAMI was partly based on the effect of initial solution pH.

5 Conclusions

From this report, efforts were made to remove toxic metals from water through adsorption process using ligands supported on silica and nanofibres respectively.

For the silica supported ligands, it is evident that a better extraction is achieved at a higher pH than lower pH. In this particular study, a pH-value of 5.9 was obtained as optimum. The reason may well be because the ligands are less protonated at the higher pH. This leaves the cavity, as well as the donating atoms exposed and complexation can take place.

When comparing the capacities of the ligands supported upon different silica supports, it was found that Si gel (60 Å) was the most effective support to use. It did not always have the highest yields, but in all the extraction experiments, some extraction was obtained when Si gel (60 Å) was used as the support. A reason for this result may be because of the more favourable BET results concerning the surface area of Si gel (60 Å). The area of the Si gel (60 Å) is more accessible and can be modified more easily. MCM-41 is also a very good support to use, but it is more expensive to make than Si gel (60 Å) and the pore openings are very small which might prevent the ligands and metal ions from entering. This leads to crowding of the ligands on the surface of MCM-41 which in turn leads to less contact area for the metal ions. SBA-15 and HMS showed the least effective results as supports for all of the ligands. Their BET results showed that the usable surface areas were much smaller than that of Si gel (60 Å) or that of MCM-41.

There was no affinity for As^{5+} or Hg^{2+} at either low or high pH levels. There is slight selectivity for Cd^{2+} extraction by 18-c-6, THTD and THTUD. Cr^{6+} is selectively extracted by all the ligands, independent of the support that was used. Sr^{2+} is selectively extracted by 15-c-5 and to a lesser extent by 18-c-6. Uranyl showed the same preferential affinity towards 18-c-6 and 15-c-5.

It was shown that the extraction increased for the same ligands as soon as a spacer was introduced except for the extraction of the uranyl. As the length of the spacer increased, the extraction of the immobilised ligands increased as well except for the uranyl extraction. The reason is that the metal ions can come into better contact with the ligands because the ligands have more flexibility to move about in the solution, and that there is less interference from the Si supports. Extraction experiments with just the supports were also conducted. The amount of metal ions extracted was below 2.5% and can be considered to be zero.

It should be noted that regeneration proved impossible as the supports lose their ligands when regenerated under the conditions tested. Therefore, the reusability of these materials was in doubt and further efforts are required to stabilize the ligand on the support.

Another support in nano-metre diameter was used to support ligands. Polyacrylonitrile electrospun into nanofibres was used to support 2-pyridine amidoxime ligand. The removal for Pb^{2+} in batch adsorption experiment was carried out by investigating various parameters namely the effect of initial pH, initial concentration, and the contact time. The effect of initial pH played the most important role in adsorption of Pb^{2+} as the removal was greatly increased as pH increased. PAN-PyAMI performed better compared to PAN-nfs with an optimum pH of 4.9 during adsorption. This is as a result of selectivity of the ligands supported on PAN-nfs. The maximum adsorption capacity of PAN-PyAMI for Pb^{2+} was 22.5%, while PAN-nfs had a capacity of only 8%. The PAN-nfs supports contributed to the adsorption better than the silica support (2.5%). This may be due to the fact that PAN-nfs is a nano-material with higher surface area. Therefore, perhaps, immobilising more ligands on nano-materials could yield better results. At pH-value 4.9, PAN-PyAMI adsorbed more Pb^{2+} as it could significantly remove more of Pb^{2+} (22.5%) than Sr^{2+} (10.5%) in the same aqueous solution. PAN-PyAMI was regenerated using EDTA but could not be regenerated using HNO_3 . This is the advantage the ligand supported on nanofibres has over the silica supported ligands. The regenerability might be due the fact that the polymer chosen for this study (PAN) has functional groups that could react well with the ligand to form fairly stable support-ligand bonds, but further investigations are needed.

The capacities of both the silica supported ligands and the nanofibres supported ligands are fairly higher when compare to the adsorbents reported in the review paper published as part of this research (Bode-Aluko et al., 2017a). From this research, adsorption is still the simplest method for toxic metals removal as the methods reported in this research are not cumbersome and could be set-up in a simplified batch manner. This study has opened another avenue for extraction of toxic metals; therefore, further research should be carried on the immobilisation of ligands on nanofibres for adsorption and metal separation purposes. The stability of the ligand-support bonds should be looked into in order to overcome the instability in acids.

6 References

- ABNEY, C., LIU, S. and LIN, W. (2013). Tuning amidoximate to enhance uranyl binding: A density functional theory study. *Journal of Physical Chemistry* **117** 11558-11565.
- AGRAWAL, A., PAL, C. and SAHU, K.K. (2008). Extractive removal of chromium (VI) from industrial waste solution. *Journal of Hazardous Materials* **159** 458-464.
- AKCAY, H., OGUZ, A. and KARAPIRE, C. (2003). Study of heavy metal pollution and speciation in Buyak Menderes and Gediz river sediments. *Water Research* **37** (4) 813-822.
- AKITA, S. and TAKEUCHI, H. (1990). Sorption and separation of metals from aqueous solution by a macromolecular resin containing tri-n-octylamine. *Journal of Chemical Engineering of Japan* **23** (4) 439-443.
- ANJUM, N.A., GILL, S.S. and TUTEJA, N. (2017). *Enhancing Cleanup of Environmental Pollutants: Volume 2, Non-Biological Approaches*. Springer.
- ARMITAGE, P.D., BOWES, M.J. and VINCENT, H.M. (2007). Long-term changes in macroinvertebrate communities of a heavy metal polluted stream: the river Nent (Cumbria, UK) after 28 years. *River Research and Applications* **23** (9) 997-1015.
- ARNOLD, P.L., PATEL, D., BLAKE, A.J., WILSON, C. and LOVE, J.B. (2006). Selective oxo functionalization of the uranyl ion with 3d metal cations. *Journal of the American Chemical Society* **128** (30) 9610-9611.
- ATKINS, T., RICHMAN, J. and OETTLER, W. (1978). Macrocyclic Polyamines: 1, 4, 7, 10, 13, 16-Hexaazacyclooctadecane. *Organic Syntheses*, 86-86.
- AVDEEF, A., SOFEN, S.R., BREGANTE, T.L. and RAYMOND, K.N. (1978). Coordination Chemistry of Microbial Iron Transport Compounds. 9. Stability Constants for Catechol Models of Enterobactin. *Journal of the American Chemical Society* **100** 5362 -5370.
- BAI F, YE G, CHEN, G., WEI, J., WANG, J. and CHEN, J. (2013). New macrocyclic ligand incorporated organosilicas: Co-condensation synthesis, characterization and separation of strontium in a simulated high level liquid waste. *Reactivity and functional polymers* **73** 228-236.

- BARAKAT, M.A. (2011). New trends in removing heavy metals from industrial wastewater. *Arabian Journal of Chemistry*, **4** 361-377.
- BARNARD, B.F. (2008). The synthesis, stability and structures of two novel macrocyclic ligands and their complexes, MSc Thesis, University of Stellenbosch.
- BEER, P., HOPKINS, P. and MCKINNEY, J. (1999). Cooperative halide, perchlorate anion-sodium cation binding and pertechnetate extraction and transport by a novel tripodal tris (amido benzo-15-crown-5) ligand. *Chemical Communications* **13** 1253-1254.
- BERNASEK, E. (1957). Pyridineamidoximes, *Journal of Organic Chemistry* **6208** 1263.
- BHARDWAJ, N. and KINDU, S. (2010). Electrospinning: A fascinating fiber fabrication technique. *Biotechnology Advances* **28** 325-347.
- BILBA, D., BEJAN, D. and TOFAN, L. (1998). Chelating Sorbents in Inorganic Chemical Analysis. *Croatica Chemica Acta* **71 (1)** 155-178.
- BODE-ALUKO, C.A., PEREAO, O., FATOBA, O. and PETRIK, L. (2017b). Surface-modified polyacrylonitrile nanofibres as supports. *Polymer Bulletin* **74** 2431-2442.
- BODE-ALUKO, C.A., PEREAO, O., NDAYAMBAJE, G. and PETRIK, L. (2017a). Adsorption of Toxic Metals on Modified Polyacrylonitrile Nanofibres: A Review. *Water, Air and Soil Pollution*, 228:35 DOI 10.1007/s11270-016-3222-3.
- BORKOWSKY, L. and CAHILL, C. (2003). Topological evolution in uranyl dicarboxylates: synthesis and structures of one-dimensional $\text{UO}_2(\text{C}_6\text{H}_8\text{O}_4)(\text{H}_2\text{O})_2$ and three-dimensional $\text{UO}_2(\text{C}_6\text{H}_8\text{O}_4)$. *Inorganic chemistry* **42** 7041-7045.
- BRAUN, T. and GHERSINI, G. (1975). *Extraction chromatography*, Elsevier Scientific Publications Co., New York.
- CARBONI, M., ABNEY, C.W., TAYOR-PASHOW, K., VIVERO-ESCOTO, J. and LIN, W. (2013). Uranium sorption with functionalized mesoporous carbon materials. *Industrial and engineering chemistry research* **52** 15187-15197.
- CASNATI, A., BARBOSO, S., ROUQUETTE, H., SCHWING-WEILL, M., ARNAUD-NEU, F., DOZOL, J. and UNGARO, R. (2001). New efficient calixarene amide ionophores for the selective removal of strontium ion from nuclear waste: synthesis, complexation, and extraction properties. *Journal of the American Chemical Society* **123 (49)** 12182-12190.

- CHEN, W., YUAN, H., WANG, J., LIU, Z., XU, J., YANG, M. and CHEN, J. (2003). Synthesis, structure, and photoelectronic effects of a Uranium–Zinc–Organic coordination polymer containing infinite metal oxide sheets. *Journal of the American Chemical Society* **125** 9266-9267.
- CHOPPIN, G., THAKUR, P. and MATHUR, J. (2006). Complexation thermodynamics and structural aspects of actinide-aminopolycarboxylates. *Coordination chemistry review* **250** 936-947.
- CHRISTEN, J.J., EATOUGH, D. and IZATT, R. (1974). Synthesis and ionic binding of synthetic multidentate macrocyclic-compound. *Chemical reviews* **74** (3) 351-384.
- COMARMOND, J., PAYNE, T., HARRISON, J., THIRUVOTH, S., WONG, H., AUGHTERSON, R., LUMPKIN, G., MÜLLER, K. and FOERSTENDORF, H. (2011). Uranium sorption on various forms of titanium dioxide – influence of surface area, surface charge, and impurities. *Environmental science and technology* **45** 5536-5542.
- CONSTABLE, E.C. (1999). *Coordination chemistry of macrocyclic compounds*, Oxford University Press Oxford.
- CRINI, G. (2005). Recent developments in polysaccharide-based materials used as adsorbents in wastewater treatment. *Progress in Polymer Science* **30** 38-70.
- DASSENAKIS, M., SCOULLOS, M., FOUFA, E., KRASAKOPOULOU, E., PAVLIDOU, A. and KLOUKINIOTOU, M. (1998). Effects of multiple source pollution on a small Mediterranean river. *Applied Geochemistry* **13** (2) 197-211.
- DENG, S., BAI, R. and CHEN, J. (2003). Aminated polyacrylonitrile fibers for lead and copper removal. *Langmuir* **19** 5058-5064.
- DENIZILI, A., BÜYÜKTUNCEL, E., SAID, Z., GENÇ, Ö. and PISKIN, E. (1998). New Dye-Ligand: Procion Red MX-3B Carrying Poly (EGDMA-HEMA) Microbeads for Removal of Copper Ions. *Journal of Macromolecular Science, Part A: Pure and Applied Chemistry* **35** (6) 919-932.
- DEORKAR, N. and KHOPKAR, S. (1989). Separation of uranium (VI) as chloride complex by solvent extraction with dicyclohexyl-18-crown-6. *Journal of Radioanalytical and Nuclear Chemistry* **130** (2) 433-441.
- DEORKAR, N.V. and TAVLARIDES, L.L. (1997). Zinc, cadmium, and lead separation from aqueous streams using solid-phase extractants. *Industrial & Engineering Chemistry Research* **36** (2) 399-406.
- DOMINGO, J. and CORN, M. (1993). *Handbook of Hazardous Materials*, Academic press, Inc. Boston.

- DRAYE, M., FAVRE-REGUILLON, A., FAURE, R. and LEMAIRE, M. (2008). Radiation chemistry of cis-syn cis dicyclohexano-18-crown-6: Acidity and uranyl nitrate dependence. *Radiation physics and chemistry* **77** 581-584.
- ELDRIDGE D.S., CRAWFORD, R.J. and HARDING, I.H. (2015). The role of metal ion-ligand interactions during divalent metal ion adsorption. *Journal of Colloid and Interface Science* **454** 20-26.
- ESSAWY, H. and IBRAHIM, H. (2004). Synthesis and characterization of poly (vinylpyrrolidone-co-methylacrylate) hydrogel for removal and recovery of heavy metal ions from wastewater. *Reactive and Functional Polymers* **61** (3) 421-432.
- FENG, Q., WANG, X., WEI, A., WEI, Q., HOU, D., LUO, W., LIU, X. and WANG, Z. (2011). Surface Modified Polyacrylonitrile Nanofibers and Application for Metal Ions Chelation. *Fibers and Polymers* **12** 1025-1029.
- FENTON, R.R., GAUCI, R., JUNK, P.C., LINDOY, L.F., LUCKAY, R.C., MEEHAN, G.V., PRICE, J.R., TURNER, P. and WEI, G. (2002). Macrocyclic ligand design. Structure-function relationships involving the interaction of pyridinyl-containing, mixed oxygen-nitrogen donor macrocycles with cobalt (II), nickel (II), copper (II), zinc (II), cadmium (II), silver (I) and lead (II). *Journal of the Chemical Society, Dalton Transactions* **10** 2185-2193.
- FU, F. and WANG, Q. (2011). Removal of heavy metal ions from wastewaters: A review. *Journal of Environmental Management* **92** 407-418.
- GLOE, K. (2005). *Macrocyclic chemistry*. Springer.
- GLOE, K., GRAUBAUM, H., WÜST, M., RAMBUSCH, T. and SEICHTER, W. (2001). Macrocyclic and open-chain ligands with the redox switchable trithiadiazapentalene unit: synthesis, structures and complexation phenomena. *Coordination Chemistry Reviews* **222** (1) 103-126.
- GONZÁLEZ, O., PÉREZ, H., NAVARRO, P., ALMEIDA, L., PACHECO, J. and MONTES, M. (2009), Use of different mesostructured materials based on silica as cobalt supports for the Fischer-Tropsch synthesis. *Catalysis Today* **148** (1) 140-147.
- GORDEN, A.E., XU, J., RAYMOND, K.N. and DURBIN, P. (2003). Rational design of sequestering agents for plutonium and other actinides. *Chemical reviews* **103** (11) 4207-4282.
- GREEN, B. and HANCOCK, R. (1982). Useful resins for the selective extraction of copper, nickel and cobalt, *Journal of the Southern African Institute of Mining and Metallurgy* **82** 303-315.

GREENE, R. (1972). 18-Crown-6: a strong complexing agent for alkali metal cations. *Tetrahedron letters* **13 (18)** 1793-1796.

GRÜNER, B., PLEŠEK, J., BÁČA, J., DOZOL, J.F., LAMARE, V., CÍSAŘOVÁ, I., BĚLOHRADSKÝ, M. and ČÁSLAVSKÝ, J. (2002). Crown ether substituted cobalt bis (dicarbollide) ions as selective extraction agents for removal of Cs and Sr 2 from nuclear waste. *New Journal of Chemistry* **26 (7)** 867-875.

GUPTA, B., DEEP, A. and MALIK, P. (2001). Extraction and recovery of cadmium using Cyanex 923. *Hydrometallurgy* **61 (1)** 65-71.

HANCOCK, R., MELTON, D., HARRINGTON, J., MCDONALD, F., GEPHART, R., BOONE, L., JONES, S., DEAN, N., WHITEHEAD, J. and COCKRELL, G. (2007). Metal ion recognition in aqueous solution by highly preorganized non-macrocyclic ligands. *Coordination Chemistry Reviews* **251** 1678-1689.

HANJRA, M.A. and QURESHI, M.E. (2010). Global water crisis and future food security in an era of climate change. *Food Policy* **35 (5)** 365-377.

HASSABALLA, H., STEED, J.W., JUNK, P.C. and ELSEGOOD, M.R. (1998). Formation of lanthanide and actinide oxonium ion complexes with crown ethers from a liquid clathrate medium. *Inorganic chemistry* **37 (18)** 4666-4671.

HONG, G., LI, X., SHEN, L., WANG, M., WANG, C., YU, X. and WANG, X. (2015). High recovery of lead ions from aminated polyacrylonitrile nanofibrous affinity membranes with micro/nano structure. *Journal of Hazardous Materials* **295** 161-169.

HORZUM, N., SHAHWAN, T., PARLAK, O. and DEMIR, M. (2012). Synthesis of amidoximated polyacrylonitrile fibers and its application for sorption of aqueous uranyl ions under continuous flow. *Chemical Engineering Journal* **213** 41-49.

HOSSAIN, M. (2013). Effect of solvent type on removal and recovery of hexavalent chromium from industrial wastewater. *Desalination and Water Treatment* **52** 3147-3157.

HUSKENS, J. and SHERRY, A.D. (1996). Synthesis and characterization of 1, 4, 7-triazacyclononane derivatives with methylphosphinate and acetate side chains for monitoring free MgII by ³¹P and ¹H NMR spectroscopy. *Journal of the American Chemical Society* **118 (18)** 4396-4404.

IGWE, J.C. and ABIA, A. (2006). Sorption kinetics and intraparticulate diffusivity of As (III) bioremediation from aqueous solution, using modified and unmodified coconut fiber. *Ecletica Quimica* **31 (3)** 23-29.

ISLAM, M.S., AHMED, M.K., RAKNUZZAMAN, M., HABIBULLAH-AL-MAMUN, M. and ISLAM, M.K. (2015). Heavy metal pollution in surface water and sediment: A preliminary assessment of an urban river in a developing country. *Ecological Indicators* **48** 282-291.

IZATT, M., TERRY, R., HAYMORE, B., HANSEN, L., DALLEY, N., AYONDET, A. and CHRISTENSEN, J. (1976). Calorimetric Titration Study of the Interaction of Several Uni- and Bivalent Cations with 15-Crown-5, 18-Crown-6, and Two Isomers of Dicyclohexo- 18- crown-6 in Aqueous Solution at 25°C and $p = 0.1$. *Journal of the American Chemical Society* **98** 7620-7626.

IZATT, N.E., BRUENING, R.L., KRAKOWIAK, K.E. and IZATT, S.R. (2000). Contributions of Professor Reed M. Izatt to Molecular Recognition Technology: from laboratory to commercial application. *Industrial & Engineering Chemistry Research* **39 (10)** 3405-3411.

IZATT, R.M., BRUENING, R.L., BRUENING, M.L., TARBET, B.J., KRAKOWIAK, K.E., BRADSHAW, J.S. and CHRISTENSEN, J.J. (1988). Removal and separation of metal ions from aqueous solutions using a silica-gel-bonded macrocycle system, *Analytical Chemistry* **60 (17)** 1825-1826.

JAISHANKAR, M., TSETEN, T., ANBALAGAN, N., MATHEW, B.B. and BEEREGOWDA, K.N. (2014). Toxicity, mechanism and health effects of some heavy metals. *Interdisciplinary toxicology* **7(2)** 60-72.

JAL, P.K., PATEL, S. and MISHRA, B.K. (2004). Chemical modification of silica surface by immobilization of functional groups for extractive concentration of metal ions. *Talanta* **62** 1005-1028.

JURBERGS, H. and HOLCOMBE, J. (1999). Comparison of silica-immobilized poly (L-cysteine) and 8-hydroxyquinoline for trace metal extraction and recovery. *Journal of Analytical Atomic Spectrometry* **14 (8)** 1209-1214.

JURBERGS, H.A. and HOLCOMBE, J.A. (1997). Characterization of immobilized poly (L-cysteine) for cadmium chelation and preconcentration. *Analytical Chemistry* **69 (10)** 1893-1898.

KALTSOYANNIS, N. and SCOTT, P. (1999). *The elements*. Oxford University Press.

- KAMPALANONWAT, P. and SUPAPHOL, P. (2014). The Study of Competitive Adsorption of Heavy Metal Ions from Aqueous Solution by Aminated Polyacrylonitrile Nanofiber Mats 11th Eco-Energy and Materials Science and Engineering (11th EMSES). *Energy Procedia* **56** 142-151.
- KANNAN, S., RAJ SHANMUGASUNDARA, S. and FUN, H. (2001). Crown ether compounds of actinides bis(β -diketonate). Synthesis, characterization and molecular structures of $[\text{UO}_2(\text{TTA})_2\text{H}_2\text{O}]_2(\text{benzo-15-crown-5})$ (1) and $[\text{UO}_2(\text{TTA})_2(\mu\text{-H}_2\text{O})]_2(\text{H}_2\text{O})_2(\text{dibenzo-18-crown-6})$. *Polyhedron* **20** 2145-2150.
- KANTIPULY, C., KATRAGADDA, S., CHOW, A. and GESSER, H. (1990). Chelating polymers and related supports for separation and preconcentration of trace metals. *Talanta* **37** (5) 491-517.
- KARKHANEI, E., ZEBARJADIAN, M. and SHAMSIPUR, M. (2001). Complexation of Ba^{2+} , Pb^{2+} , Cd^{2+} , and UO_2^{2+} ions with 18-crown-6 and dicyclohexyl-18-crown-6 in nitromethane and acetonitrile solutions by a competitive NMR technique using the ^7Li Nucleus as a probe. *Journal of solution chemistry* **30** 323-333.
- KHEZAMI, L. and CAPART, R. (2005). Removal of chromium(VI) from aqueous solution by activated carbons: kinetic and equilibrium studies *Journal of Hazardous Material* **123** 223-231.
- KIM, J., NORQUIST, A. and O'HARE, D. (2003). Incorporation of U(IV) into metal-organic framework solids, $[\text{UO}_2(\text{C}_4\text{H}_4\text{O}_4)]\cdot\text{H}_2\text{O}$, $[\text{UO}_2\text{F}(\text{C}_5\text{H}_6\text{O}_4)]\cdot 2\text{H}_2\text{O}$ and $[(\text{UO}_2)_{1.5}(\text{C}_8\text{H}_4\text{O}_4)_2]_2[(\text{CH}_3)_2\text{NCOH}_2]\cdot\text{H}_2\text{O}$. *Journal of chemical society Dalton transactions* **2003** 2813-2814.
- KOROBEINYK, A.V., WHITBY, R.L. and MIKHALOVSKY, S.V. (2012). High temperature oxidative resistance of polyacrylonitrile-methylmethacrylate copolymer powder converting to a carbonized monolith. *European Polymer Journal* **48**, 97-104.
- KOYAMA, H. and YOSHINO, T. (1972). Syntheses of some medium sized cyclic triamines and their cobalt (III) complexes. *Bulletin of Chemical Society of Japan* **45** 481-484.
- KUMAR, J., KIM, J., LEE, J. and YOON, H. (2011). A brief review on solvent extraction of uranium from acidic solutions. *Separation and Purification Reviews* **40** 77-125.
- KUMARI, R. (2011). Preliminary mercury emission estimates from non-ferrous metal smelting in India. *Atmospheric Pollution Research* **2**(4) 513-519.

- KUMBASAR, R.A. (2010). Extraction of cadmium from solutions containing various heavy metal ions by Amberlite LA-2 Journal of Industrial and Engineering Chemistry **16** 207-213.
- KUMBASAR, R.A. (2013). Selective extraction of Cadmium from multicomponent acidic leach solutions by emulsion liquid membrane using amberlite LA2 as extractant, Separation Sciences and technology **48** 1841-1850.
- KURNIAWAN, T., CHAN, G., LO, W. and BABEL, S. (2006). Physicochemical treatment techniques for wastewater laden with heavy metals. Chemical Engineering Journal **118** 83-98.
- KWON, T. and JEON, C. (2012). Desorption and regeneration characteristics for previously adsorbed indium ions to phosphorylated sawdust, Journal of Environmental Engineering Research **17 (2)** 65-67.
- LASSETER, T.L., CLARE, B.H., ABBOTT, N.L. and HAMERS, R.J. (2004). Covalently modified silicon and diamond surfaces: resistance to nonspecific protein adsorption and optimization for biosensing. Journal of the American Chemical Society **126 (33)** 10220-10221.
- LEWIS, R.J. (1996). *Sax's Dangerous Properties of Industrial Materials*, 8th Ed., Vol. III, Van Nostrand Reinhold, New York.
- LUCKAY, R., HANCOCK, R.D., CUKROWSKI, I. and REIBENSPIES, J.H. (1996). Study of protonation of 1, 4, 7-tris (2-hydroxyethyl)-1, 4, 7-triazacyclononane, and its complexes with metal ions, by crystallography, polarography, potentiometry, molecular mechanics and NMR. Inorganica Chimica Acta **246 (1)** 159-169.
- MADRAKIAN, T., AFKHAMI, A. and MOUSAVI, A. (2007). Spectrophotometric determination of trace amounts of uranium (VI) in water samples after mixed micelle-mediated extraction. Talanta **71 (2)** 610-614.
- MADZIVIRE, G. (2012). Chemistry and speciation of potentially toxic and radioactive elements during mine water treatment, Ph.D. thesis, University of the Western Cape.
- MAHMOUD, M.E. and AL-BISHRI, H.M. (2012). Adjusted pH for the selective separation of cadmium from lead by nano-active silica-functionalized- [Bmim+][Tf2N-] ionic liquid. Separation Science Technology **48** 931-940.
- MAHMOUD, M.E. and SOLIMAN, E.M. (1997). Study of the selective extraction of iron (III) by silica-immobilized 5-formyl-3-aryloxy-salicylic acid derivatives. Talanta **44 (6)** 1063-1071.

- MARSHALL, M.A. and MOTTOLA, H.A. (1983). Synthesis of silica-immobilized 8-quinolinol with (aminophenyl) trimethoxysilane, *Analytical Chemistry* **55 (13)** 2089-2093.
- MARTELL, A.E. and HANCOCK, R.D. (1996). *Metal complexes in aqueous solutions*. Plenum Press, New York.
- MAYANI, V.J., ABDI, S., KURESHY, R., KHAN, N., AGRAWAL, S. and JASRA, R. (2006). Synthesis and characterization of (< i> S)-amino alcohol modified M41S as effective material for the enantioseparation of racemic compounds. *Journal of Chromatography A* **1135 (2)** 186-193.
- MEENA, A.K., KADIRVELU, K., MISHRA, G.K., RAJAGOPAL, C. and NAGAR, P.N. (2008). Adsorptive removal of heavy metals from aqueous solution by treated sawdust (*Acacia arabica*). *Journal of Hazardous Materials* **150 (3)** 604-611.
- MSDS “All the information was obtained from the MSDS from the various suppliers”
- MUNDRA, S., PAI, S. and SUBRAMANIAN, M. (1987). Synergistic extraction of uranyl ion with acylpyrazolones and dicyclohexano-18-crown-6. *Journal of Radioanalytical and Nuclear Chemistry* **116 (1)** 203-211.
- MUSYOKA, S., NGILA, C., MOODLEY, B., KINDNESS, A., PETRIK, L. and GREYLING, C. (2011). Oxolane-2,5-dione modified electrospun cellulose nanofibers for heavy metals Adsorption. *Journal of Hazardous Materials* **192** 922-927.
- MYASOEDOVA, G., ANTOKOL'SKAYA, I. and SAVVIN, S. (1985). New chelating sorbents for noble metals. *Talanta* **32 (12)** 1105-1112.
- NATARAJ, S., YANG, K. and AMINABHAVI, T. (2012). Polyacrylonitrile-based nanofibers – A state-of-the-art review. *Progress in polymer science* **37** 487-513.
- NDAYAMBAJE, G., LAATIKAINEN, K., LAATIKAINEN, M., BEUKES, E., FATOBA, O., VAN DER WALT, N., PETRIK, L. and SAINIO, T. (2016). Adsorption of nickel(II) on polyacrylonitrile nanofiber modified with 2-(20-pyridyl)imidazole. *Chemical Engineering Journal* **284** 1106-1116.
- NEGHLANI, P., RAFIZADEH, M. and TARONI, F. (2011). Preparation of aminated-polyacrylonitrile nanofiber membranes for the adsorption of metal ions: Comparison with microfibers. *Journal of Hazardous Materials* **186** 182-189.
- NILCHI, A., BABALOU, A.A. and RAFIEE, R. (2008a). Adsorption properties of amidoxime resins for separation of metal ions from aqueous systems. *Reactive and Functional Polymer* **68** 1665-1670.

- NILCHI, A., RAFIEE, R. and BABALOU, A.A. (2008b). Adsorption Behavior of Metal Ions by Amidoxime Chelating Resins. *Macromolecular Symposia* **274** 101-108.
- PAKADE, V., CUKROWSKA, E., DARKWA, J., TORTO, N. and CHIMUKA, L (2011). Selective removal of chromium (VI) from sulphates and other metal anions using an ion-imprinted polymer. *Journal of Water Resource* **37 (4)** 529-38.
- PEARSON, R.G. (1963). Hard and soft acids and bases. *Journal of the American Chemical Society* **85 (22)** 3533-3539.
- PEKEL, N. and GUVEN, O. (2003). Separation of uranyl ions with amidoximated poly(acrylonitrile/N-vinylimidazole) complexing sorbents. *Colloids and surfaces a physicochemical engineering aspects* **212** 155-161.
- PEKEL, N., SAHINER, N. and GUVEN, O. (2000). Development of new chelating hydrogels based on N-vinyl imidazole and acrylonitrile. *Radiation Physics and Chemistry* **59** 485-491.
- PEREAO, O.K., BODE-ALUKO, C., NDAYAMBAJE, G., FATOBA, O. and PETRIK, L.F. (2016). Electrospinning: Polymer Nanofibre Adsorbent Applications for Metal Ion Removal. *Journal of Polymer and Environment* DOI 10.1007/s10924-016-0896-y.
- PIODA, L.A., WACHTER, H., DOHNER, R. and SIMON, W. (1967). Komplexe von Nonactin und Monactin mit Natrium-, Kalium-und Ammonium-Ionen, *Helvetica chimica acta* **50 (5)** 1373-1376.
- POOLE, C.F. (2003). New trends in solid-phase extraction. *TrAC Trends in Analytical Chemistry* **22 (6)** 362-373.
- POWELL, K.J., BROWN, P.L., BYRNE, R.H., GAJDA, T., HEFTER, G., LEUZ, A.K., SJOBERG, S. and WANNER, H. (2009). Chemical speciation of environmentally significant metals with inorganic ligands. Part 3: the Pb^{2+} , OH^- , Cl^- , CO_3^{2-} , SO_4^{2-} , and PO_4^{3-} systems (IUPAC technical report). *Pure and Applied Chemistry* **81** 2425-2476.
- PYELL, U. and STORK, G. (1992). Preparation and properties of an 8-hydroxyquinoline silica gel, synthesized via mannich reaction. *Fresenius' journal of analytical chemistry* **342(5)** 281-286.
- QING-ZHU, L., LI-YUAN, C. and JING, Z. (2009). Lead desorption from modified spent grain, *Transactions of Nonferrous. Metals Society of China* **19** 1371-1376.

RAWAT, N., MOHAPATRA, P., LAKSHMI, D., BHATTACHARYYA, A. and MANCHANDA, V. (2006). Evaluation of a supported liquid membrane containing a macrocyclic ionophore for selective removal of Strontium from nuclear waste solution. *Journal of membrane science* **275** 82-88.

RODRÍGUEZ, A.M., GÓMEZ-LÍMÓN, D. and ALGUACIL, F.J. (2005). Liquid-liquid extraction of cadmium (II) by Cyanex 923 and its application to a solid-supported liquid membrane system. *Journal of Chemical Technology and Biotechnology* **80 (9)** 967-972.

SABATINI, L. and FABBRIZZI, L. (1979). Fitting of nickel (II) ion into two 14-membered tetraaza macrocycles. Blue-to-yellow conversion and the oxidation and reduction behaviour. *Inorganic chemistry* **18(2)** 438-444.

SADEGHI, S. and SHEIKHZADEH, E. (2009). Solid phase extraction using silica gel modified with murexide for preconcentration of uranium (VI) ions from water samples. *Journal of hazardous materials* **163(2)** 861-868.

SADEGHI, S., AZHDARI, H., ARABI, H. and MOGHADDAM, A. (2012). Surface modified magnetic Fe₃O₄ nanoparticles as a selective sorbent for solid phase extraction of uranyl ions from water samples. *Journal of Hazardous Materials* **215** 208-216.

SAEED, K., HAIDER, S., OH, T. and PARK, S. (2008). Preparation of amidoxime-modified polyacrylonitrile (PAN-oxime) nanofibres and their applications to metal ions adsorption. *Journal of Membrane Science* **322** 400-405.

SAKAMA, M., IMURA, H., KUZE, K. and SASAYA, A. (2007). Investigation of uranium and thorium activities and their isotopic ratios in environmental water samples in Tokushima, Japan, using extraction chromatography and samarium coprecipitation. *Journal of Radioanalytical and Nuclear Chemistry* **273(1)** 187-193.

SALAMONE, J.C. (1998). *Concise polymeric materials encyclopedia*, CRC press.

SANTOS, M.R. and AIROLDI, C. (1996). Urea derivatives anchored on silica gel, *Journal of colloid and interface science* **183(2)** 416-423.

SEEBER, G., BRUNNER, P., BUCHMEISER, M.R. and BONN, G.K. (1999). Poly(7-oxanorborn-2-ene-5,6-dicarboxylate)-coated silica prepared by ring-opening metathesis polymerization for the selective enrichment of radioactive lanthanides, *Journal of Chromatography A* **848(2)** 193-202.

- SHAMSIPUR, M., GHIASVAND, A.R. and YAMINI, Y. (1999). Solid-phase extraction of ultratrace uranium (VI) in natural waters using octadecyl silica membrane disks modified by tri-n-octylphosphine oxide and its spectrophotometric determination with dibenzoylmethane. *Analytical Chemistry* **71** (21) 4892-4895.
- SHARMA, B., SINGH, S. and SIDDIQI, N.J. (2014). Biomedical implications of heavy metals induced imbalances in redox systems. *BioMed research international* **2014** 640754.
- STEPINSKI, D.C., JENSEN, M.P., DZIELAWA, J.A. and DIETZ, M.L. (2005). Synergistic effects in the facilitated transfer of metal ions into room-temperature ionic liquids. *Green Chemistry* **7**(3) 151-158.
- STIKKER, A. (1998). WATER TODAY AND TOMORROW: Prospects for overcoming scarcity. *Futures* **30**(1) 43-62.
- SZIGETHY, G. and RAYMOND, K.N. (1999). Designing of ligands using crown ethers. *Inorganic Chemistry* **38** 308.
- TAKEDA, T., SAITO, K., UEZU, K., FURUSAKI, S., SUGO, T. and OKAMOTO, J. (1991). Adsorption and Elution in Hollow-Fiber-Packed Bed for Recovery of Uranium from Seawater. *Industrial and Engineering Chemistry Research* **30** 185-190.
- TAKESHITA, K., WATANABE, K., NAKANO, Y. and WATANABE, M. (2003). Solvent extraction separation of Cd (II) and Zn (II) with the organophosphorus extractant D2EHPA and the aqueous nitrogen-donor ligand TPEN. *Hydrometallurgy* **70** (1) 63-71.
- TASKER, P., PLIEGER, P. and WEST, L. (2004). Metal complexes for hydrometallurgy and extraction. *Comprehensive Coordination Chemistry II* **9** 759-808.
- TIAN, G., WANG, J., SHEN, Y. and RAO, L. (2005). Extraction of strontium from HLLW using N, N, N', N'-tetraisobutyl 3-oxa-glutaramide. *Solvent extraction and ion exchange*, **23** (4) 519-528.
- TOPOLSKA, K., SAWICKA-KAPUSTA, K. and CIESLIK, E. (2004). The effect of contamination of the Krakow region on heavy metals content in the organs of bank voles (*Clethrionomys glareolus*, Schreber, 1780). *Polish Journal of Environmental Studies* **13** 103-109.
- TUNCA, U. and YAGCI, Y. (1994). Crown ether-containing polymers, *Progress in polymer science* **19**(2) 233-286.

- TUTU, H., MCCARTHY, T.S. and CUKROWSKA, E.M. (2008). The chemical characteristics of acid mine drainage with particular reference to sources, distribution and remediation: The Witwatersrand Basin, South Africa as a case study. *Applied Geochemistry* **23(12)** 3666-3684.
- WADDELL, T.G., LEYDEN, D.E. and DEBELLO, M.T. (1981). The nature of organosilane to silica-surface bonding. *Journal of the American Chemical Society* **103(18)** 5303-5307.
- WAI, C.M., KULYAKO, Y., YAK, H.K., CHEN, X. and LEE, S.J. (1999). Selective Extraction of Strontium with Supercritical Fluid Carbon Dioxide. *Chemical Communication* 2533-2535.
- WANG, Y., LIN, S. and JUANG, R. (2003). Removal of heavy metal ions from aqueous solutions using various low-cost adsorbents. *Journal of hazardous materials* **102 (2)** 291-302.
- WASSINK, B., DREISINGER, D. and HOWARD, J. (2000). Solvent extraction separation of zinc and cadmium from nickel and cobalt using Aliquat 336, a strong base anion exchanger, in the chloride and thiocyanate forms. *Hydrometallurgy* **57 (3)** 235-252.
- WINDE, F. (2006). Challenges for sustainable water use in dolomitic mining regions of South Africa- A case study of Uranium pollution Part 1: Sources and pathways. *Physical Geography* **27 (4)** 333-347.
- WINDE, F. and SANDHAM, L. (2004). Uranium pollution in South Africa streams. An overview of the situation on gold mining area of the Witwatersrand. *Geojournal Kluiver Academic publishers* **61** 131-149.
- WOOD, D.J., LAW, J.D. and Tullock, P.A. (1997). Extraction of lead and strontium from hazardous waste streams by solvent extraction with 4',4', (5')-Di-(t-butylidicyclohexano)-18-crown-6. *Solvent Extraction and Ion Exchange* **15** 65-78.
- WORLD HEALTH ORGANIZATION (2011). *Radiological aspects: Guidelines for Drinking water Quality*. Third edition, Geneva, World Health Organization 197-209.
- WU, Y., KIM, S., TOZAWA, D., ITO, T., TADA, T., HITOMI, K., KURAOKA, E., YAMAZAKI, H. and ISHII, K. (2012). Equilibrium and kinetic studies of selective adsorption and separation for strontium using DtBuCH18C6 loaded resin. *Journal of nuclear science and technology* **49 (3)** 320-327.
- YAKSHIN, V., TSARENTO, N., KOSHCHEEV, A., TANANAEV, I. and MYASOEDOV, B. (2010). Selective extraction of uranium from hydrochloric acid solutions with macrocyclic endoreceptors. *Radiochemistry* **52 (4)** 358-362.
- YAVUZ, Ö., ALTUNKAYNAK, Y. and GÜZEL, F. (2003). Removal of copper, nickel, cobalt and manganese from aqueous solution by kaolinite. *Water research* **37 (4)** 948-952.

YE, G., BAI, F., WEI, J., WANG, J. and CHEN, J. (2012). Novel polysiloxane resin functionalized with dicyclohexano-18-crown-6 (DCH18C6): Synthesis, characterization and extraction of Sr(II) in high acidity HNO₃ medium. *Journal of Hazardous Materials* **225** 8-14.

YIN, C. (2010). Emerging usage of plant-based coagulants for water and wastewater treatment. *Process Biochemistry* **45** (9) 1437-1444.

YUAN, L., LIU, Y., SHI, W., LI, Z., LAN, J., FENG, Y., ZHAO, Y., YUAN, Y. and CHAI, Z. (2012). A novel mesoporous material for uranium extraction, dihydroimidazole functionalized SBA-15. *Journal of material chemistry* **22** 17019-17025.

ZAPOROZHETS, O., PETRUNIOCK, N., BESSARABOVA, O. and SUKHAN, V. (1999). Determination of Cu (II) and Zn (II) using silica gel loaded with 1-(2-thiasolyazo)-2-naphthol *Talanta* **49** (4) 899-906.

ZHANG, A., CHEN, C., WANG, W. and WEI, Y. (2008). Adsorption behavior of Sr(II) and some typical co-existent metals contained in high level liquid waste onto a modified macroporous silica-based polymeric DtBuCH18C6 composite. *Solvent extraction and ion exchange* **26** 624-642.

ZHANG, A., WEI, Y. and KUMAGAI, M. (2004). Synthesis of a novel macroporous silica-based polymeric material containing 4, 4, (5)-di(tert-butylcyclohexano)-18-crown-6 functional group and its adsorption mechanism for strontium. *Reactive and functional polymers* **61** 191-202.

ZHANG, A., XIAO, C., LIU, Y., HU, Q., CHEN, C. and KURAOKA, E. (2010). Preparation of macroporous silica-based crown ether materials for strontium separation, *Journal of porous material* **17** 153-161.

ZOU, W., ZHAO, L. and HAN, R. (2009). Removal of uranium (VI) by fixed bed ion-exchange column using natural zeolite coated with manganese oxide. *China journal chemical engineering* **17** 585-593.